

EEG-69  
DOE/AL58309-69

SENSITIVITY ANALYSIS OF PERFORMANCE  
PARAMETERS USED IN MODELING THE WIPP

Dale F. Rucker

Environmental Evaluation Group  
7007 Wyoming Blvd NE, Suite F-2  
Albuquerque, NM 87109

and

P.O. Box 3149, 505 North Main Street  
Carlsbad, NM 88221

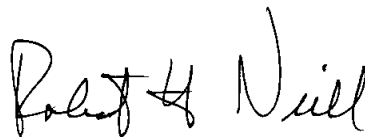
May 1998



## FOREWORD

The purpose of the New Mexico Environmental Evaluation Group (EEG) is to conduct an independent technical evaluation of the Waste Isolation Pilot Plant (WIPP) Project to ensure the protection of the public health and safety and the environment. The WIPP Project, located in southeastern New Mexico, is being constructed as a repository for the disposal of transuranic (TRU) radioactive wastes generated by the national defense programs. The EEG was established in 1978 with funds provided by the U.S. Department of Energy (DOE) to the State of New Mexico. Public Law 100-456, the National Defense Authorization Act, Fiscal Year 1989, Section 1433, assigned EEG to the New Mexico Institute of Mining and Technology and continued the original contract DE-AC04-79AL10752 through DOE contract DE-AC04-89AL58309. The National Defense Authorization Act for Fiscal Year 1994, Public Law 103-160, continues authorization.

EEG performs independent technical analyses of the suitability of the proposed site, the design of the repository, its planned operation, and its long-term integrity, suitability and safety of the transportation systems, suitability of the Waste Acceptance Criteria and the generator sites' compliance with them, and related subjects. These analyses include assessments of reports issued by the DOE and its contractors and other federal agencies and organizations as they relate to the potential health, safety, and environmental impacts from WIPP. Another important function of EEG is the independent environmental monitoring of background radioactivity in air, water, and soil, both on-site and off-site.

A handwritten signature in black ink, appearing to read "Robert H. Neill". The signature is written in a cursive, somewhat stylized font.

Robert H. Neill  
Director

## EEG STAFF

Sally C. Ballard, B.S., Laboratory Scientist  
William T. Bartlett, Ph.D., Health Physicist  
Radene Bradley, Secretary III  
James K. Channell, Ph.D., Environmental Engineer/Health Physicist  
Lokesh Chaturvedi, Ph.D., Deputy Director & Engineering Geologist  
Patricia D. Fairchild, Secretary III  
Donald H. Gray, M.A., Environmental Specialist  
Jim W. Kenney, M.S., Environmental Scientist/Supervisor  
Lanny King, Assistant Environmental Technician  
Betsy J. Kraus, M.S., Technical Editor/Librarian  
Robert H. Neill M.S., Director  
Dale F. Rucker, M.S., Performance Assessment Engineer  
Jill Shortencarier, Executive Assistant  
Matthew K. Silva, Ph.D., Chemical Engineer  
Susan Stokam, Administrative Secretary  
Ben A. Walker, B.A., Quality Assurance Specialist  
Brenda J. West, B.A., Administrative Officer

# TABLE OF CONTENTS

FOREWORD.....	iii
EEG STAFF.....	iv
EXECUTIVE SUMMARY.....	xv
1. Introduction.....	1
1.1. Performance Assessment.....	1
1.2. Repository Design and Site Characterization.....	4
1.2.1. Castile Formation.....	4
1.2.2. Salado Formation.....	5
1.2.3. Rustler Formation.....	6
1.2.4. Dewey Lake RedBeds, Santa Rosa, and Gatuna Formations.....	6
1.2.5. The Repository.....	7
1.2.5.1. Room Collapse and Post Closure.....	7
1.2.5.2. Gas Generation and Waste Backfill.....	9
1.2.5.3. Panel Closure.....	10
1.2.5.4. Shaft Seals.....	10
1.2.5.5. Borehole Plugs.....	11
1.2.6. Potential Pathways for Release.....	12
1.3. Scope.....	12
2. Performance Assessment Review.....	14
2.1. Scenarios of the Performance Assessment.....	14
2.1.1. Undisturbed Performance.....	14
2.1.2. Disturbed Performance-Human Intrusion.....	14
2.1.3. Probabilistic Performance.....	16
2.2. Computer Models.....	16
2.2.1. BRAGFLO.....	17
2.2.2. NUTS.....	17
2.2.3. PANEL.....	18
2.2.4. CUTTINGS_S.....	18
2.2.5. BRAGFLO_DBR.....	19
2.2.6. SECOFL2D.....	20

2.2.7. SECOTP2D.....	21
2.2.8. CCDFGF .....	21
2.3. Parameters.....	22
2.4. Sensitivity and Uncertainty Analysis of Performance Assessment Parameters.....	24
2.4.1. Repository Conditions.....	25
2.4.1.1. Repository Pressure.....	25
2.4.1.2. Brine Saturation.....	27
2.4.1.3. Brine Flow.....	27
2.4.2. Cuttings and Cavings.....	27
2.4.3. Spallings.....	28
2.4.4. Direct Brine Release.....	28
2.4.5. Culebra Transport.....	28
3. Concerns.....	30
3.1. Conservatism.....	30
3.2. Parameter Issues.....	30
3.2.1. Brine Reservoir Interception.....	31
3.2.2. Actinide Solubility.....	31
3.2.3. Chemical Retardation.....	32
3.2.4. Castile Reservoir Parameters.....	32
3.2.5. Potash Mining.....	33
3.2.6. Spallings' Calculations.....	33
4. Probability Modeling of Drill Intrusion Rates.....	35
4.1. Summary.....	35
4.2. Introduction.....	35
4.3. Methodology.....	35
4.4. Results.....	37
4.5. Conclusions.....	38
5. Individual and Combined Influence of Plutonium Solubility on Direct Brine Release and the Probability of Hitting Castile Brine.....	39
5.1. Summary.....	39
5.2. Introduction.....	39
5.3. Methodology .....	40
5.4. Results.....	42

5.5. Conclusions.....	45
6. Transport Modeling of $K_d$ s.....	47
6.1. Summary.....	47
6.2. Introduction.....	47
6.3. Methodology.....	47
6.4. Transport Modeling of Plutonium.....	48
6.5. Probability Modeling of Actinides.....	55
6.6. Conclusions.....	55
7. Castile Brine Reservoir Parameters.....	57
7.1. Summary.....	57
7.2. Introduction.....	57
7.3. Reservoir Parameters.....	57
7.3.1. Productivity Ratio.....	58
7.3.1.1. Castile Brine Volume.....	60
7.3.1.2. Rock Compressibility of Castile Reservoir.....	60
7.3.2. Castile Reservoir Pressure.....	61
7.3.3. Castile Reservoir Permeability.....	61
7.3.4. Other Parameter Changes.....	62
7.3.4.1. Waste Permeability.....	62
7.3.4.2. Residual Brine Saturation.....	62
7.4. Methodology.....	63
7.4.1. BRAGFLO Calculations.....	63
7.4.2. CUTTINGS_S Calculations.....	65
7.4.3. BRAGFLO_DBR Calculations.....	66
7.5. Results.....	68
7.5.1. BRAGFLO Results.....	68
7.5.1.1. The Repository.....	68
7.5.1.2. Fluid Flow Through the Borehole.....	72
7.5.2. Cuttings, Cavings, and Spallings Results.....	74
7.5.2.1. Cuttings and Cavings.....	75
7.5.2.2. Spallings.....	76
7.5.3. Direct Brine Release.....	77
7.5.4. Probability Modeling with Results from Castile Simulation.....	81
7.6. Conclusions.....	81

8. Culebra Flow and Transport Using BLM Map for Economic Potash	
Resources of Eddy County.....	84
8.1. Summary.....	84
8.2. Introduction.....	84
8.3. Methodology.....	87
8.4. Results.....	87
8.4.1. Culebra Flow.....	87
8.4.2. Culebra Transport.....	91
8.4.2.1. Plutonium Transport Calculations with $K_d=0$ .....	91
8.4.2.2. Uranium Transport Calculations with LHS Generated $K_d$ s.....	92
8.5. Probabilistic Modeling of Uranium and Plutonium.....	95
8.6. Conclusions.....	96
9. GASOUT Modeling of the WIPP.....	99
9.1. Summary.....	99
9.2. Introduction.....	99
9.3. Discussion.....	102
9.4. Base Case.....	105
9.5. Sensitivity to Permeability and Initial Repository Pressure.....	108
9.6. Sensitivity to Gas Viscosity.....	111
9.7. Sensitivity to Mud Column Density.....	112
9.8. Sensitivity to Waste Porosity.....	113
9.9. Conclusions.....	114
10. Solubility Modeling Assuming No MgO Backfill and with MgO Mineral Phase of Nequehonite.....	117
10.1. Summary.....	117
10.2. Introduction.....	117
10.3. Methodology.....	119
10.4. Results.....	122
10.5. Conclusions.....	124
REFERENCES.....	125
ACRONYMS.....	130



LIST OF EEG REPORTS.....131

## LIST OF TABLES

Ex-1. Solubility Factors for SOLCIM and SOLSIM.....	xix
1.1. Release Limits as Stated in 40 CFR Part 191, Subpart B.....	2
4.1. Total Normalized Release Limits at Different Deep Drilling Rates.....	38
5.1. Solubility of Plutonium a Determined by Experiment and FMT Calculations.....	40
5.2. Releases for PANEL Simulations at $10^{-3}$ Probability.....	45
6.1. Maximum Releases of Plutonium-239 and Total for All Actinides to the Culebra.....	54
7.1. Castile Reservoir Parameter Suggestions.....	64
7.2. Fraction of Steel and Cellulosics Remaining After 10,000 Years for CCA and Castile Simulations for S2 and S3.....	71
9.1. Input Assumptions for Base Case Study and from Hansen at al. (1997) .....	104
9.2. Permeability Values Used to Calculate Waste Permeability in the CCA.....	109
10.1. Median Solubility Values Used in Various Performance Assessment Calculations.....	119
10.2. Solubility Factors for SOLCIM and SOLSIM.....	120

## LIST OF FIGURES

Ex-1. Overall Mean of Normalized Releases for Modeling of Increased Solubilities Using Nesquehonite and 'No Backfill' Values Compared to CCA Values.....	xxi
1.1. DOE's CCDF of Normalized Releases, Showing Overall Mean for all Release Types.....	3
1.2. Stratigraphic Cross Section of the Geologic Region around WIPP.....	5
1.3. Areal View of the Underground WIPP Facility.....	8
1.4. Shaft Seal System at the WIPP.....	11
2.1. Major Codes with Linkages.....	17
2.2. Mean CCDFs for Specified Release Modes.....	23
3.1. Releases from an S3 Scenario (Replicate 1) for Microbial Decay.....	31
4.1. CCDFGF Flowchart.....	36
4.2. Total Normalized Release Limits for Changing Drilling Rates.....	37
5.1. Flowchart of PANEL Simulations.....	41
5.2. Blowout Releases for Increased Solubility.....	43
5.3. Blowout Releases for CCA Calculations.....	43
5.4. Overall Mean of Blowout Normalized Releases.....	44
5.5. Total Normalized Releases with Increasing Probability of Hitting the Castile Brine Reservoir .....	45
5.6. Overall Mean of Blowout Releases with Increasing Solubility.....	46
6.1. Flowchart of SECOTP2D Runs.....	48
6.2. Integrated Discharge vs. Vector Number for Partial Mining Scenario at 10,000 Years.....	50
6.3. Plutonium Concentration (kg/m <sup>3</sup> ) for Replicate 1, Vector 4, Partial Mining.....	51
6.4. Integrated Discharge vs. Vector Number for Full Mining Scenario at 10,000 Years with 1% Plutonium having a K <sub>d</sub> of Zero.....	52
6.5. Plutonium Concentration (kg/m <sup>3</sup> ) for Replicate 1, Vector 58, Full Mining.....	53
6.6. Total Normalized Releases from Culebra for 1% K <sub>d</sub> =0 ml/g for Plutonium Simulation.....	54
6.7. Total Normalized Releases for all Actinides Crossing the LWB.....	55
7.1. Location of Boreholes in the Castile Formation that were used to Characterize the Castile Brine Reservoir.....	58
7.2. Productivity Ratio of the CCA for Replicate 1.....	59
7.3. Flowchart for BRAGFLO Calculations.....	63
7.4. Flowchart of CUTTINGS_S Simulations.....	64
7.5a. Flowchart of BRAGFLO_DBR.....	66
7.5b. Flowchart of BRAGFLO_DBR (cont.) .....	67

7.6. Volume Averaged Pressures of 10,000 Year Time History for Left) Scenario 2 and Right) Scenario 3.....	69
7.7. Net Inflow of Brine from Castile Reservoir for CCA and Castile Simulation for Left) Scenario 2 and Right) Scenario 3.....	70
7.8. Total Gas Volumes Generated from Corrosion and Microbial Degredation for CCA and Castile Simulation for Left) Scenario 2 and Right) Scenario 3.....	71
7.9. Volume Averaged Brine Saturation In Waste Panels for CCA and Castile Simulation for Left) Scenario 2 and Right) Scenario 3.....	72
7.10. Cumulative Brine Flow up the Borehole from Waste Panels to the Top of the Panel for Castile Simulation of Left) Scenario 2 and Right) Scenario 3.....	73
7.11. Scatter Plot for Volume of Brine Reaching the Top of the Waste Panels through an Intrusion Borehole and Permeabilities from Regions of the Disposal System.....	74
7.12. Brine Volume (m <sup>3</sup> ) Reaching the Top of the Rustler Formation for the Castile Simulation for Left) Scenario 2 and Right) Scenario 3.....	75
7.13. Waste Removed (m <sup>3</sup> ) by Cuttings and Cavings vs. Waste Shear Strength, Scenario 2, at Time 4,000 Years Post Closure.....	76
7.14. Frequency Distribution of Spalled Blowout Volume from an Initial Intrusion at 1000 Years (Scenario 3) and a Subsequent Intrusion Into Panel 5 At 1,200 Years.....	78
7.15. Frequency Distribution of Direct Brine Release Volumes (m <sup>3</sup> ) for CCA and Castile Simulation for Left) Scenario 2 and Right) Scenario 3.....	79
7.16. Direct Brine Release (m <sup>3</sup> ) for Scenario 3 for Castile Simulation for the Second Intrusion At 1,200 Years for Left) Volume Averaged Waste Room Pressure (MPa) and Right) Volume Averaged Waste Room Saturation (Unitless) .....	80
7.17. Scatter Plot of the Pressure in the Repository (MPa) for Castile Simulation, Scenario 3, 1,200 Years Post Closure Versus Inundated Steel Corrosion Rate.....	80
7.18. CCDF for Castile Simulation and CCA.....	82
8.1. Areal Extent of Known Potash Reserves from the BLM Map.....	85
8.2. Flowchart of SECOFL2D Simulations.....	86
8.3. Regional Flow Contours of Vector 11. Left) CCA and Right) MM Scenario.....	88
8.4. Regional Flow Contours of Vector 62. Left) CCA and Right) MM Scenario.....	88
8.5. Transmissivity Field (Log <sub>10</sub> m <sup>2</sup> /s) of Vector 62.....	89
8.6. Velocity Profile of Vector 62 on Local Grid. Top) CCA and Bottom) MM Scenario.....	90

8.7. Left) Plutonium Fractional Discharge across the LWB for Chapter 6 Results (Full Mining) and MM Scenario with both having 1% of the Initial Mass with a $K_d=0$ (ml/g). Right) Frequency Distribution of Both Mining Scenarios for Vectors with Significant Discharge across the LWB.....	91
8.8. Discharge in EPA Units at 10,000 Years from CCA NUTS Concentrations for the Results Presented in Chapter 6 and MM Scenario. Left) Scenario 2 and Right) Scenario 3.....	92
8.9. Discharge of Uranium across the LWB for MM Scenario for LHS Generated $K_d$ s.....	93
8.10. Uranium Isopleths for Vector 62 with Retardation of 2.0, MM Scenario.....	94
8.11. Integrated Discharge of Mass Across the LWB from 0 to 100,000 Years, with Blowout Section from 0 to 10,000 Years.....	95
8.12. CCDF Curves for Overall Mean Releases from Culebra, Comparing Modified Mining to CCA Mining.....	96
9.1. Verification of Typical Case presented in Hansen et al. (1997) for Left) Mud Column Acceleration, Middle) Mud Column Velocity, and Right) Bottomhole Pressure.....	105
9.2. Contiguous Tensile Radial Failure and Mud Motion Velocity vs. Time for Base Case at Late Times.....	106
9.3. Pressure Distribution Through the Repository After Intrusion.....	107
9.4. Contiguous Failed Volume as a Function of Increasing Waste Permeability for Different Waste Strengths.....	110
9.5. Left) Tensile Failed Volume as a Function of Mud Column Density for Different Waste Strengths Right) Mud Column Motion as a Function of Mud Column Density.....	113
9.6. Porosity Versus Pressure Profiles for Undisturbed Scenarios of the CCA.....	114
10.1. Flowchart for NUTS Time Intrusion Calculations.....	120
10.2. Overall Mean of Normalized Releases for Modeling of Increased Solubilities Using Nesquehonite and 'No Backfill' Values Compared to CCA Values.....	121
10.3. Overall Mean from all Release Mechanisms for Solubility Modeling with Nesquehonite.....	122
10.4. Nesquehonite Solubility Calculations Combined with Culebra Transport Calculations from Chapters 6 and 8.....	123



## EXECUTIVE SUMMARY

### Introduction

The sensitivity of the performance assessment calculations in the Department of Energy's (DOE) Waste Isolation Pilot Plant (WIPP) Compliance Certification Application (CCA) (U.S. DOE 1996) was first investigated by Helton (1996) in order to understand the impact of several key parameters. His analysis used scatter plots and stepwise correlations to determine consistency among repository parameters. However, his analysis only applied to the actual range and distributions of sampled parameters used in the CCA calculations. Changes to either the range or distribution of one parameter may strongly affect the importance of other parameters, because estimates of releases vary by orders of magnitude for different combinations of parameter values. A case in point is the brine reservoir compressibility, which has been determined to have insignificant influence on the total release. The values chosen for brine reservoir pressure and volume used in the CCA calculations reduced the importance of the brine reservoir on the calculated releases, therefore eliminating the compressibility. It is entirely possible that this brine reservoir parameter would be one of the most important contributors to large releases in calculations using more appropriate brine reservoir parameter values of pressure and volume.

The scope of the sensitivity analysis performed by Helton (1996) prompted the Environmental Evaluation Group (EEG) to conduct an independent analysis, by changing selected values or the range of selected values that were used in the CCA. This type of sensitivity analysis would distinguish the important parameters of repository performance, while testing the robustness of the codes involved. The analysis also allowed for the testing of the limit to which the disposal system would fail under extreme conditions. This is also useful in characterizing the important parameters.

### Borehole Intrusion Rate

The consequence of future human intrusion scenarios into the WIPP was investigated in the CCA, as required by EPA in 40 CFR Part 194 (U.S. EPA 1996b), and included the possibility of mining and deep and shallow drilling for resources.

The 40 CFR Part 194.33 criteria state that the likelihood of a drilling intrusion into the Delaware Basin be calculated by considering the frequency of drilling over the past 100 years for all resources and that rate be used for the 10,000 year future of the WIPP. A total of 46.8 boreholes per km<sup>2</sup> per 10,000 years were estimated based on past drilling of resources at depths greater than 655 meters (2150 feet), which equal 10,804 boreholes per century in 23,102.1 km<sup>2</sup> (area of Delaware Basin).

The above drill intrusion rate for the 10,000 year future of the WIPP was used by DOE in the CCDFGF model. Due to the uncertainty in predicting future human activities, the effect of altering this rate on the CCA calculations has been assessed in this report.

The modeling associated with an increased borehole rate shows that a factor of approximately 23 is needed to reach the U.S. Environmental Protection Agency (EPA) release limit at a probability of  $10^{-1}$  from values used in the CCA. The overall mean for the highest release tested at 0.468 boreholes/km<sup>2</sup>/yr exceeds 10 EPA Unit limit at the  $10^{-3}$  probability on the CCDF curve. This high rate of bore hole intrusion, however, does not seem to be likely, as the number of boreholes drilled in the Basin in 10,000 years would have to exceed one million per century, or 4,680 boreholes per km<sup>2</sup> per 10<sup>4</sup> years.

### **Probability of Brine Encounter at WIPP**

The probability of encountering brine at the WIPP from an intrusion into a Castile brine reservoir is uncertain. The parameter describing the probability was set to 8% in the CCA, and changed to a range of probabilities from 1% to 60% in the EPA's Performance Assessment Verification Test (PAVT). Since the extent of the reservoir beneath the WIPP is unknown, the influence of this parameter was tested at higher values at 50% and 100%. These values were based on the potential that the Castile brine reservoir encountered by WIPP-12 (Chaturvedi et al. 1997) extends below the waste area.

The modeling presented in this report only compared CCA release values to the proposed higher probability of encounter, and found the parameter to be unimportant in the CCA. The increase in releases from the 8% to 100% was only 0.1 EPA units (35 Ci). However, the synergistic effect of changing multiple parameters, especially those that affect a Castile brine reservoir directly (pressure, volume, rock compressibility, etc.) may have a more profound result on the calculations, though these changes would have to result in releases of at least 1 EPA unit to significantly impact the CCDFs.

### **Castile Brine Reservoir Parameters**

A pressurized Castile brine reservoir that may underly the WIPP has been the subject of many controversies on its extent and importance (EEG 1997b; EEG 1997d; Silva 1994; U.S. DOE 1997a; Beauheim 1997). The scientists who conducted the performance assessment calculations of the CCA recognized the fact that the brine could play a significant role in the degradation of wastes and waste containers, if an inadvertent drilling intrusion were to pass through the repository to the brine pockets below, by assigning two of the six scenarios to



calculate the effects of the breach. However, reservoir parameters used in the CCA were derived from borehole information that are mainly outside the domain of the WIPP repository. The borehole distances ranged from 3.75 miles to over 11 miles from the repository center. New values were assigned to several parameters that describe a Castile brine reservoir based on WIPP-12 data that is more closely identified to the conditions at the repository. The WIPP-12 borehole was originally drilled in 1978 and deepened in 1981. After brine was encountered at WIPP-12, EEG recommended that the site be relocated to the south and DOE concurred. Brine flow occurred when coring reached a depth of 3012 feet (D'Appolonia 1982). While extending the borehole to depths greater than 3900 feet, a total of 80,000 barrels were allowed to flow from the borehole.

The parameters associated with describing a Castile brine reservoir include reservoir volume, rock compressibility, reservoir pressure, and permeability. Assuming an inadvertent human intrusion, modeling of these parameters began with the two-phase flow code, BRAGFLO, and ended with calculations of solid and liquid waste released to the accessible environment. The outcome showed that there is no significant change in releases for the CCDF due to small changes in the reservoir parameters. However, it is expected that the CCDF curve would move closer to the EPA limit if the solubility of actinides in brine were increased above that assumed in the CCA and PAVT.

### **Solubility Modeling of Actinides**

For brine to escape the repository and travel upwards through the borehole under blowout conditions, 1) pressures must be significant to overcome the hydrostatic force of the drilling fluid, and 2) sufficient brine must be available for transport. Both conditions have been met in many of the realizations in the performance assessment calculations of the CCA. However, due to the proposed low solubility of actinides in brine, the consequence of a direct release of brine to the surface was minimal. For example, the mean release of radionuclides in the CCA through a direct brine release was 0.04 EPA Units (14 Ci) at the  $10^{-3}$  probability, compared to spillings or cuttings and cavings, each having releases of 0.2 EPA Units (70 Ci).

The physical and chemical characteristics of the repository used in the CCA were questioned by the EPA. The EPA changed several disposal system parameters to test their range of uncertainty. Using EPA's values, DOE reran the calculations for the Performance Assessment Verification Test (PAVT). Some of the changes involved the solubility of the actinides in a brine solution assuming a different speciation of minerals associated with the MgO backfill material, which lowered the median solubility limit for most actinides. The new set of solubility values came from the same FMT code used to establish the original set of numbers. No new

experiments were conducted to verify any of the values.

The results of the PAVT showed a large overall increase in the amount of brine brought to the surface upon intrusion, yet only nominal increase in release of actinides. This was expected, since the median solubilities decreased by as much as 2 orders of magnitude for the +4 radionuclides. The effect on compliance from the changes shifted the CCDF for the direct brine release scenario closer to the compliance limit by 0.15 EPA Units. The changes in consequence are minimal, since 10 EPA Units of release are needed to fail compliance at the  $10^{-3}$  probability.

Based on the observations of Reed et al. (1994; 1996) and Rao (1996), EEG questioned the CCA assumption that plutonium would exist only in +3 and +4 oxidation states. Hence, EEG conducted bounding calculations on solubility. The solubility values were only nominal increases above the CCA values for plutonium in the +3 or +4 oxidation state for Salado Brine, but upwards of 10000 for Castile Brine.

The results of the EEG modeling showed that increases in solubility using CCA brine release volumes had limited effect on compliance with an overall increase on the mean CCDFs by 0.09 EPA Units. Even when the solubility was increased to absurdly high values, the maximum release was limited by the availability of the actinide source. At a solubility of  $8 \times 10^{-3}$  M (compared to the CCA's  $4.4 \times 10^{-6}$  M for Pu+4 in Salado Brine), the overall mean for direct brine release was increased from 0.04 to 1.3 EPA Units.

The second set of EEG modeling experiments changed the solubilities of actinides in several mineral species of MgO between the conversion of brucite to magnesite. Calculations by Novak (1997) estimated solubility values for the major oxidation states (III, IV, V, and VI) at WIPP in the presence of magnesite, nesquehonite, hydromagnesite, and no backfill. The release calculations of the CCA assumed the long-term mineral species for MgO to be magnesite, and the PAVT assumed hydromagnesite. Yet, laboratory experiments could not prove the existence of either, and only showed hydromagnesite-like or proto hydromagnesite (Papenguth et al. 1997). These other mineral species looked more like nesquehonite (Neill et al. 1998), making it arduous to justify either mineral phase assumed by the DOE and EPA.

Bounding calculations were performed on conditions resulting in the highest solubilities in the repository. These included nesquehonite and no backfill. For the nesquehonite simulations, it was assumed that the mineral would persist for the entire proposed history of the repository. Only median solubility values were used, as opposed to the CCA, which generated a set of expected values from a range of -2 to +1.4 orders of magnitude from the median to capture the

uncertainty. The assumption that the intermediate species being long-lived is an overestimate on the expected conditions, and the EEG does not suggest that MgO not be used as a backfill material. The models were established to better understand the performance of the repository.

Table Ex-1 shows the solubility factors used to achieve solubility values from Novak (1997). The values have been log transformed for use in the input files to change the values that were established in the CCA. For example, SOLAM3-SOLCIM for nesquehonite increases the solubility of Am+3 in Castile Brine by 1.516 orders of magnitude, whereas SOLAM3-SOLSIM decreases the solubility by 0.277 orders of magnitude. The changes were made in the source term files, for the running of PANEL and NUTS.

In addition to solubility changes from the CCA, the Salado flow files from the PAVT were used for transport calculations of NUTS and PANEL. The PAVT calculations exhibited higher repository pressures, hence larger direct brine releases upon intrusion. The maximum effect would be noticed with both changes together.

Table Ex-1 shows that the solubility of the +4 actinides (Pu+4, U+4, and Th+4) in the presence of nesquehonite is higher than without any MgO backfill. This would suggest that the scenario with backfill has larger releases than without.

Figure Ex-1 shows the overall mean of all processes combined as they relate to compliance. In addition, the PAVT direct brine releases were run with the slightly higher CCA solubilities. The most distinct feature of the figure is the shoulder of the high solubility models that extend below the  $10^{-1}$  probability limit. The “shouldering” is the effect of increased releases due to the direct brine release. Since the Pu+4 and Th+4 (although minor) solubilities increased over 5 orders of magnitude, the release due to this mechanism is expected to increase significantly as well. For example, the CCA median value for +4 actinide solubilities in Castile brine was  $6 \times 10^{-9}$  M. If one assumes  $100 \text{ m}^3$  of  $\text{Pu}^{239}$  contaminated brine, then it is expected that the release is  $2.5 \times 10^{-5}$  EPA Units. If the solubility is increased by  $10^{5.23}$  as seen in Table Ex-1, then it is expected that 4.24

	nesquehonite		No Backfill	
	SOLCIM	SOLSIM	SOLCIM	SOLSIM
SOLAM3	1.51616	-.27709	4.48678	3.83714
SOLPU3	1.51616	-.27709	4.48678	3.83714
SOLPU4	5.23242	2.15588	4.06695	2.05552
SOLU4	N/A	2.15588	N/A	2.05552
SOLU6	0.95861	0.96357	0.95861	0.96357
SOLTH4	5.23242	2.15588	4.06695	2.05552

Table Ex-1. Solubility Factors for SOLCIM and SOLSIM

EPA Units are released to the accessible environment. Therefore, the CCDF for higher solubilities would be closer to the EPA limit.

The consequences of higher solubilities, as seen in Figure Ex-1 are quite high. The overall mean release for the CCA and PAVT were 0.2 and 0.4 EPA Units at  $10^{-3}$  probability, respectively. The overall mean for the increased solubilities of nesquehonite and 'no backfill' are 6.0 and 8.0 EPA Units at the  $10^{-3}$  probability, respectively. The limit for compliance, according to 40 CFR Part 194 is 10 EPA Units. While these calculations, based on DOE's own solubility values, do not violate the containment requirements, they show that there is little margin for error.

### **Flow and Transport Modeling within the Culebra**

The transport of radionuclides to the accessible environment can happen two ways: upwards from the repository through a borehole to the surface into the biosphere, or laterally through the stratigraphy of highly conductive layers across the Land Withdrawal Boundary (LWB). The second method was investigated by modeling the Culebra aquifer. The CCA and PAVT include Culebra modeling and its consequence of transport across the LWB in the CCDF curves. The CCA showed only 1 of 300 realizations to cross the boundary in 10000 years with the PAVT showing a significantly higher impact on the Culebra. The end result of increased transport across the LWB in the PAVT had little to no overall effect on the CCDF.

The EEG's concern in the Culebra modeling began with the parameter assumptions that describe actinide behavior with the Culebra Dolomite. When the actinides migrate along flow paths after a release to the Culebra, the transport will be retarded by the interaction of the actinides with the Culebra dolomite matrix. The interaction is known as sorption. The Culebra was characterized as having a linear isotherm with the actinides, and the parameters of the isotherm, known as the partition or distribution coefficient ( $K_d$ ) were measured or inferred from laboratory experiments.

The same oxidation state analogy used for solubility was applied to the distribution coefficient; same oxidation states would exhibit similar values. Therefore, many of the actinides'  $K_d$ s were not actually measured and it is not clear what the consequence would have been with directly measured values. Though it is well known that high  $K_d$  values will retard the actinide species sufficiently to inhibit transport, it is the low  $K_d$  values that are of concern. For example, it was shown in Blaine (1997) that  $K_d$  values higher than 3 ml/g for most actinides would sufficiently retard transport. Only one actinide in the PAVT, U+6, has  $K_d$  values as low as 2 ml/g.

Some waste constituents in the inventory at WIPP may bind to the actinides and further lower

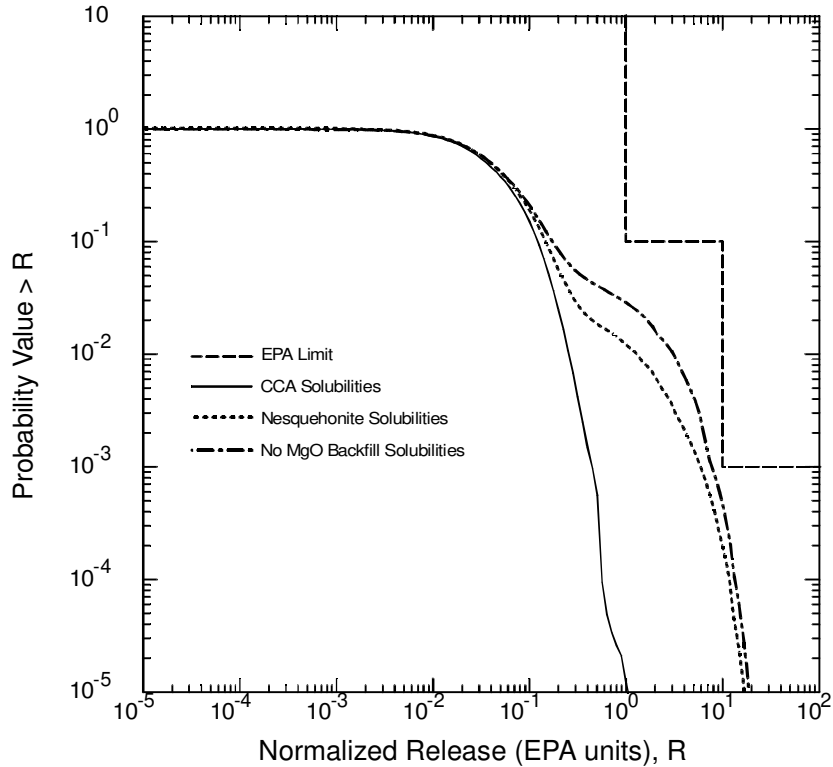


Figure Ex-1. Overall Mean of Normalized Releases for Modeling of Increased Solubilities using Nesquehonite and 'No Backfill' Values Compared to CCA Values

the  $K_d$  values. EDTA, for example, is used in industry for chelation with plutonium for quick cleanup. Other organic ligands in the waste will have similar effect. Furthermore, the lack of  $K_d$  measurements decrease the confidence in values used in the CCA and PAVT, and this prompted the EEG to continue with additional calculations, testing the effects of lowered  $K_d$ s on the disposal system and compliance.

The interaction between releases from the repository and transport of actinides require a lengthy discussion, and will not be discussed here. It is possible, due to the set up of the codes, to do calculations that assume any percentage of the actinide's mass to completely bind with EDTA and migrate unretarded through the Culebra matrix. Therefore, additional calculations were performed assuming 1% of Pu (+3 and +4) having a  $K_d=0$  ml/g.

The results of the calculations show that the overall mean of the releases through the Culebra was 0.0001 EPA Units at the  $10^{-3}$  probability. Since a large number of realizations crossed the LWB with significant releases, it was reasoned that the mass of radionuclides reaching the Culebra was the limiting factor. This was proved when the models of higher solubility were combined with transport modeling, and the overall mean for release from the Culebra was

increased to 0.31 EPA Units.

Another model was proposed by EEG in which the extent of potash mining within the controlled area (or Land Withdrawal Area-LWA) was extended to include lower grade potash ore. Potash mining occurs in the McNutt Potash Zone of the Salado, and is several hundred feet below the Culebra. The effect of potash mining in the Delaware Basin would cause subsidence to the overlying units, and hence have a possible detrimental consequence from increased transport of radionuclides. The EPA established the criteria for the mining by assigning a multiplying factor to the transmissivities of the Culebra, which increased the velocities in the mined region.

The extent of mining in the long-term future is debatable, depending on assumed future economic viability of the resource. New methods such as solution mining could extract lower grade minerals more readily. Therefore, the EEG included a larger area of potential mining in a new flow model, yet keeping the same parameter changes that were used in the CCA. It is feasible to change other parameters or include new ones, but due to the limited time available, was not thoroughly investigated.

The results of extending the areal minable region below the Culebra had little to no effect on the transport of radionuclides across the LWB, though it did change the flow patterns slightly. The limit of transport is sorption, and the PAVT values for  $K_d$  were retained for uranium. The combination of low  $K_d$  and larger mining area was studied with plutonium, again using the 1%  $K_d=0$  ml/g. Again, the amount of initial mass injected to the Culebra crossing the LWB was significantly higher, but limited by the amount reaching the Culebra.

Lastly, the effects of extended mining, low  $K_d$ s, and high solubilities were combined in an effort to test the synergistic effect of all the previous results. The overall mean for the release through the Culebra was as high as 1 EPA Unit (or 344 Ci) at a  $10^{-3}$  probability of release. The addition of the Culebra releases to the overall mean of all combined releases moved the CCDF closer to the EPA compliance limit by 12%, but did not show non-compliance.

# **SENSITIVITY ANALYSIS OF PERFORMANCE PARAMETERS USED IN MODELING THE WIPP**

## **1. INTRODUCTION**

The Waste Isolation Pilot Plant (WIPP) is intended to be the first repository for the permanent disposal of defense generated transuranic (TRU) wastes. The WIPP is located in southeastern New Mexico, 655 meters below the surface in the Salado Formation. The containment of transuranic wastes in the ancient salt beds of the Salado *"will result in extremely effective isolation of the radioactive waste"* if the repository is to remain undisturbed for 10,000 years (U.S. DOE 1996). Modeling of this undisturbed scenario encompasses the natural processes such as the salt creep closure of the excavated repository and disturbed rock zones (DRZ) which surround the repository, brine flow into the repository from under- and over-lying formations, and gas generated through degradation of waste and waste containers. The performance assessment of the repository was also required by 40 CFR Part 191 Subpart B (U.S. EPA 1996a) to consider disturbed scenarios by which a breach may occur through inadvertent drilling for resources. The release of radionuclides to the accessible environment during the 10,000 year future of the repository must be quantified to ensure compliance with the requirements stated in 40 CFR Part 191.13 (Containment Requirements). The accessible environment refers to everywhere beyond the controlled boundary, including land, air, and water. The cumulative radionuclide release through a probabilistic performance assessment must fall below specified limits within the time frame designed for containment. The estimate of probabilistic releases through these scenarios was calculated using computer codes designed specifically for the flow and transport of radionuclides through the formations that overlie the WIPP, as well as direct releases to the surface.

### **1.1. Performance Assessment**

The estimated releases from the performance assessment for WIPP were incorporated into probability distributions. One of the requirements used to judge satisfactory performance of the repository is to demonstrate that the calculated releases have a likelihood of less than 1 in 10 to exceed the quantities listed in Table 1.1 (U.S. EPA 1996a), and less than 1 in 1,000 to exceed ten times the quantities in Table 1.1. A performance assessment refers to an analysis that (1) *identifies the process and events that might affect the disposal system, (2) examines the effects of the processes and events on the performance of the system, and (3) estimates the cumulative releases of radionuclides, considering the associated uncertainties, caused by all significant process and events* (U.S. EPA 1996). In addition to the performance assessment of the disposal

Radionuclide	Release (curies) per million curies of alpha-emitting radionuclides
Americium-241, -243	100
Carbon-14	100
Cesium-135, -137	1,000
Iodine-129	100
Neptunium-237	100
Plutonium-238, -239, -240, -242	100
Radium-226	100
Strontium-90	1,000
Technetium-99	10,000
Thorium-230, -232	10
Tin-126	1,000
Uranium-233, -234, -235, -236, -238	100
Other $\alpha$ -emitting radionuclides, half-life > 20 years	100
Other $\alpha$ -emitting radionuclides, half-life < 20 years	1,000

Table 1.1. Release Limits as Stated in 40 CFR Part 191, Subpart B

system, certain assurance requirements were necessary to provide confidence that the containment of TRU wastes will be maintained for 10,000 years as stated in CFR 40 Part 191.13. For example, active institutional controls (AICs) should be exercised for as long as possible after disposal. Active institutional control simply means the maintenance of the site, remediation or cleanup of a release, and monitoring after closure of the repository. These controls can be assessed up to 100 years after disposal, after which passive institutional controls (PICs) will proceed that include markers, public records, and other methods to preserve the knowledge of the dangers of the wastes contained below. Although AICs and PICs are considered part of the assurance requirements, they were included in the containment calculations.

The performance assessment calculations were submitted to the EPA in October 1996 in the form of a Compliance Certification Application (CCA). The CCA was compiled from many years of scientific and engineering investigations, and consists of nine chapters with 58 supporting appendices that reference over 600 professional publications. The CCA also describes the DOE Quality Assurance Program and the results of independent peer reviews.



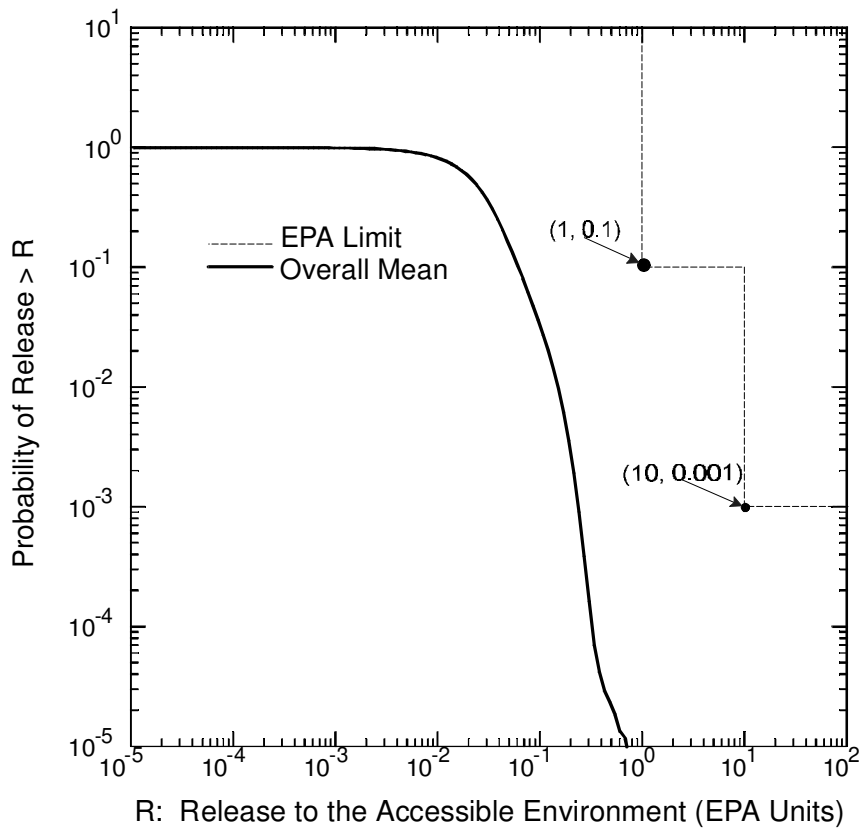


Figure 1.1. DOE's CCDF of Normalized Releases, Showing Overall Mean for all Release Types

The quantitative results from the performance assessment, shown in the CCA, are presented as complementary cumulative distribution functions (CCDFs). To facilitate comparison with 40 CFR Part 191.13, the CCDFs are plotted on a log scale with a probability-of-releases greater than the abscissa value on the ordinate axis, and release to the accessible environment in EPA units on the abscissa. Figure 1.1. shows an example of a constructed CCDF from the performance assessment of the CCA. The curve is an overall mean for all types of releases to the accessible boundary that can occur. A list of these release types are mentioned in the subsequent chapters. The EPA requirements for release, as stated in 40 CFR Part 191, are shown as points, which are the allowable cumulative releases for two probabilities.

The term 'EPA Unit' is used to describe the amount of release compared to the total allowable release limit from Table 1.1. multiplied by a waste unit factor. The waste unit factor is defined as the number of  $\alpha$ -emitting TRU radionuclides with half-lives larger than 20 years in millions of curies (U.S. DOE 1996). An estimated 3.44 million curies of waste will be disposed at the WIPP, equating to a waste unit factor of 3.44. The total number of curies allowed to be released for any

one radionuclide is 3.44 multiplied by 100. Therefore, the total number of EPA units of americium-241 is 1420, assuming an inventory of  $4.88 \times 10^5$  curies postclosure. The sum of releases in EPA units is expressed by

$$R_j = \left( \frac{1}{f_w} \right) \sum_{i=1}^n \frac{Q_{ij}}{L_i}$$

where  $R_j$  is the release under scenario  $j$ ,  $f_w$  is the waste unit factor,  $Q_{ij}$  is the cumulative release for radionuclide  $i$  under scenario  $j$  for  $n$  scenarios, and  $L_i$  is the EPA release limits from Table 1.1.

## 1.2. Repository Design and Site Characterization

The repository was designed to limit the quantity of TRU wastes from being released to the accessible environment. Long term disposal requires many barriers between the repository and environment, including both natural and engineered. The placement of the repository in the Salado Formation halite is one barrier that is very crucial to containment. The halite beds are stable and exhibit many desirable qualities for encapsulating the buried waste.

The Salado Formation is bound by the Rustler Formation above, and the Castile Formation below. The stratigraphical cross section of the area can be seen in Figure 1.2. The figure is a southwest to northeast cut through the geologic profile and shows the formations associated with the Ochoan series. The Castile is bound on the bottom by the Bell Canyon Formation, which is the first laterally transmissive unit underlying the WIPP. However, for performance assessment calculations, the Bell Canyon was omitted.

### 1.2.1. Castile Formation

The Castile Formation is 425 to 490 meters thick consisting of alternating beds of anhydrite and halite. Pressurized brine occurs in discrete pockets of the upper anhydrite layer. Several exploratory boreholes in the vicinity of the WIPP site have encountered these pressurized brine reservoirs. More than  $12720 \text{ m}^3$  of brine flowed out during deepening of the WIPP-12 borehole 1 km north of the WIPP in 1981 (D'Appolonia 1983). Hydrologic tests estimated the size of the reservoir to be  $2.7 \times 10^6 \text{ m}^3$ . Using a rock compressibility of  $10^{-10} \text{ Pa}^{-1}$ , porosity of 0.008, and a reservoir thickness of 24 meters, the diameter of an assumed cylindrical reservoir encountered by WIPP-12 would be 4 km.

### 1.2.2. Salado Formation

The Salado is the most important geological unit in the disposal system, since the repository is in this formation, and represents the primary natural barriers needed to contain the waste. The Salado is divided into three informal members: the upper, the McNutt Potash Zone and the lower. The thickness of the Salado ranges from a few meters in the eastern part of the Delaware Basin to over 600 meters at the WIPP site. Though the Salado deposits are mainly halite, sulfate minerals form many interbeds in the formation, with the most common being anhydrite, polyhalite, and gypsum. The anhydrite layers are commonly referred to as markerbeds and are numbered sequentially from top to bottom 101 through 144 (MB101 - MB 144). The repository is

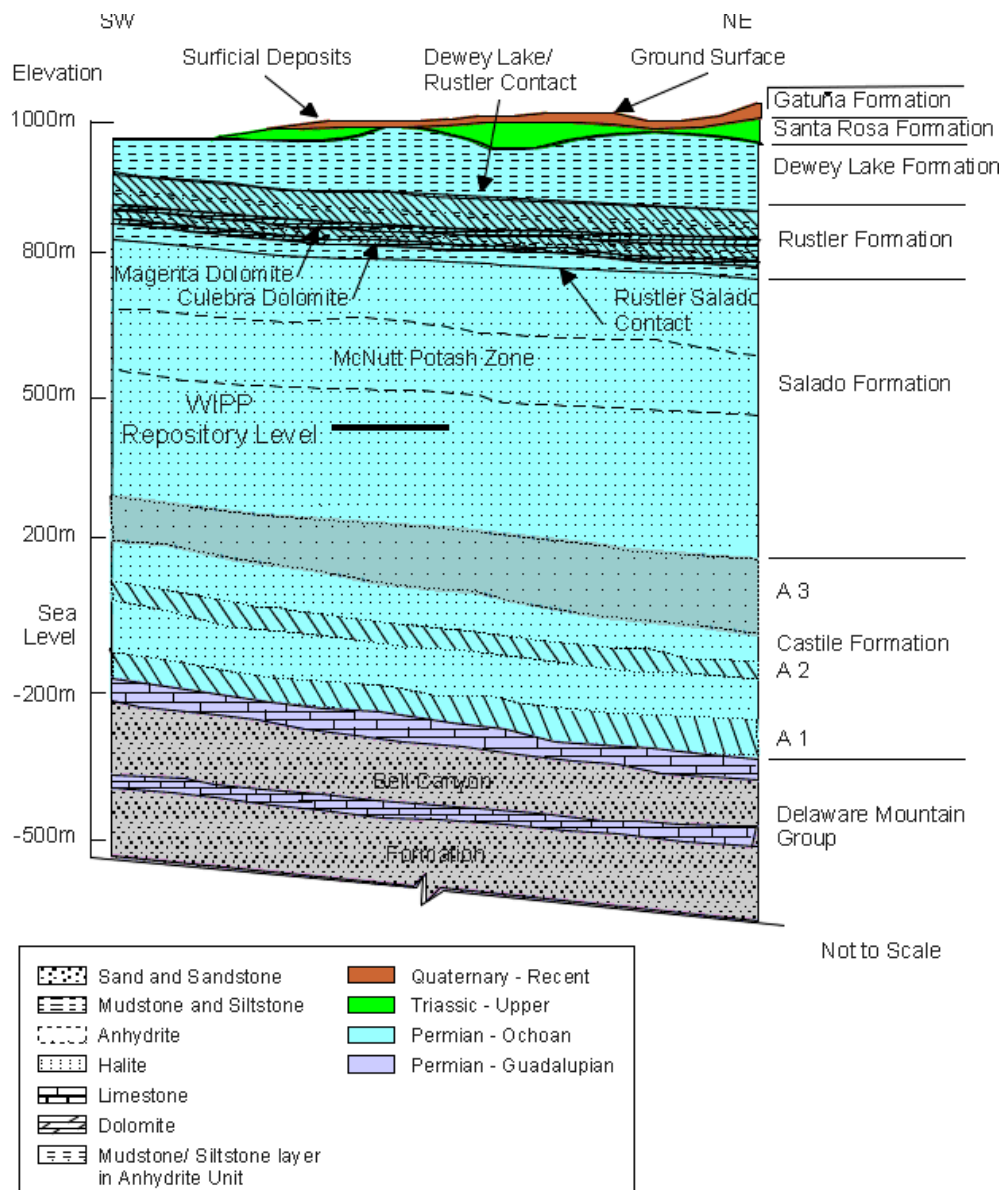


Figure 1.2. Stratigraphic Cross Section of Geologic Region around WIPP (U.S.DOE 1996)

located between MB138 and MB139.

### **1.2.3. Rustler Formation**

The Rustler Formation contains a wide variety of different types of deposits, including anhydrite, halite, carbonate, dolomite, mudstone, and sandstone. Though not as thick as the members below, the Rustler Formation is far more extensive in area. Its thickness ranges between 90 to 107 meters at the WIPP site.

Within the Rustler lies the Culebra Dolomite member, the most hydrologically transmissive unit. It is believed that this member can transport a radionuclide release to the accessible environment in a relatively short period of time upon breaching the repository. The fractured Culebra dolomite aquifer is approximately 11 meters thick at its maximum with a transmissivity up to  $10^{-3}$  m<sup>2</sup>/s. The minimum values for thickness and transmissivity are 4 meters and  $10^{-9}$  m<sup>2</sup>/s, respectively. The hydraulic head in the aquifer ranges from approximately 950 m in the north to less than 900 m in the south, showing a general north to south flow. Tracer tests show that solute travel is mainly through fractures and interconnected vugs, but can also diffuse into the dolomite matrix (U.S. DOE 1996).

Above the Culebra Dolomite lies the Tamarisk, Magenta Dolomite, and Forty-niner Members of the Rustler Formation. The Tamarisk and Forty-niner members vary significantly in composition and are much thicker than the Culebra, ranging from 26 to 56 meters and 13 to 24 meters, respectively (LaVenue et al. 1990). The Magenta Dolomite varies from 7 to 8.5 meters in thickness, is primarily composed of gypsumiferous dolomite, and is also an aquifer, but less transmissive than the Culebra.

### **1.2.4. Dewey Lake Redbeds, Santa Rosa, and Gatuna Formations**

Moving upward in stratigraphic sequence at WIPP, the Dewey Lake Redbeds lie directly above the Rustler. The Dewey Lake Formation is mainly sandstone, siltstone, and claystone. Analysis of the Dewey Lake shows that it is not hydrologically connected to the Rustler, but may actually have lateral water movement (U.S. DOE 1996).

The Santa Rosa and Gutuna Formations lie directly above the Dewey Lake, and are the closest formations to the surface at the WIPP site.

### **1.2.5. The Repository**

The repository was designed to dispose approximately 176,000 m<sup>3</sup> (6.2x10<sup>6</sup> ft<sup>3</sup>) of CH-TRU (contact handled) waste and RH-TRU (remote handled), of which no more than 7080 m<sup>3</sup> (2.5x10<sup>5</sup> ft<sup>3</sup>) can be of RH-TRU waste (U.S. Congress 1992; Silva 1994; U.S. DOE 1990). The waste contains organics such as rubber, plastic, and cloth; metals; and waste sludge. The CH-TRU waste is stored in 55-gallon drums and will be stacked three-high in rooms that are 300 feet long, 33 feet wide, and 13 feet high. The RH-TRU waste containers are 26 inches in diameter and 121 inches long, and will be placed in horizontal holes in the walls of the waste panel rooms.

The rooms are separated by 100 foot thick pillars. The repository consists of eight waste panels with seven rooms in each panel. The waste panels are separated by 60 meters (200 feet) of intact rock. Each room will contain approximately 6000 drums of CH-TRU waste and 50 canisters of RH-TRU waste.

Figure 1.3. shows the configuration of the three main area of the repository: experimental area, operations region, and waste disposal region. The experimental region was used as an area to perform geotechnical evaluations, which consisted of rock mechanics tests, waste package experiments, and brine migration tests. The operations region contains the passages to connect the surface to the waste disposal area. There are four shafts in this area: the waste handling shaft for the transport of personnel and waste to the subsurface, the air intake and exhaust shafts allowing fresh air to the underground and exhaust to leave, and the salt handling shaft for the removal of mined salt.

The waste disposal area contains the eight panels for waste storage. The main north-south and east-west access drifts in this area will also house waste after the main panels are filled and are called panels 9 and 10. The disposal area will be sealed after all panels are filled.

#### **1.2.5.1. Room Collapse and Post Closure**

Once each panel has been filled, they will be sealed to prevent the escape of actinides when the drums begin to fail from the pressures exerted by salt creep from the ceiling, floor and walls. The salt creep will consolidate the drums, producing stress fractures that will ultimately cause the waste to spill out. However, one of the main reasons for choosing salt for disposal was its mechanical response to the overpressures of the rock above. The salt will encapsulate the waste, creating a natural barrier.

The closure process of the salt begins as soon as the rooms are excavated and continues until an equilibrium state of the rock and the waste are reached (Butcher 1997). At equilibrium, the salt deformation ceases, and the waste in the room has undergone all possible compaction. The measure of compaction in the repository is the amount of change in pore volume of the waste, which continues to decrease under pressure. However, it is not likely that the salt surrounding the repository will ever come to a pure equilibrium with the waste. The waste changes form continuously throughout most of the initial time history of the repository and gases are progressively generated from degrading waste. During the time of degrading waste, the repository is expected to make minor readjustments. Waste rooms will continue to deform until all stress gradients vanish.

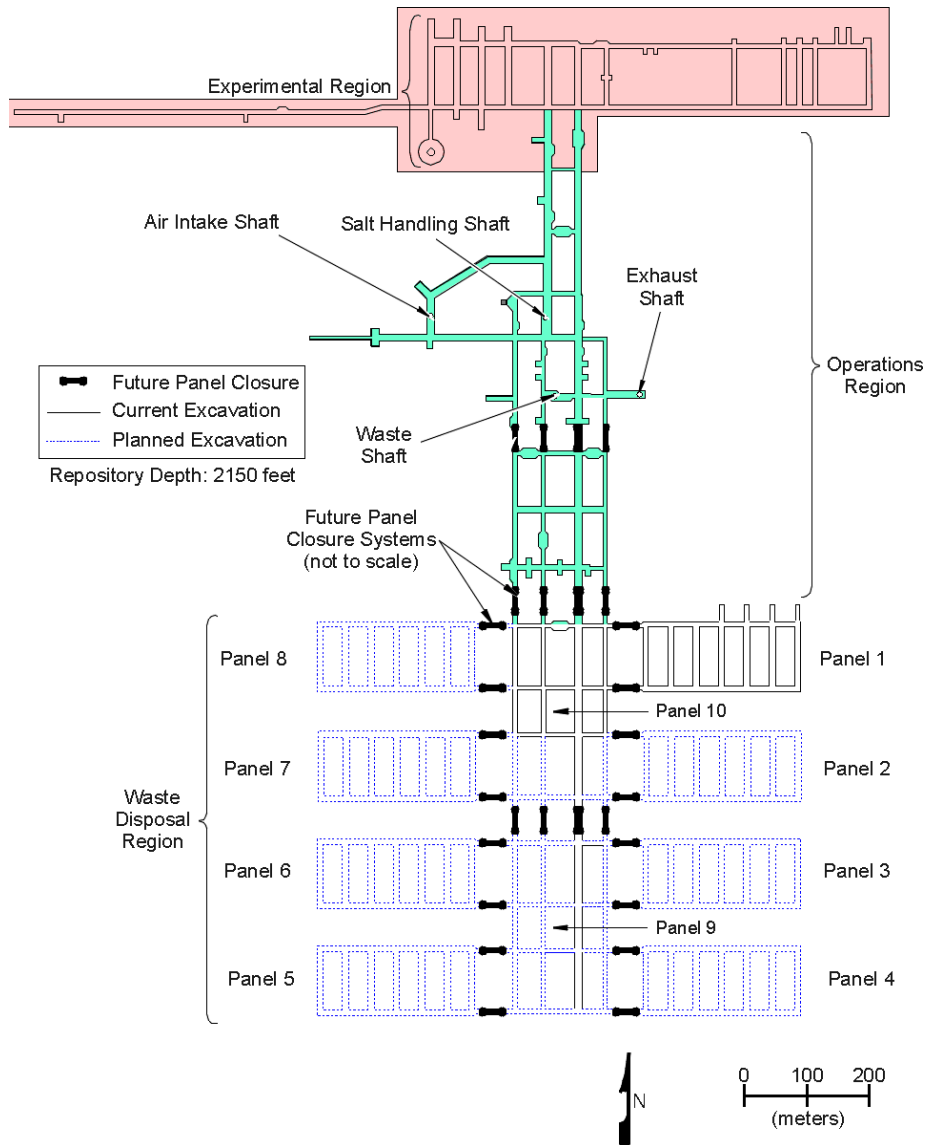


Figure 1.3. Areal View of the Underground WIPP Facility (U.S. DOE 1996)

A computer model was developed (Butcher 1997) to estimate the compaction and decrease in the pore volume of the compacted waste. The initial room height is approximately 4 meters. The drums, stacked three high will be approximately 2.7 meters, leaving 1.3 meters of air space above for the placement of backfill. After consolidation, the room heights will be compacted to roughly 2 meters, and porosity of the waste will decrease from an average of 0.7 to ~0.25.

### **1.2.5.2. Gas Generation and Waste Backfill**

Before sealing, the panel rooms will be backfilled with a buffer to reduce the amount of gas generated from degrading organic material. Several backfill materials have been considered, including bentonite clay, CaO, and MgO. MgO was selected as the backfill material based on its postulated benefits to increase the pH of the repository, which decreases the solubility of the actinides in brine. The cemented MgO, called Sorel cement, will also strengthen the repository waste.

The generation of gases in the repository, if produced in significant quantities, may affect the performance of the WIPP. An increase in CO<sub>2</sub>, for example, will decrease pH and increase the solubility of the actinides in brine. The corrosion of metals and microbial activity are seen as the major contributors of gas generation in the disposal system. A minor source of gas is the radiolysis of water, but is much less a contributor than corrosion or degradation.

The oxic corrosion of metals (iron, aluminum, aluminum-based alloys, and lead) will deplete the rooms of O<sub>2</sub> and water, thus allowing anoxic corrosion to produce large amounts of H<sub>2</sub>. The anoxic corrosion process will consume a large amount of water, depleting brine availability for other processes, such as chemical degradation or physical blowout. The rate of corrosion for metals is dependent on the pressures and quantities of CO<sub>2</sub>, H<sub>2</sub>S, N<sub>2</sub>, and other gases (Telander and Westerman 1996) and is said to vary from 0 to 1.587x10<sup>-14</sup> m of steel per second in the CCA. The values assume no CO<sub>2</sub> present.

Microbial activity from the degradation of cellulose, plastics, and rubbers will consume O<sub>2</sub> and produce CO<sub>2</sub>, N<sub>2</sub>O, N<sub>2</sub>, H<sub>2</sub>S, H<sub>2</sub>, and CH<sub>4</sub> (Brush 1995). The generation of H<sub>2</sub>S is important to corrosion, and experiments have found that steel corrosion will almost cease in H<sub>2</sub>S overpressures, and that Al corrosion was relatively high (Telander and Westerman 1996). The formation of CO<sub>2</sub> from microbial denitrification, sulfate reduction, and methogenesis will decrease the pH, increasing the solubility of the actinides in brine solution. A low pH, with values <6, has been shown to have the highest solubilities, decreasing as pH increases until the pH

reaches 10. When pH is greater than 10, the solubilities are anticipated to increase (U.S. DOE 1996).

The MgO backfill will react with the brine to produce brucite ( $\text{Mg}(\text{OH})_2$ ). Brucite will then react with the  $\text{CO}_2$  to produce magnesite ( $\text{Mg}(\text{CO}_3)$ ), or any mineral species of magnesite (nesquehonite and hydromagnesite). One mole of MgO will react with one mole of water and one mole of carbon dioxide to produce one mole of magnesite. Thus, the one-to-one relationship of carbon dioxide and MgO consumption is important in respect to the amount of MgO needed as backfill to consume the  $\text{CO}_2$ . The CCA estimates that a maximum  $1.4 \times 10^9$  moles of gas will be generated and the DOE has therefore planned to emplace  $1.875 \times 10^9$  moles of MgO (83,150 tons) in the repository.

The effectiveness of the MgO to mix completely with the  $\text{CO}_2$  has invited much debate, and even DOE's own Peer Review Group reassembled on three separate occasions to examine further evidence. Their final report on the subject can be found in Wilson et al. (1997). The EEG also outlined a number of concerns (Neill et al. 1998), including the exact mineral phases of the MgO species that will persist as it forms complex minerals with carbonate.

### **1.2.5.3. Panel Closure**

Figure 1.3. shows the location of plugs for each panel access drifts. The intent of the barriers was not to aid in long term repository performance, but to prevent potentially high levels of unacceptable volatile organic waste from seeping into the operations area (U.S. DOE 1996). The closure system design allows for a two layer protection scheme, which consists of an explosion- (or construction-) isolation wall and a concrete barrier. These barriers are separated by 20 feet of space called the isolation zone.

### **1.2.5.4. Shaft Seals**

The four shafts in the operations region of the repository will be sealed after the decommissioning of the WIPP repository. The sealing allows for additional barriers of isolation from the accessible environment, and are not technically "engineered barriers", since they represent an effort to fix the damage to the natural barriers. The seal will consist of 13 elements, layered throughout the shaft length with the purpose to limit fluid flow in the column with high density/low permeability materials (Sandia 1996). Figure 1.4. shows the layout of the shaft seal system. Some materials that will fill the shaft include: concrete, clay, salt, asphalt, earthen fill, and cementitious grout. The performance assessment calculations included degradation of the materials in the shaft over time.



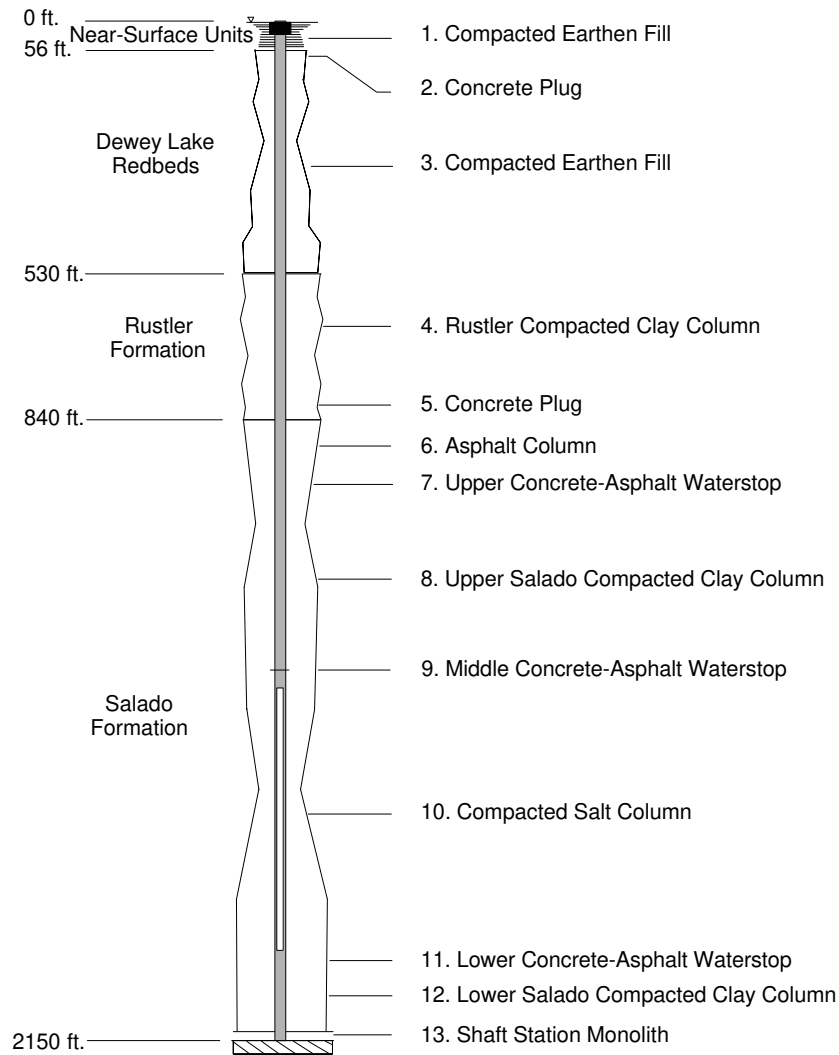


Figure 1.4. Shaft Seal System at the WIPP (Modeled after Figure 4.1 of Sandia 1996)

### 1.2.5.5. Borehole Plugs

The last barrier to be implemented in the repository is the plugging of boreholes, which play a role in projected future human intrusion scenarios. The borehole plugs are expected to reduce the amount of water from overlying formations from entering the repository, and the contaminated brine from escaping to the surface. The DOE plans to use mainly cement or grout with mud and clay, compacted to closely match the physical properties of the surrounding rock. The plug will fill the entire length of the borehole casing.

There are several designs being considered for the borehole plug. These consist of a one-, two-, and three-plug configuration. Based on a survey of current plugging practice, the DOE has assigned probabilities for usage to each configuration and these are incorporated into the

probabilistic modeling of future events. The two-plug configuration is the most common type, with the three-plug being less likely, and the single concrete plug being the least likely to be used.

### **1.2.6. Potential Pathways for Release**

Though there are several safeguards to reduce the possibility of release of radionuclides to the accessible environment, it is not totally improbable that the waste may escape from the disposal system. In undisturbed performance, the radionuclides could be transported through fissures and fractures of the weaker anhydrite units above and below the repository. Marker beds 138 and 139 provide potential pathways for escape, especially when the pressures in the repository reach a level, above lithostatic, that will induce further fracturing. Fluid injection in nearby oil/gas wells for the secondary and tertiary recovery of resources may also induce fracturing at WIPP levels, and possibly leak into the repository (Silva 1996; Bredehoeft 1997a,1997b). However, the probability and consequence of fluid injection has yet to be determined as a possible mechanism for release.

Disturbed performance of the disposal system allows several pathways of release upon breach of the repository. If the repository is sufficiently pressurized, then the blowout of solid waste material may entrain radionuclides, and be brought to the surface via the intruding borehole. Also, a breach of the pressurized repository may bring radionuclides dissolved in contaminated brine up to the hydrologically transmissive units above the repository and possibly to the surface. If contaminated brine reaches the Culebra aquifer, radionuclides may be transported to the accessible environment with the groundwater.

## **1.3 Scope**

A basic understanding of the performance assessment (PA) calculations of the CCA is needed to understand much of the work in this report. The report starts with an overview of the PA, repository design, and site characterization of the WIPP disposal system.

Background is provided to allow the reader to move into a detailed description of the PA presented in Chapter 2. The chapter explains the organization of the PA and how the different mechanisms of flow and transport for release scenarios are split into the computer codes. A discussion of the parameters will be followed by an uncertainty analysis description of the PA.

Chapter 3 discusses EEG's outstanding concerns of the calculations performed in the CCA and the parameters used in modeling. The remaining chapters address the sensitivity of the different parameters. The modeling started simply, investigating less complicated parameters and

models and then moved to more complex scenarios. A summary and conclusion for each model study are presented in the modeling chapters.

## **2. PERFORMANCE ASSESSMENT REVIEW**

To understand the long term behavior characteristics of the disposal system, the probabilities and future occurrences must be determined. A set of scenarios have been analyzed for the potential effect of the repository on the accessible environment. These scenarios have undergone a formal screening by DOE to eliminate features, events, and processes (FEPs) that are unimportant to the performance of the disposal system. The scenarios are based on the FEPs that are predicted to be both potentially likely and have significant consequence, and categorized as having an influence on either the undisturbed or disturbed performance of the repository.

The purpose of FEPs screening is to identify those FEPs that need not be included in the PA calculations based on either low probability, or low consequence, or regulations. A FEP was screened out of inclusion based on probability when it is expected that there is less than one chance in 10,000 that the event or processes will occur in 10,000 years. A FEP may also be excluded if the consequence to the overall calculations of the CCDFs are less than  $10^{-4}$  EPA units. In addition EPA promulgated criteria to allow for certain human initiated events to be eliminated from consideration (tunneling, excavation, deliberate drilling, fluid injection for resource recovery, etc.).

### **2.1. Scenarios of the Performance Assessment**

#### **2.1.1. Undisturbed Performance**

Undisturbed performance, as stated in the 40 CFR 191.12, is defined as *“the predicted behavior of a disposal system, including consideration of the uncertainties in predicted behavior, if the disposal system is not disrupted by human intrusion or the occurrence of unlikely natural events”*. The undisturbed scenario forms the base case for PA calculations and includes only natural events and human influences that do not affect the repository directly. Some low probability FEPs that were screened out are regional tectonics, fault movement, seismic activity, and volcanic activity.

#### **2.1.2. Disturbed Performance - Human Intrusion**

The disturbed performance of the repository must include human initiated events as stated in the 40 CFR Part 194. However, there are only two disturbed events that were considered for the long term performance of the repository: deep drilling (E), and mining (M) with all others being screened out. The drilling events were subcategorized into two scenarios, one for drilling only into the repository waste panels (E2), and the other for drilling through the waste panel into the

underlying pressurized brine reservoir of the Castile formation (E1). A combination of the two drilling scenarios were also considered, noted as an E1E2 scenario. A third type of drilling, shallow drilling for underground sources of drinking water (E3), was eliminated from the performance assessment calculations based on low probability due to the groundwater being nonpotable in the Culebra Dolomite aquifer.

Mining at the WIPP may occur in combination with drilling (ME1, ME2, ME1E2), potentially producing a more rapid transport to the accessible environment through the Culebra aquifer than drilling alone. The mining for resources, such as potash in the McNutt Potash Zone of the Salado Formation for example, can cause subsidence in layers above the Salado. The subsidence could result in greater fracturing of the Culebra possibly causing faster transport of radionuclides to the accessible environment.

Although the drilling intrusion scenarios were narrowed down to two types, the time at which they can occur during the repository future are too numerous to simulate directly. Over one thousand future drilling times could occur during the life of the repository, requiring unachievable computer time and storage requirements. Therefore, the intrusion times were reduced to two separate times for each of the E1 and E2 intrusion type, and a single, two-time drill intrusion of E1E2 scenario. A total of six scenarios (S1 through S6), including one undisturbed scenario, were created for the performance assessment calculations.

S1 - undisturbed

S2 - E1 at 350 years postclosure

S3 - E1 at 1000 years postclosure

S4 - E2 at 350 years postclosure

S5 - E2 at 1000 years postclosure

S6 - E2 at 800 years followed by an E1 at 2000 years postclosure

The times at which these scenarios occur are mainly used as reference times for additional calculations. The computer models use these reference times to calculate an intermediate step for determining individual futures. The individual futures are then scaled to the 10,000 possible futures during the construction of the CCDFs assuming a linear interpolation between calculated times. However, these interpolations become more complicated as radioactive decay and ingrowth are incorporated into the CCDF. A more detailed description of how the computer models interact and the calculated times for the construction of the CCDFs is described below.

### **2.1.3. Probabilistic Performance Assessment**

The performance of the disposal system was quantified in a probabilistic analysis, in which key parameters for model input were stochastically varied over a wide range of values. The ranges were intended to accommodate the uncertainty in the disposal system and was modeled using codes designed to simulate the transport of radionuclides through the system. The simulations (or realizations) were incorporated into a probabilistic process that determined the average behavior of the repository. Monte Carlo analysis is the general name for the technique used for probabilistic analysis of the WIPP.

A Monte Carlo analysis uses a probabilistic approach on the selection of values from parameter ranges for the input to the models for performance assessment. The chosen values represent one of many in a set of separate calculations (vectors) that are used for the probabilistic assessment. For example, the halite permeability of the Salado Formation around the WIPP was found to vary from  $1 \times 10^{-24} \text{ m}^2$  to  $1 \times 10^{-21} \text{ m}^2$  (U.S. DOE 1996-Appendix PAR). This parameter was assigned a uniform distribution and a set of vectors were created by sampling from the distribution. The vectors were then used as input to the two phase brine and gas flow code, BRAGFLO, to create a set of outputs for the calculation of a distribution function that would best describe the performance of the disposal system. The halite permeability is one of 57 parameters used in the Monte Carlo analysis of the CCA.

## **2.2. Computer Models**

In order to accomplish the numerical modeling of the WIPP repository, several computer codes were written to quantify the long term behavior of the waste disposal. These codes can be broken into several categories with each major code having smaller supporting codes to pre- and post-process data. The major codes include:

- (1) BRAGFLO - Salado Flow
- (2) NUTS and PANEL - Salado Transport
- (3) CUTTINGS - Borehole calculations of cuttings, cavings, and spall
- (4) BRAGFLO\_DBR - Direct brine release from the repository
- (5) SECOFL2D - Culebra Flow
- (6) SECOTP2D - Culebra Transport
- (7) CCDFGF - Probabilistic modeling of the 10000 year future

Figure 2.1. shows the relationships between the codes.

### 2.2.1. BRAGFLO

BRAGFLO (BRine And Gas FLOW) models the processes occurring in the repository and the surrounding rock, including two-phase fluid flow, anhydrite fracturing, and gas generation. These processes are simulated on a simplified two-dimensional, north-south cross-section of the disposal system from the overlying units above the Dewey Lake down to the Castile formation. The geometry of BRAGFLO's irregular grid spans 46,629.88 m in the north-south direction and 939.06 m vertically. The code was used to calculate brine pressure, saturation, and flow over the entire 10,000 year future of the repository for each of the six scenarios.

### 2.2.2. NUTS

NUTS (NUclide Transport System) models the migration rate, distance, concentration, and level of radioactivity of radionuclides transported from the repository to the surrounding formations. The equations are solved on the same grid as used in BRAGFLO using BRAGFLO's brine flow rates, porosities, pressures, and saturation. The NUTS code was used to calculate transport times at 100, 3000, 5000, 7000, and 9000 years postclosure for scenarios S1 through S5.

Of the 33 assumed radionuclides that will be in the WIPP waste, only five lumped isotopes were simulated using NUTS to reduce computer time and memory requirements. The lumped isotopes are assumed to have equivalent decay and transport characteristics of the remaining isotopes, and account for approximately 99% of the activity of radionuclides in the repository. The five lumped isotopes are:  $^{241}\text{Am}$ ,  $^{239}\text{Pu}$ ,  $^{238}\text{Pu}$ ,  $^{234}\text{U}$ ,  $^{230}\text{Th}$ .

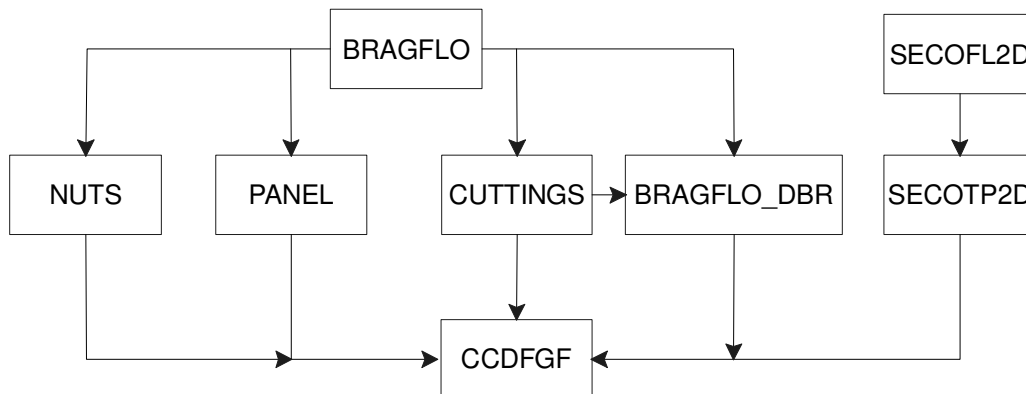


Figure 2.1. Major Codes with Linkages

Computationally, NUTS is a very slow code to run. Therefore, it was first used to simulate a nonreactive passive tracer to test which BRAGFLO flow velocity calculations would transport radioactive isotopes to the accessible environment. Several BRAGFLO simulations were screened out and no longer needed for the calculations. The simulations exhibiting a tracer release and having a mass in excess of  $10^{-7}$  kgs across the accessible environment underwent a complete transport analysis. For the CCA, replicate 1, only one vector was not screened out of the complete analysis for Scenario 1, 23 for S2, 21 for S3, 6 for S4, and 6 for S5. Thus, only 57 out of 500 vectors were needed for running the NUTS simulations.

The complete analysis included an 'isotope' simulation and a 'time shifted' simulation on the unscreened vectors. The isotope simulation establishes the transport of an undisturbed performance. The isotope simulation results are then used as input for the time shifted calculations at 100, 3000, 5000, 7000, and 9000 years post closure.

### **2.2.3. PANEL**

PANEL calculates the "*mobilized radioactive load in the brine phase of the brine/gas mixture that seeps or flows through the repository's decommissioned waste panels*" (U.S. DOE 1996-Appendix PANEL). Simply, PANEL was used to model the release of radionuclides in a direct brine release scenario to the surface and to model the upper bound of long term releases to the Culebra in the S6 scenario. The times at which PANEL was calculated were 100, 350, 1,000, 4,000, 6,000, and 9,000 years post closure.

PANEL uses BRAGFLO's information, much like NUTS, on a more simplified scale. PANEL represents each waste room as a well mixed grid cell, and solves integrated analytical equations with 50 year time stepping. PANEL simulated the release of 21 of the 33 isotopes from the repository in less time than the NUTS simulation of 5 isotopes.

### **2.2.4. CUTTINGS\_S**

CUTTINGS\_S calculates the cuttings, cavings, and spallings from an intrusion borehole through the disposal system. CUTTINGS\_S receives its initial and boundary conditions from BRAGFLO and can simulate the effects of multiple boreholes. BRAGFLO also provides repository pore pressures, saturations, and porosities for solid removal calculations.

The cuttings and cavings portion of the code models the direct removal of wastes brought to the surface by the drilling cooling liquid (usually a mud brine) and is the sum of the material cut by the drill bit and eroded material. The eroded material is a function of fluid shear stress acting on



the borehole wall and the strength of the waste.

The third type of removal of wastes calculated by CUTTINGS\_S is through the process of spall. If the repository is significantly pressurized (above hydrostatic), then a portion of the solid waste could be forced to separate from the bulk mass of waste inward toward the borehole by high pressures in the repository. The amount of spillings removed is dependent upon the waste shear strength and permeability. If the permeability is too low, then it is assumed that the flow of gas to the borehole is too slow to cause a waste blowout up the borehole. Berglund (1994) identified the "threshold" permeability at  $10^{-16} \text{ m}^2$ , below which the blowout would cease. The CCA used a value of  $1.7 \times 10^{-13} \text{ m}^2$  for waste permeability in the repository after compaction. For a comparison of the significance of spillings, the maximum release due to spalling calculated in the performance assessment was  $4.0 \text{ m}^3$  with a maximum release of  $3.0 \text{ m}^3$  for cuttings and cavings combined.

The scenarios of S1 through S5 were used to calculate borehole times other than those specified in Section 2.1.2. The results of pressures and saturations from the undisturbed scenario (S1) were used as the initial conditions for a first time borehole intrusion at 100, 350, 1000, 3000, 5000, and 10000 years. The CUTTINGS\_S simulations for scenarios S2 through S5 were like the S6 scenario (E1E2), and the initial intrusion at either 350 or 1000 years in the BRAGFLO calculations was used to calculate conditions at 550, 750, 1200, 1400, 2000, 3000, 4000, 5000, and 10000 years.

The spillings portion of the CUTTINGS\_S was deemed inadequate by the Conceptual Models Peer Review Committee. The peer review (U.S. DOE 1996-Appendix Peer1) reported on the uncertainty in the conceptual model and its inadequacy to calculate the channel flow of waste to the borehole. However, with additional calculations of another spillings code, the spilled releases of the CCA were considered reasonable by the Peer Review Committee (Wilson et al. 1997). Based on a semi-analytical model of spall (Hansen et al. 1997) which calculated a maximum release of  $0.25 \text{ m}^3$  at repository pressures of 14.8 MPa, the CCA values of 0.5 to  $4.0 \text{ m}^3$  were accepted by the committee. Chapter 9 of this reports explains this new model and some problems associated with the analysis.

### **2.2.5 BRAGFLO\_DBR**

BRAGFLO\_DBR (BRine And Gas FLOW, Direct Brine Release) calculates the brine released from an intrusion borehole through the repository. The released brine was not assessed in the CUTTINGS code, as that code only calculated the solids removed during drilling. For a direct

brine release to occur, certain conditions must exist in the repository. The repository pressure must be above 8 MPa. This pressure is the hydrostatic pressure at the depth of the repository, which accounts for the column of mud in the borehole that the waste brine must overcome and the frictional forces in the borehole. There must also be enough mobile brine present in the waste panels to flow up the borehole to the surface.

The BRAGFLO\_DBR uses the BRAGFLO code, converted to a repository scale model. The model is set up on an areal, two-dimensional grid. The direct brine release can occur at any time during the 10000 year period of the repository, and the saturation and pressure history from the S1 to S5 BRAGFLO calculations are used as initial and boundary conditions. The code calculates a brine release that lasts between 3 and 11 days.

Intrusion times, other than that specified for the different scenarios, were calculated in the same way that CUTTINGS\_S intrusion times were calculated. The BRAGFLO intrusion times at 350 or 1000 years postclosure for either an E1 or E2 intrusion were used to establish initial conditions for a direct brine release of a subsequent E2 intrusion at later times. These times correspond with the intrusion times of CUTTINGS\_S.

### **2.2.6. SECOFL2D**

SECOFL2D simulates the single-phase flow of groundwater through the Culebra Dolomite member of the Rustler formation. The Culebra member is of particular importance, since this is the most transmissive unit in the disposal system. Radionuclides released from the repository can be transported up an intrusion borehole into the aquifer and be transported to the accessible environment in a short period of time, relative to other units within the subsurficial disposal system.

The Culebra is considered to be a confined aquifer in steady-state. The equations are solved on two grids, regional and local. The regional domain is solved first for the discrete hydraulic head to be used as boundary conditions on a much smaller, finer local grid. Figure 8.1 of this report shows the regional grid in relation to the Land Withdrawal Boundary (LWB) of the WIPP site.

The effects of potash mining in the McNutt member of the Salado formation is considered in modeling of the Culebra aquifer. The subsidence of the mined area may adversely effect the fractured dolomite, creating even more fractures. To simulate the additional fractures, a scaling factor was used to increase transmissivity in a full and partial mining scenario. The scenarios are based on the extent of allowable mining in the region of the Land Withdrawal Boundary. The

scaling factor was sampled from a uniform distribution for a range of 1 to 1000.

### **2.2.7. SECOTP2D**

The transport of radionuclides through the Culebra Dolomite was accomplished with the code, SECOTP2D. The transport code used the local grid velocities of SECOFL2D to calculate the concentration of the actinide species on a nonuniform grid. SECOTP2D reported the mass of simulated actinides that crossed the Land Withdrawal Boundary through time.

The transport calculations of the radionuclides used in the performance assessment first assumes that the initial mass to be injected into the Culebra will be 1 kg. This is a unit mass, that is coupled with predicted mass that reaches the Culebra through a NUTS calculation. The transport of the same five lumped isotopes of NUTS was also transported in SECOTP2D.

### **2.2.8. CCDFGF**

The results of the numerical simulation from NUTS, PANEL, CUTTINGS\_S, BRAGFLO\_DBR, and SECOTP2D were summarized into tabular form for input to CCDFGF. The NUTS information includes the time integrated discharge of  $^{241}\text{Am}$ ,  $^{239}\text{Pu}$ ,  $^{234}\text{U}$ , and  $^{230}\text{Th}$  up the borehole to the Culebra. The information from PANEL includes the time integrated discharge of  $^{241}\text{Am}$ ,  $^{239}\text{Pu}$ ,  $^{234}\text{U}$ , and  $^{230}\text{Th}$  from the waste panels. The tables from CUTTINGS\_S include the volume of cuttings, cavings, and spallings. The flow of brine up the borehole after intrusion is summed in the tables of BRAGFLO\_DBR, and the time integration of mass across the accessible environment is located in the tables from SECOTP2D. All together, they represent the possible discrete calculations from a breach into the repository, on a purely deterministic basis.

As a final step to the modeling of the disposal system, complementary cumulative distribution functions (CCDFs) were created to represent the probabilistic future of the repository and to calculate the potential cumulative releases. The CCDF is used to compare release limits specified in 40 CFR Part 191. For the CCA performance assessment, there were only three modes that produced nonzero releases to the accessible environment: cuttings and cavings, spallings, and direct brine release. The calculated amount of radionuclides released through the Culebra was considered negligible.

The sequence of future events simulated for the disposal system was generated by the random sampling of eight individual "events" that could occur at the WIPP. Each sequence is given equal weight in the 10,000 possible futures, and are combined with the results of the numerical

simulations. The individual events are (1) the interval time between drilling intrusion, (2) the location of the drilling intrusions, (3) the drill bit diameter used for drilling intrusion, (4) range of borehole permeabilities, (5) the activity of the waste penetrated by a drill intrusion, (6) the borehole plug configuration, (7) penetration of the Castile brine reservoir, and (8) the occurrence of mining.

Each sampled future requires the determination of a normalized release to the accessible environment. The releases were calculated from the deterministic calculations of the above computer codes. The releases were then scaled and ordered from lowest to highest according to normalized releases. The CCDF is then plotted by summing the probabilities of all futures at a given EPA release limit, with the probabilities of all futures exceeding the summed value. Figure 2.2 shows the individual releases summed to a total release for all pathways, with cuttings and cavings showing the highest releases, spillings, then direct brine release with the least. CCA calculated releases to the accessible environment from transport modeling within the Culebra Dolomite were always less than  $10^6$  EPA Units.

### **2.3. Parameters**

The complexity of the disposal system required the use of computational models to quantify the effects of scenarios in the performance assessment calculations. The computer codes required specific information about the initial and boundary conditions and the parameters needed to quantify the physical system. The parameters were obtained from data surveyed through various experiments or observations. However, when no data were available, expert judgement was employed.

A careful distinction is needed between parameters and data. Parameters are based on the supporting data and are values used in the model calculations. Data are commonly spread over a range for a particular observation/experiment, and statistical quantities are used to summarize that range (minimum, maximum, mean, and mode). A distribution type is assigned to the parameter range, and can be either uniform, loguniform, normal, lognormal, cumulative (delta or otherwise specified), student's-T, or triangular.

There are approximately 3500 parameters used in the performance assessment modeling of the WIPP disposal system, 57 of which are not constants. The constants represent one value, whereas nonconstants have an assigned range and distribution type. Of the 57 ranged parameters, 24 have uniform distributions, which suggests the lack of information about the data.

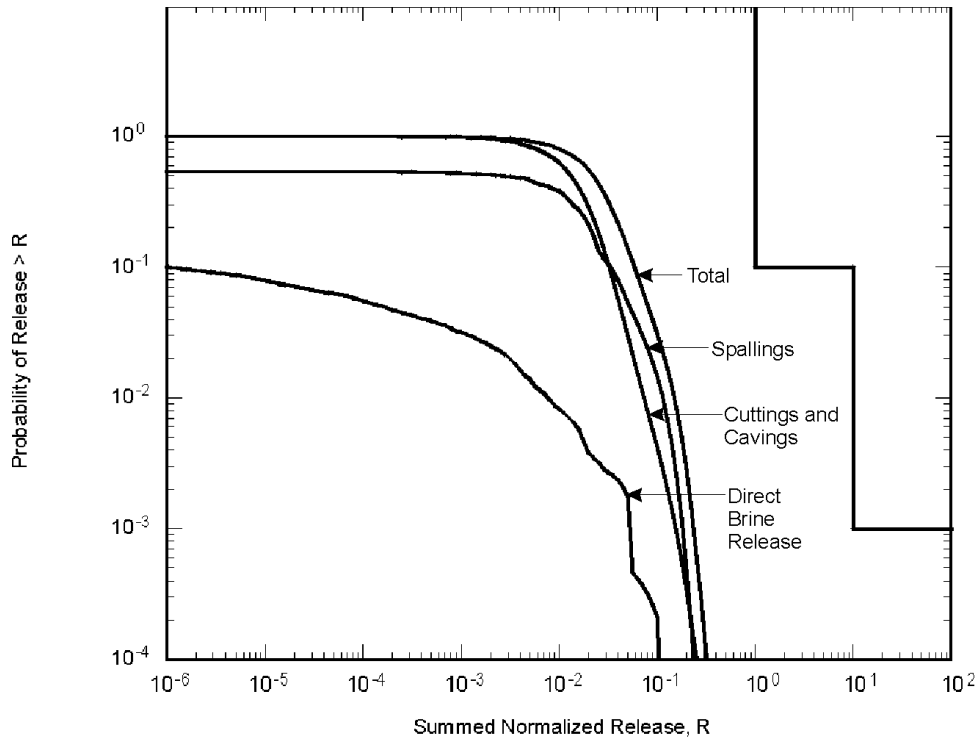


Figure 2.2. Mean CCDFs for Specific Release Modes (U.S. DOE 1996)

A uniform distribution is assigned to a parameter if nothing is known other than its range. However, if the range spanned several orders of magnitude, a loguniform distribution was assigned. This is also equivalent to a uniform distribution applied to a log-scaled parameter.

A range that is representative of a parameter cannot be directly implemented into the computational models. Instead, that range is broken up into several sampled values that fall within the probable range of data, based on the distribution type assigned to that range. For the performance assessment calculations 100 samples were created for each parameter to cover the likelihood of that value existing in the disposal system.

The 5700 total samples were represented by 100 vectors, each with 57 parameters. The vectors were created through the Latin-Hypercube Sampling (LHS) technique. The LHS allows sampling from the outer wings of a distribution with relatively small sample sets, as opposed to other procedures like a strict Monte Carlo method, where sampling is biased more towards higher probability-of-occurrence segments of the distribution. Although the parameters are selected individually through sampling, user-specified correlations are permitted between parameters.

The creation of the LHS sampled vectors uses a random number generated from a seed value

from which the random number generator begins and is specified by the user. The seed value allows duplication of sampled results if the same number is used again for quality assurance measures. For CCA calculations, three separate seed numbers were used to generate three sets of sampled vectors. These are referred to as replicates, and are numbered R1 through R3.

Results of the performance assessment calculations are sensitive to the sampled parameter values. As seen in Figure 2.2, the parameters chosen for the CCA demonstrated compliance of the disposal system. The figure, however, only shows the mean for all individual vectors. Individual CCDF vectors are averaged based on the probability of the parameter occurring during the future of the repository. If only a single vector, for example, were to have parameter values that were to show noncompliance with 40 CFR 191, then that vector could have been averaged out by vectors that show smaller releases. The parameters underwent analyses to test the system and to fully understand the behavior of the repository.

## **2.4. Sensitivity and Uncertainty Analysis of Performance Assessment**

### **Parameters**

The sampling of parameters in the CCA calculations is intended to capture the uncertainty in the understanding of the repository environment and those processes that may occur in the event of human intrusion. The purpose of sensitivity analysis is to determine which of the sampled parameters have the greatest influence on the uncertainty of the calculated release to the accessible environment. The sensitivity analysis is based on the use of statistical manipulations to discover the key dependencies in the CCA calculations. This overview summarizes the major conclusions drawn from the DOE's sensitivity analysis report (Helton 1996).

The sensitivity analysis used stepwise correlations and scatter plots. Stepwise correlation is a powerful tool to rank the relative influence of the various parameters. If only a few parameters are important, and the effect of these parameters is consistent, then the correlations work well. Often, however, the effects of some parameters are not consistent. An example is the influence of corrosion rate on spallings. Pressure tends to increase with corrosion rate. Spallings increases with pressure above 8 MPa, but is insensitive to pressure below 8 MPa. Thus, spallings is only weakly correlated with corrosion rate. Scatter plots are very useful for spotting inconsistent correlations and for revealing large changes in system behavior. Scatter plots, however, can be unreliable in determining relative importance because they are qualitative rather than quantitative. Scatter plots are two or three dimensional plots of points defined by measures of interest and one or two parameters. These allow a visual determination of sensitivities.

One inherent limitation in the sensitivity analysis presented by Helton is that the sensitivity to parameters only applies to the actual range and distributions of sampled parameters used in the CCA calculations. Changes to either the range or distribution of one parameter may strongly effect the importance of other parameters, because release estimates vary by orders of magnitude for different combinations of parameter values. A case in point is the brine reservoir compressibility, which has been determined to have insignificant influence on the total release. The brine reservoir pressure and reservoir volume characteristics used in the CCA calculations reduce the importance of the brine reservoir to the calculated releases. It is entirely possible that the brine reservoir would be one of the most important contributors to large releases in calculations using more appropriate characteristics.

The description that follows refers to sampled vectors and histories. A sampled vector is a single random selection of parameter values used to define the physical characteristics of both the repository and relevant human intrusion processes such as spillings. One hundred vectors were used for one replicate of the calculations. Three replicates were used to demonstrate the stability of the averaged results to different sets of vectors. Describing the results in terms of vectors refers to the six scenario calculations performed at fixed intrusion times for each vector. A time history describes the timing of events such as potash mining and drilling intrusions. Ten thousand time histories were generated and applied to each sample vector. Describing the results in terms of time histories refers to probabilities averaged over either a single replicate or all three replicates. The abscissa of the CCDF curves is the probability of a release magnitude for a single history. The lowest cumulative release probability in any CCDF calculated for the CCA is  $10^{-4}$ , one over 10,000. The mean and percentile cumulative release probabilities can be less than  $10^{-4}$  because of averaging over 100 or 300 sampled vectors.

## **2.4.1. Repository Conditions**

### **2.4.1.1. Repository Pressure**

Repository pressure at the time of intrusion is a critical condition that influences spillings release, direct brine release, and flow to the Culebra. The factors controlling repository pressure are complex and change over time. Prior to an intrusion, the pressure uncertainty is almost entirely controlled by gas generation. After an intrusion, gas flow up the borehole can keep the repository near atmospheric pressure. At high borehole permeability, brine flows down the borehole from the Culebra causing the pressure to eventually reach hydrostatic equilibrium with the Culebra.

By far the most important influence on gas pressure prior to an intrusion is the switch for microbial degradation of cellulose and plastics. Fifty percent of the vectors assume no microbial degradation, twenty-five percent have degradation of cellulose only and twenty-five percent include both cellulose and plastics. Microbial degradation is so fast that it tends to exhaust supplies in less than 1,000 years. Hence, the rate hardly matters and the switch parameter becomes the most important indicator of large releases. The numerical values for this parameter are set to capture a lack of understanding of the possibility of microbial degradation.

Microbial generation produces either 0,  $1.5 \times 10^6$ , or  $4.6 \times 10^6$  moles of gas in the first 1,000 years depending on the microbial generation switch. Steel corrosion generates up to  $7.5 \times 10^6$  moles averaging roughly  $3 \times 10^6$  moles after 10,000 years. If microbial degradation produces gas then the steel corrosion rate is increased by a factor of 13. Steel corrosion is rate-controlled throughout the 10,000 years for slow corrosion rates, but only at early times, first 2,000 to 4,000 years, for microbial enhanced fast rates. This makes the steel corrosion rate the second most important parameter in controlling repository pressure and the third most important parameter in determining overall releases to the accessible environment. The rate of steel corrosion is effected by the height of the capillary rise of brine from the repository floor, which is approximated by a sampled parameter known as “waste wicking”. The waste wicking parameter value is important at early times but less so than the base corrosion rate.

Steel corrosion is dependent on the availability of its two ingredients, steel and brine. Brine is readily available through the 10,000 years with slow corrosion rates. At faster rates the lack of brine inhibits corrosion. The mechanisms controlling brine availability are described later, in order to keep the focus here on gas generation. In one of the undisturbed vectors, and in some 30% of the disturbed cases, steel is exhausted in the lower panel but never in the upper panel. Steel consumption does not appear to be greater as a result of interception of the brine reservoir.

After an intrusion, the borehole permeability effects the flow of gas up the borehole which depressurizes the repository. Only about 10% of the vectors have repository pressures above the critical 8 MPa threshold for more than 2,000 years after a drilling intrusion. Very high permeability almost completely determines the repository pressure at 10,000 years. If the permeability is greater than  $2.5 \times 10^{-12} \text{ m}^2$  then the repository fills with brine and the pressure reaches hydrostatic equilibrium with the Culebra within a few thousand years of the intrusion. If the permeability is slightly less, down to roughly  $2 \times 10^{-12} \text{ m}^2$ , then gas vents to the surface as fast as it is generated, inhibiting brine flow down the borehole and thus holding the repository pressure to near atmospheric. The influence of borehole permeability on post intrusion



pressures causes this parameter to rank sixth in importance to total releases. Even the diminished brine reservoirs of the CCA analysis have a strong effect on repository pressure in the case of a brine reservoir interception.

#### **2.4.1.2. Brine Saturation**

Brine saturation in the repository is important to the direct brine release calculation and to repository pressure through steel corrosion. Unlike pressure, saturation predictions are different between the upper and lower panels of the BRAGFLO model. Brine saturation depends on brine inflow and the consumption of brine by steel corrosion. The brine inflow is less per panel for the upper panels compared to the lower panel. Because the lower panel is down dip it is expected that it would receive more brine inflow. Saturation also depends on gas pressure because the repository swells in response to pressure increases. The upper panel is much less likely to have a saturation that exceeds the sampled residual gas saturation of the waste. Most vectors show brine saturation going to zero in the upper panel over the 10,000 years because of steel corrosion.

#### **2.4.1.3. Brine Flow**

As mentioned earlier, the availability of brine becomes important if the steel corrosion rates are fast. The largest source of brine in early times is the disturbed rock zone (DRZ). This flow averages about 13,000 m<sup>3</sup>, most of which enters the repository in the first thousand years. The DRZ porosity is a function of halite porosity which is a sampled parameter. Halite porosity has the fifth largest correlation with total releases of the 57 sampled parameters. The marker beds contribute an average of 3,000 m<sup>3</sup>. Although one vector produces 70,000 m<sup>3</sup> from the marker beds, less than 10% of the vectors are above 10,000 m<sup>3</sup>. The anhydrite permeability and repository pressures have the greatest impact on brine flow through the marker beds. Anhydrite permeability ranks ninth in importance to total releases.

#### **2.4.2. Cuttings and Cavings**

Cuttings and cavings are the largest releases in most of the generated drilling intrusion histories. Only cavings, not cuttings, is effected by sampled parameters. Cuttings release varies due to the sampling of 569 CH-TRU waste streams or the average RH-TRU radionuclide concentration. Waste stream sampling creates about a three order of magnitude variation in cuttings release per intrusion. Cavings is dependent on the sampled value of waste shear resistance. The volume of cuttings, 0.3 m<sup>3</sup>, plus cavings varies between 0.4 and 3. m<sup>3</sup>.

### **2.4.3. Spallings**

Repository conditions necessary to produce spallings occurs for 80% of the sampled vectors, but spallings only occurs in just over half the time histories. However, spallings along with cavings contribute to the largest release estimates in the CCA. The release estimates from the two mechanisms are roughly equivalent at the critical 10% probability level, as seen in Figure 2.2. The conceptual model uncertainty in the spallings model is enormous. The calculations for a given set of repository conditions could be low by an order of magnitude or more. In addition, the potential influence of repository pressure uncertainty is also enormous. At this time, uncertainty in the spallings conceptual model makes it difficult to assess the CCA calculations in terms of compliance.

### **2.4.4. Direct Brine Release**

Direct brine release contributes only marginally to the overall release estimates and to only 48% of the sampled vectors. Considering the vector average, the direct brine release is larger than the median combined cuttings, cavings and spallings releases in less than 0.4 percent of the time histories. The largest calculated direct brine release was 0.2 normalized EPA Units, i.e. 20% of the release limit.

The releases strongly depend on several factors, including brine saturation and repository pressure. These two conditions are not independent. Large gas pressures usually mean low brine saturation and vice versa. The largest releases are associated with the larger pressures and higher saturations. However, the parameter that correlates best with the direct brine release is the residual brine saturation for the waste area. This parameter describes the minimum amount of brine that is necessary for brine movement through the waste. Direct brine release will occur only if the brine saturation is above the minimum value and the hydraulic conductivity of the waste will be small for saturations near the residual which inhibits brine flow into the waste.

### **2.4.5. Culebra Transport**

Releases to the accessible environment through the Culebra were negligible in the CCA calculations. Large amounts of radionuclides reached the Culebra from the intrusion borehole, but only for a few vectors. More than one EPA Unit of radionuclides reached the Culebra in approximately 10% of the sample vectors. The largest release to the Culebra was 20 EPA Units. However, the transport of the radionuclides limited the amount reaching the accessible environment with the partition coefficient for sorption isotherms being the limiting factor. As the retardation increases (calculated from the partition coefficient), the transport distance decrease.

Other factors that have a small effect on the increase of nuclide transport are fluid velocity and fracture spacing.

### 3. CONCERNS

The EEG's concerns of the computational efficacy of the CCA performance assessment for the WIPP disposal system does not imply any lack in scientific integrity by the DOE. Instead, it allows an unbiased investigation to ensure the robustness and completeness of the work to dispose of TRU waste effectively. However, it is believed that some of the parameters and ranges used in modeling the performance assessment of WIPP may be in error, or lack justification (Clemo et al. 1996). The DOE applied "conservatism" to many of the parameter and ranges, assuming that a larger range would incorporate all the experimental evidence. Without conducting a full scale sensitivity analysis on the parameters, this conservative approach becomes less meaningful.

#### 3.1. Conservatism

By claiming conservatism in the performance assessment calculations, the DOE took shortcuts on some of its scientific investigations. Conservatism was claimed for many conceptual models and parameters to show that the process would over predict releases to the accessible environment. However, it is not easy to forecast the implications of such assumed conservatism. The calculated releases may diverge from the actual releases, and a bound on the difference is very difficult. For example, an investigation into the microbial decay parameter, which is a major gas producer in the repository, shows one of three choices, (1) no degradation, (2) gas generation through microbial activity of cellulose, and (3) biodegradation of cellulose with rubber and plastics. The switch concedes to a 50% probability on any generation of gas through microbial activity. This estimated value was assumed to be conservative, since the possibility of degradation was unknown and no experiments were conducted to prove the possibility of gas generation with the addition of a magnesium oxide backfill. The MgO backfill is predicted to increase repository pH to 10 (U.S. DOE 1996). *"In general, rigorous microbial activity ceases above pH 10.5, although there may be few exceptions."* (Biddle et al. 1987). Figure 3.1. shows that there were higher average releases associated with lower microbial activity for an intrusion associated with the S3 Scenario due to the availability of brine. Other scenarios showed the opposite behavior.

#### 3.2. Parameter Issues

EEG's main issues with the assumptions used in the performance assessment calculations were outlined in the letters to the DOE and EPA on September 11, 1996 (EEG 1996), February 7, 1997 (EEG 1997a), and March 14, 1997 (EEG 1997b). Some major issues which will be discussed in this report are as follows:

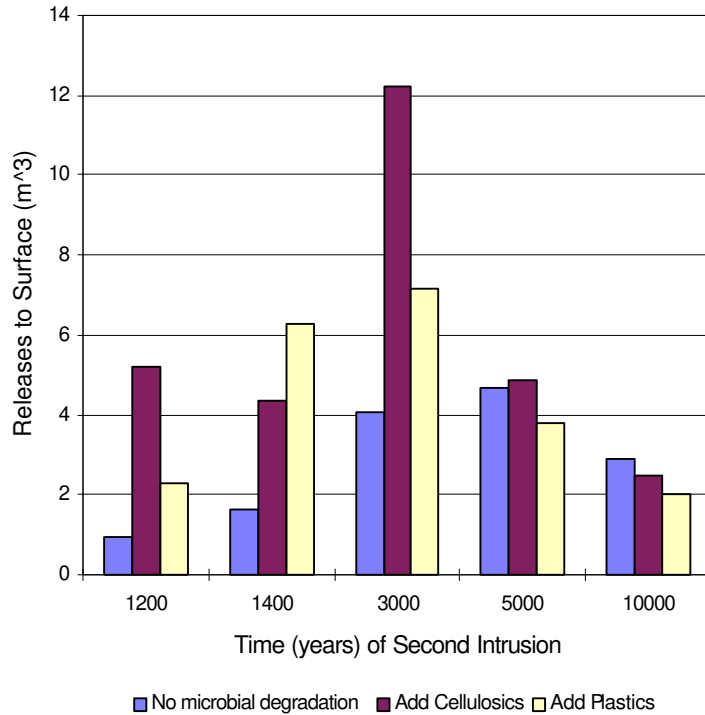


Figure 3.1. Releases from S3 Scenario (Replicate 1) for Microbial Decay

### 3.2.1. Brine Reservoir Interception

For performance assessment calculations in the CCA, an 8% probability was assigned to the parameter for intercepting a pressurized brine reservoir in the Castile formation. This seems unjustified, considering the data that was overlooked for the WIPP-12 borehole, located within the WIPP site. The reservoir at WIPP-12 was estimated to contain 2.7 million m<sup>3</sup> of brine, and extends more than 3 km in diameter. The values assumed in the CCA for the volume of the reservoir ranged from 32,000 to 160,000 m<sup>3</sup>. A value of at least 60% probability should be assigned to the parameter. This report explores the consequence of higher probabilities of encountering a brine reservoir.

### 3.2.2 Actinide Solubility

The solubility of actinides play an important role in the performance assessment calculations. The parameter determines how much of the radionuclide mass per cubic meter of brine will be transported from the repository up the borehole to the Culebra or to the surface. More specifically, the solubility of plutonium, which constitutes 87% of the initial radioactivity in the waste, was modeled as oxidation states III and IV in the CCA calculations with a 50% probability that it will be one or the other. DOE maintains that the conditions of the repository will be a reducing environment, not allowing the actinide to go above an oxidation state of IV, which would

inherently increase the solubility by 10,000 in some cases. Furthermore, experiments were never conducted to establish the solubilities of Pu(III) and Pu(IV), and were extrapolated from thermodynamic data conducted on Nd(III). Therefore, modeling experiments were conducted by the EEG to test the impact of solubility of actinides in brine.

### **3.2.3. Chemical Retardation in the Culebra**

The chemical retardation in the Culebra determines how the radionuclides will react with the surrounding dolomite matrix. Retardation infers that the contaminants will sorb onto the matrix, and the amount is determined by a coefficient called the partition (or distribution coefficient,  $K_d$ ). DOE made laboratory measurements of  $K_d$  for various actinides (Brush and Storz 1996).

The EEG has a number of concerns on  $K_d$ , which were raised in a meeting between Sandia and EEG. First, the applicability of the oxidation state analogy for Pu(III) from Pu(V), which was initially from Am(III), seemed weak at best. Several of EEGs' consultants noted that the assumptions for this analogy were based on questionable data and interpretations of experiments conducted with dilute groundwater from the Yucca Mountain site, a proposed high level waste repository in Nevada (Neill et al. 1998). Similarly, Pu(IV) was derived from Th(IV).

Another concern for the  $K_d$  values was the range and distributions used to establish these parameters in the LHS sampling method. The uranium data, for example, exhibited negative values in experimentation. Though physically impossible, they should have been averaged into the parameter's range. The lower end of  $K_d$  for uranium was 0.03 ml/g in the CCA, but should have been zero, due to the extreme uncertainty in the value. A model value of 3 ml/g was shown (Blaine 1997) to retard any actinide sufficiently from crossing the LWB. Therefore, it is very important to assign the correct values with a large enough uncertainty of  $K_d$  for actinides that exhibit values less than 3 ml/g.

These and other issues surrounding the  $K_d$  issue prompted the EEG to conduct their own transport modeling study, which changes the  $K_d$ s for several key parameters.

### **3.2.4. Castile Reservoir Parameters**

The pressurized brine pockets contained within the Castile formation were grossly under represented in the performance assessment calculations. After the submittal of the CCA, recommendations were made (Beauheim 1997) to characterize the formation by what is referred to as the "productivity ratio". This ratio is the product of the volume and the pore compressibility to porosity. The recommended range for this ratio was 0.0007 to 0.04 m<sup>3</sup>/Pa based on values from the ERDA-6 and WIPP-12 borehole data, respectively.

It should be noted that the ERDA-6 borehole lies outside the WIPP area at approximately 5 miles northeast from the repository center. The WIPP-12 well, on the other hand, is only 1 mile north of the site and values to describe the Castile for disposal system modeling would be more representative if this borehole data is used.

### **3.2.5. Potash Mining**

The extent of potash mining above the repository horizon for PA calculations included the possibility of two scenarios, which included partial and full mining. The two scenarios were based on the possible future extent of mining both inside and outside the disposal system with respect to ore grade. The extent of the partial mining maps were established on historically leased areas with economic grade ore, and the full mining was based on the a report by the New Mexico Bureau of Mines and Mining Resources (U.S. DOE 1996-Appendix Mass).

The BLM has established a map on the possible economic minable ore around the WIPP site. The CCA has identified this as the most conservative mapping of ore, but has refused to include it stating that a significant volume of potash is not minable by today's economic conditions. Furthermore, the BLM map does not include nonminable regions for the existence of hydrocarbon holes. The EEG conducted a modeling study, which extends the area of minable resources, while keeping all other modeling philosophy the same as it was in the CCA. The EEG does not believe that this resolves the modeling problems associated with that used in the CCA, and extensive modeling will be conducted in the future.

### **3.2.6. Spallings' Calculations**

The issue of spallings is very sensitive, with respect to codes, performance, and parameters. Initially, the DOE used a spallings code to calculate the effects of high repository pressures on releases during a human intrusion scenario in the CCA. The code was found inadequate by the Conceptual Models Peer Review Group (U.S. DOE 1996-Appendix Peer 5). However, the committee found the results in the CCA to be "reasonable" with further evidence from additional modeling.

This further evidence uses more realistic conceptual models than were presented in the CCA, implemented in a series of spreadsheets and numerical codes. Further investigation of the codes, by the EEG, found them to be inadequate to model all expected repository conditions. For example, a slightly lower waste permeability than that in the CCA, caused the results (volume of failed material that could reach the surface) to be quite unrealistic, with values as high as 500 m<sup>3</sup>. Other parameters used in the code, such as gas viscosity and drilling mud density, also cause unexpected values. It is EEG's belief that none of the codes, in their present

form, can adequately model all expected repository conditions to establish “justifiable” values for releases to compare with 40 CFR Part 194.



## **4. PROBABILITY MODELING OF DRILL INTRUSION RATES**

### **4.1. Summary**

This investigation included changing the deep drilling intrusion rates at the WIPP to estimate the safety margin between assumed drilling rates and the drilling rate that first violates the standards for compliance. The CCA used a drilling rate of  $4.68 \times 10^{-3}$  boreholes/km<sup>2</sup>/yr over the 10,000 year period of the repository. The rates were increased in two simulations. Additional modeling was also performed with a  $2.34 \times 10^{-3}$  boreholes/km<sup>2</sup>/yr drilling rate to investigate the potential for larger spallings releases due to higher pressures with a less frequent drilling rate. The results show a linear relationship between drilling rates and release limits. A factor of safety of 23 was calculated for the CCA drilling rate, with all other factors remaining the same as used in the CCA.

### **4.2. Introduction**

The consequence of future human intrusion scenarios into the Waste Isolation Pilot Plant was investigated in the CCA (U.S. DOE 1996). These scenarios were established according to the EPA guidelines in 40 CFR Part 194 (U.S. EPA 1996b), and included the possibility of mining and deep and shallow drilling for resources.

The guidelines state in 40 CFR Part 194.33 that the likelihood of a drilling intrusion into the Delaware Basin for the future 10,000 years must be calculated by considering the frequency of drilling for all resources over the past 100 years. These numbers were calculated in the CCA, Appendix DEL (Tables DEL-3 through DEL-7) and were used to calculate the CCDF curves for the performance assessment calculations of the CCA. A total of 46.8 boreholes per km<sup>2</sup> were estimated based on past drilling of resources at depths greater than 2150 meters, which equal 10,804 boreholes in 23,102.1 km<sup>2</sup> (area of Delaware Basin).

The drill intrusion rate for the 10,000 year future of the WIPP was directly implemented in the CCDF model, and was calculated to be equal to 0.00468 boreholes/km<sup>2</sup>/yr. However, since the future human activities are uncertain, the rate was changed to test the effects on the CCA calculations. The rates were increased by one and two orders of magnitude, and also decreased by one-half. New CCDF curves were generated based on the changes.

### **4.3. Methodology**

The modeling of new drill intrusion rates were started at the code CCDFGF. All steps up to generating the new CCDF curves were exactly the same as CCA calculations. The files needed to conduct the modeling were fetched from the CMS library. Figure 4.1. lists the steps involved

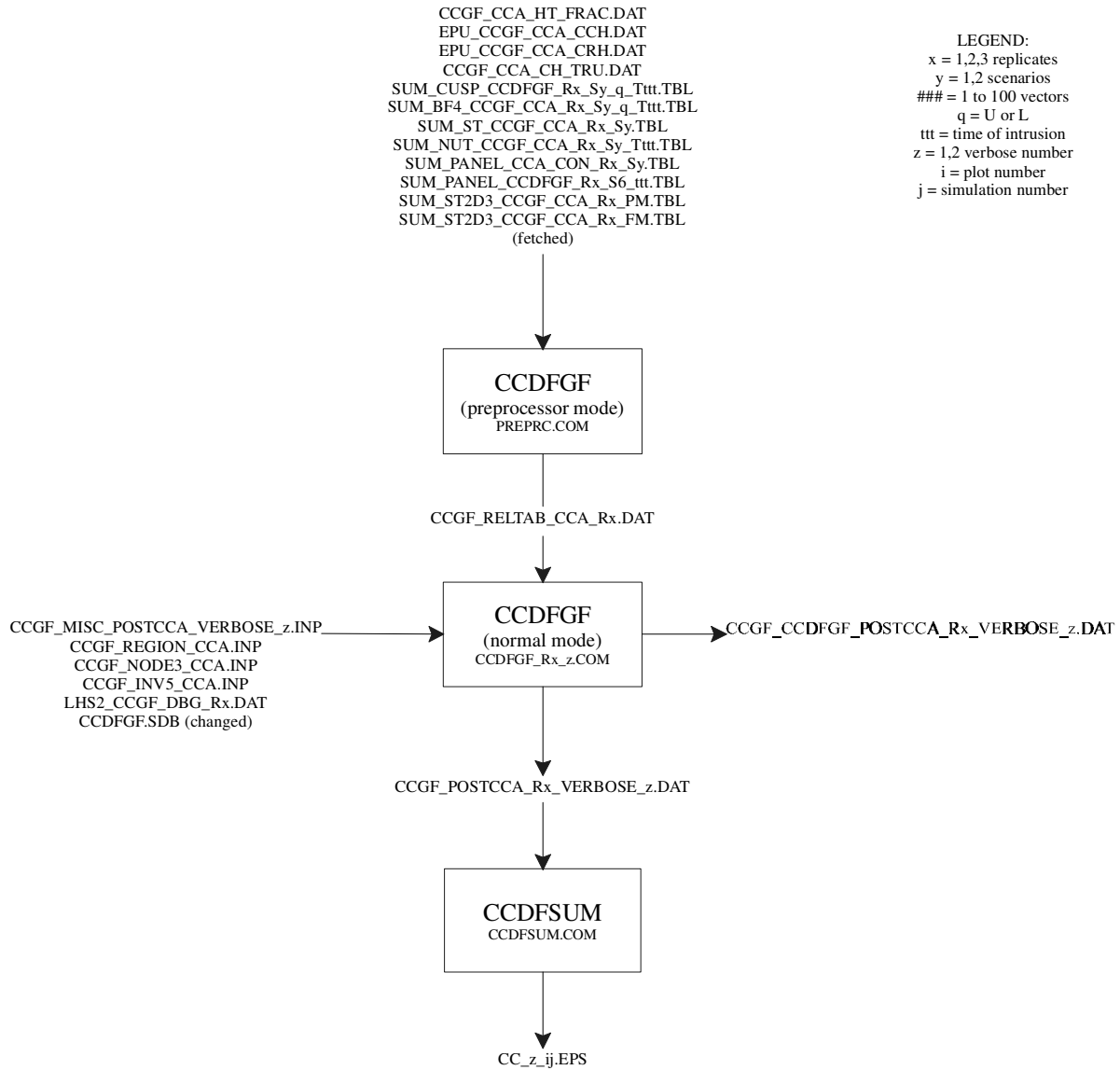


Figure 4.1. CCDFGF Flowchart

in the modeling process with all input and output files.

The change of the drill intrusion rate was made in the file CCDFGF.SDB, a secondary database file used in both preprocessing mode and normal mode of the CCDFGF code. The parameter LAMBDA<sub>D</sub> (number 3494) was changed, and the specifications can be found in Appendix PAR, Table PAR-53 of the CCA (U.S. DOE 1996). Drilling rates were changed to  $4.68 \times 10^{-2}$  boreholes/km<sup>2</sup>/yr,  $4.68 \times 10^{-1}$  boreholes/km<sup>2</sup>/yr, and  $2.34 \times 10^{-3}$  boreholes/km<sup>2</sup>/yr in three successive simulations.

Minor changes had to be made to the CCDFGF code in order to accommodate the higher drill intrusion rates. Currently, the maximum number of boreholes allowed in the code is 100; MAXBH in CCDFGF.FOR limited the total number. Therefore, the variable MAXBH was increased from 100 to 100,000 in every subroutine of CCDFGF.FOR to allow for a greater number of boreholes. The code was recompiled with the specifications used for the CCA.

The CCDFGF was first run in preprocessor mode to generate the release table data, then in normal mode. The output files created by the normal mode of CCDFGF were postprocessed by CCDFSUM, which created the printable ADOBE style postscript files.

#### 4.4. Results

New CCDF curves were calculated for the changed drill intrusion rates, and are plotted in Figure 4.2, which also shows the results from the CCA. As expected, the increasing rate produces an increase in releases, in as much to exceed the EPA maximum release limit at  $4.68 \times 10^{-1}$  boreholes/km<sup>2</sup>/yr. The relationship between drilling rate and actinide release also seems to be approximately linear; one order of magnitude increase in drilling rate produces approximately one order of magnitude increase in release. Table 4.1. lists the releases for all three simulations and the results for the CCA at a release probability of  $10^{-3}$ . All releases are in EPA Units.

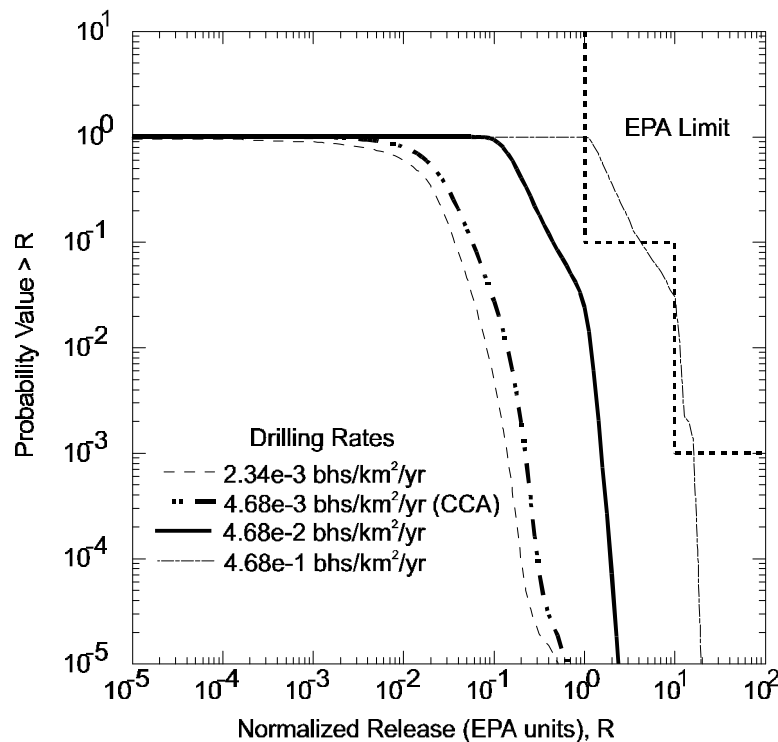


Figure 4.2. Total Normalized Release Limits for Changing Drilling Rates

Simulation	Deep Drilling Rate (bhs/km <sup>2</sup> /yr)	Total Normalized Releases at a probability of 10 <sup>-1</sup> (U.S. EPA Units)	Total Normalized Releases at a probability of 10 <sup>-3</sup> (U.S. EPA Units)
1 (CCA)	4.68x10 <sup>-3</sup>	0.059	0.21
2	4.68x10 <sup>-2</sup>	0.44	1.7
3	4.68x10 <sup>-1</sup>	4.1	17
4	2.34x10 <sup>-3</sup>	0.035	0.12

Table 4.1. Total Normalized Release Limits at Different Deep Drilling Rates

The drilling rate was also reduced by half to test a hypothesis about the increased gas pressures with less intrusions. The effect would most likely be seen in the low probability range, however the releases decreased linearly with respect to drilling rate.

#### 4.5. Conclusions

Drilling rates were changed from the original CCA calculations to test the effects of future uncertainty. The changes included two CCDFGF simulations which increased the deep drilling rates by one and two orders of magnitude, and a simulation that decreased the deep drilling rate by one-half. The results are presented in Table 4.1. and Figure 4.2..

The future drilling rate used in the CCA, as specified by the EPA, estimated that the number of boreholes for the next 10,000 years was an average from the last 100 years. Of course there is no possible way to predict human scenarios and the numbers used were more or less arbitrary. However, the present study looks at several different drilling rates, and concludes that the relationship is approximately linear between releases and drilling rates. A drilling rate 23 times greater than that prescribed by EPA and used in the CCA is needed to reach the EPA release limit at a probability of 10<sup>-1</sup> from values used in the CCA. The overall mean for the highest release at 0.468 boreholes/km<sup>2</sup>/yr exceeds the EPA limit of 10 EPA Units at a probability of 10<sup>-3</sup>. While the drilling rate in the immediate vicinity of WIPP has been documented to be higher than 0.3 boreholes/km<sup>2</sup>/yr, that drilling rate was not anticipated to be sustained for any length of time (Silva, 1994).

## **5. INDIVIDUAL AND COMBINED INFLUENCE OF PLUTONIUM SOLUBILITY ON DIRECT BRINE RELEASE AND THE PROBABILITY OF HITTING CASTILE BRINE**

### **5.1. Summary**

This investigation describes the influence of plutonium solubility and the probability of hitting Castile brine on the potential and consequences of brine release to the surface through blowout. The effects of these two parameters on the performance assessment, without changes to other parameters, are investigated both individually and in combination. Results are presented as a comparison of CCDF for blowout and the total normalized surface release. Changing these parameters to more realistic values than used in the CCA increases releases but not substantially. Even calculations using plutonium solubility set to unrealistically high values do not exceed the EPA standards for potential radioactive nuclide releases to the accessible environment through a direct brine release scenario. At the largest solubility values, the entire plutonium inventory is in solution. The release is, however, limited by the fraction of repository brine brought to the surface.

The codes PANEL and CCDFGF are the primary codes used in this investigation. The investigation made use of the intermediate results of the performance assessment calculations. The PANEL code created intermediate data files that are used later to incorporate plutonium solubility influences in investigations of other parameters such as the Castile brine reservoir parameters.

### **5.2. Introduction**

The standards issued by the EPA for the safe disposal of TRU waste at WIPP require a performance assessment of the WIPP repository in order to provide a reasonable assurance that the potential radioactive nuclide releases to the accessible environment will not exceed the limits established by the EPA. The DOE has submitted an application (CCA) for the EPA to certify that the DOE has demonstrated compliance with the EPA standards. One of the potential pathways for radionuclide release to the environment is through unintended drilling into the repository in the distant future. If the pressure buildup in the repository due to chemical reactions in the waste is sufficiently large then venting of the repository through a borehole could bring radioactive brine to the surface. The EEG contends that the oxidation states within the repository assumed for plutonium in the CCA performance assessments are in error. The oxidation state assumption has a major influence on the amount of plutonium that may be in solution in the repository brine and hence on the amount plutonium brought to the surface as a consequence of drilling.

The oxidation states of plutonium in certain WIPP brines have been the subject of some recent studies (Reed et al. 1994, 1996; Rao 1996) and conclusions show that plutonium will exist in oxidation state VI, reducing to V in some instances. However, modeling of plutonium for the CCA was conducted on Pu(III) and Pu(IV) using solubilities predicted by the FMT code, contrary to the above experiments. The range for the plutonium solubility in the Salado brine for the CCA was  $4.4 \times 10^{-8}$  M to  $1.1 \times 10^{-4}$  M. The range for plutonium solubility in Castile brine was  $5.7 \times 10^{-11}$  M to  $1.4 \times 10^{-7}$  M. The changed oxidation states will effect the solubility of plutonium in the waste, and change the amount of actinide release to the surface and Culebra.

The solubility of plutonium was changed from values used for oxidation states III and IV to those measured in Reed et al. (1996). The solubility of plutonium in the Salado brine was increased by a factor of 20, and fell within the range suggested by the FMT calculations. A more substantial change was made in the solubility of plutonium in the Castile brine, increasing by almost 4 orders of magnitude. Table 5.1. lists the solubilities used in the CCA, suggested by DOE (1996) using the FMT calculations, and the experimental results shown by Reed et al. (1996).

### 5.3. Methodology

The solubility change was implemented in the PANEL calculations for blowout considerations only; the changes impacted the direct brine release portion of the CCDFs. The change was made to the source term file ALG\_ST\_CCA\_Sy.inp, where Sy are the scenario numbers 1 and 2. Only the first two scenarios are needed to obtain Salado and Castile brine radionuclide concentrations.

The changed parameter in the source term file, DIS (dissolved solubility), was converted to a constant equalling the solubilities measured in Reed et al. (1996) using ALGEBRA. It was previously a sampled parameter, with a range of -2 to 1.4 orders of magnitude difference from that in the FMT calculations. This was the only changed parameter, and the steps involved prior to running the CCDFGF code follow the PANEL Concentration simulations in Stockman et al. (1997). The flowchart in Figure 5.1. shows the steps involved through the entire process. The changed input file for ALGEBRA is identified in Figure 5.1. as input to the ALGEBRA Source Term.

	FMT Calculations	Reed et al. 1996
Castile Brine	$5.7 \text{ e-}9 \text{ M}$	$8.0 \text{ e-}5 \text{ M}$
Salado Brine	$4.4 \text{ e-}6 \text{ M}$	$9.0 \text{ e-}5 \text{ M}$

Table 5.1. Solubility of Plutonium as Determined by Experiment and FMT Calculations

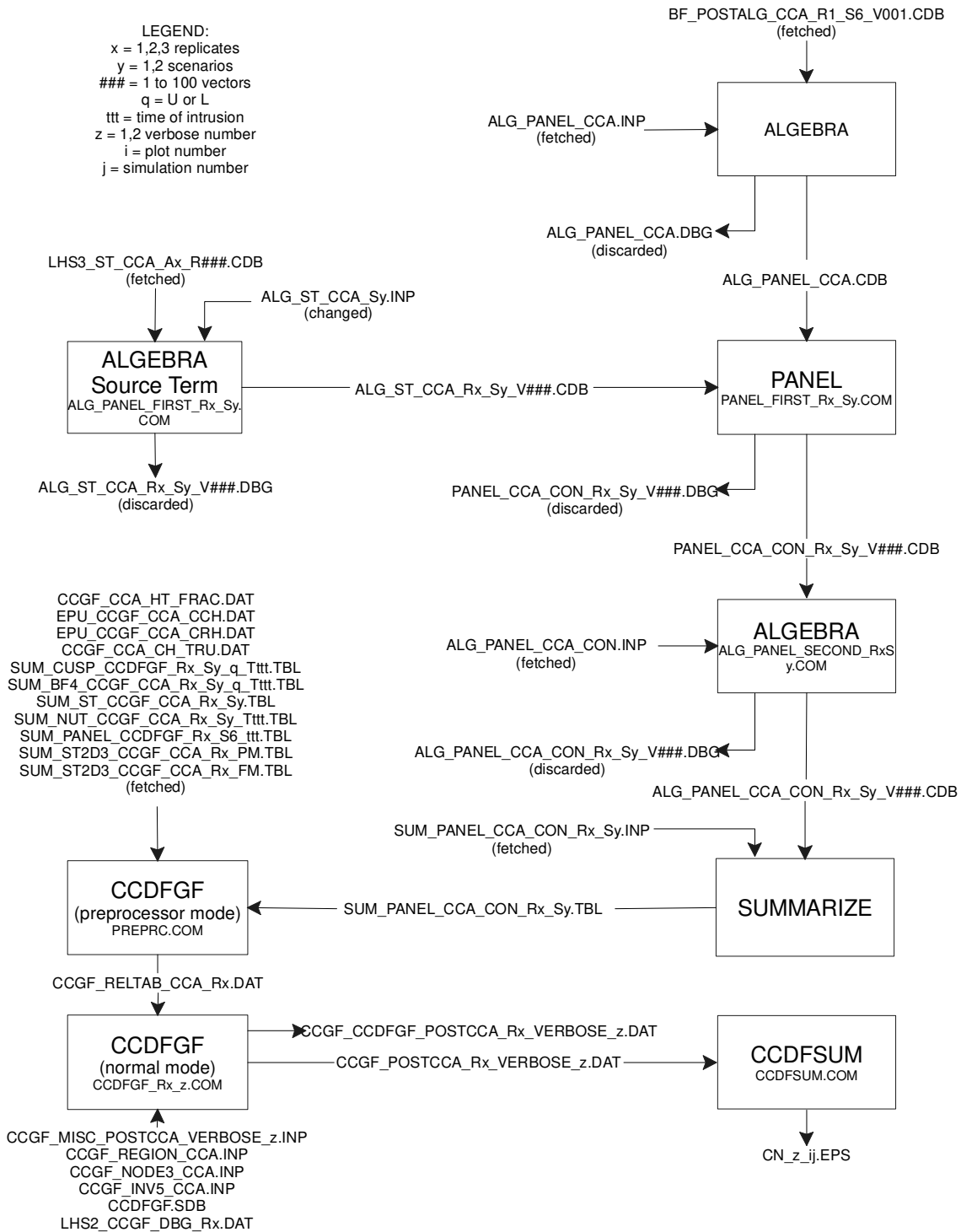


Figure 5.1. Flowchart of PANEL Simulations

Figure 5.1. shows a listing of all the programs needed to run the entire PANEL concentration simulation, and are represented as rectangles. The rectangles list the names of the executable code and the script (if available) used to run the code. Arrows in and out of the rectangle show which files went into and came out of the code execution.

Script files were created to automate the process of running all one hundred vectors for each replicate and scenario for each step. These script files also help to ensure reproducibility of the calculations. Any additional files needed for code execution were fetched from the CMS library, and erased after use. For example, LHS files were needed to run the source term portion of ALGEBRA. The files LHS3\_ST\_CCA\_Ax\_R###.CDB (where Ax represents the replicate number and R### are the vectors 1-100) were fetched from the library LHS, and discarded afterward to conserve drive space.

The PANEL calculations were postprocessed by SUMMARIZE and used in CCDFGF to generate new CCDF plots. The CCDFGF was first run in the pre-processor mode, then in normal mode to produce the results. The CCDFGF calculations were then post-processed by CCDFSUM to produce postscript files that are printable.

## 5.4. Results

The CCDF plot created from CCDFSUM for blowout calculations can be seen in Figure 5.2., with the corresponding CCA plot in Figure 5.3.. Each line represents the probability of a magnitude of release in EPA Units for different vectors of sampled parameter values. The plots are from replicate R1. The highest release from a vector at  $10^{-3}$  probability is less than 1.0 EPA Units. However, this is an increase from the CCA calculations which show the highest vector at less than 0.2 EPA Units at the same probability level.

The plot in Figure 5.4. shows an overall mean increase in blowout normalized release for the increased solubility and the CCA calculations. At the  $10^{-3}$  probability level, the release increases in EPA Units from 0.04 to approximately 0.13. This does not violate the EPA release limit, which limits a release of 10.00 EPA Units (3440 Ci) at  $10^{-3}$  probability.

Further experimentation of the blowout calculations included changing the parameter which controls the probability of a drill intrusion into the Castile brine. In the CCA calculations, this parameter was set to 8 %. The influence of this parameter was tested at higher values at 50 and 100%. These values were based on the potential that the Castile reservoir size encountered by WIPP-12 (Chaturvedi et al. 1997) extends below the waste area. It should be noted that the



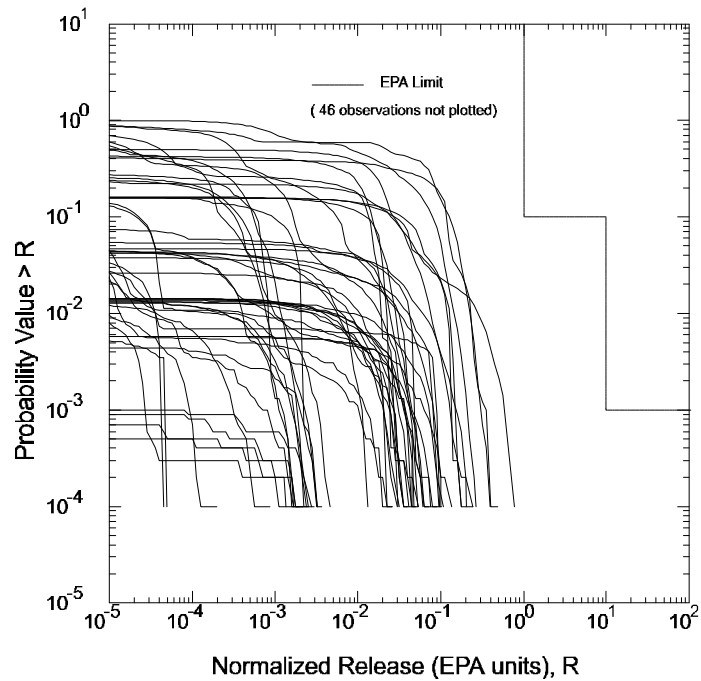


Figure 5.2. Blowout Releases for Increased Solubility

probability parameter is located in the 'Region and Panel Parameters File' (CCGF\_REGION\_CCA.INP) at position 9, but is overwritten by parameter 3493 in the secondary database file (CCDFGF.SDB).

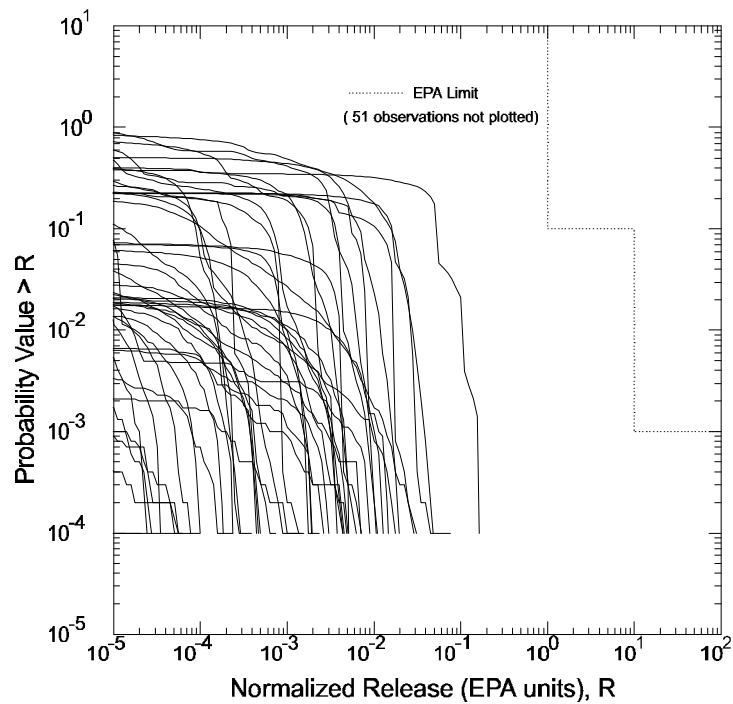


Figure 5.3. Blowout Releases for CCA Calculations

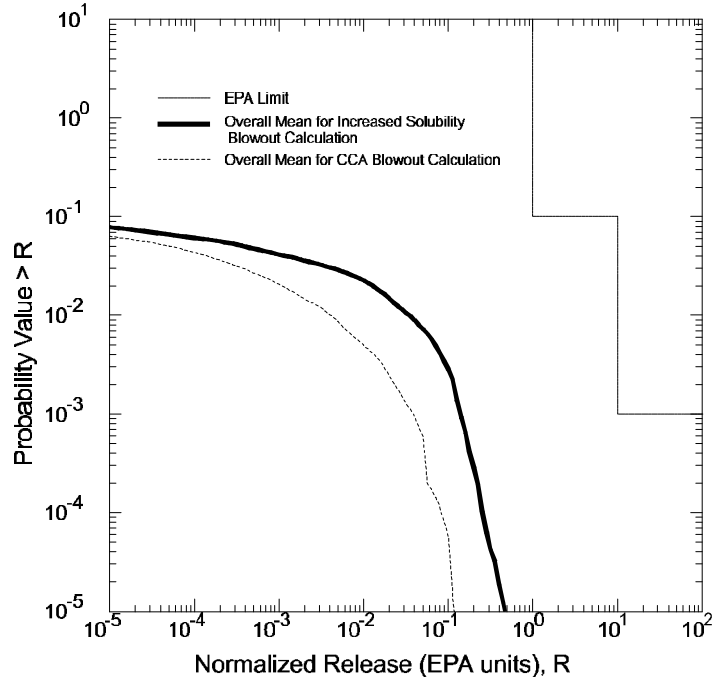


Figure 5.4. Overall Mean of Blowout Normalized Releases

Figure 5.5. shows the overall mean from the total normalized release calculations from the three simulations of 8, 50, and 100% probability as it compares to the CCA. The greatest release came from the 100% probability of Castile brine intrusion, with a value of 0.31 EPA Units at a probability of  $10^{-3}$ , which is less than the 10.0 EPA Units established by the EPA as the maximum allowable release limit. The calculated releases at the 10% level are only slightly effected.

Lastly, the solubility of the plutonium in the Castile and Salado brines was increased further to test the limits and compare values for the previous simulations. The solubilities were increased from  $8.0 \times 10^{-5}$  M and  $9.0 \times 10^{-4}$  M to  $8.0 \times 10^{-4}$  M,  $8.0 \times 10^{-3}$  M, and  $8.0 \times 10^{-1}$  M for both brines. These values have no justification other than testing the limits of the code with respect to more suitable values. The probability of hitting a brine reservoir was returned to 8%. The results were plotted in Figure 5.6., showing the increased solubilities compared to the the CCA calculations and solubility of  $8.0 \times 10^{-5}$  M and  $9.0 \times 10^{-5}$  M in the Castile and Salado, respectively. For each increased solubility simulation, the release increased to a threshold limit at approximately  $8.0 \times 10^{-3}$  M, above which the solubility had no further effect on the calculations. All releases stayed below the EPA limit, with the maximum reaching 1.3 EPA Units at solubilities of  $8.0 \times 10^{-3}$  M and above.

Table 5.2. lists all simulations conducted showing releases at  $10^{-3}$  probability.

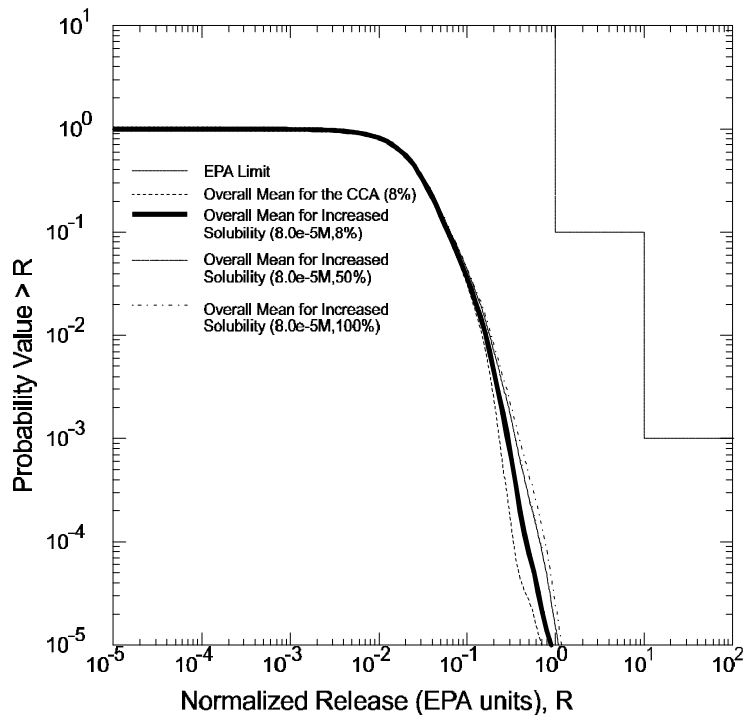


Figure 5.5. Total Normalized Releases with Increasing Probability of Hitting Castile Brine Reservoir

## 5.5. Conclusions

Additional PANEL simulations were performed to test the effect of plutonium solubility on the CCDF calculations in the CCA. The solubility was changed in both the Castile and Salado brine from a ranged parameter to a constant value. Six simulations were conducted that tested the overall effectiveness of the changes, which included changes in the solubility and Castile brine intrusion probability. Table 5.2. lists the results from each simulations as compared to the CCA calculations.

Simulation Number	Simulation Description	Blowout Release Overall Mean (U.S. EPA Units)	Total Release Overall Mean (U.S. EPA Units)
1	CCA	0.04	0.21
2	$8.0 \times 10^{-5} \text{M}$ , 8% probability	0.13	0.29
3	$8.0 \times 10^{-5} \text{M}$ , 50% probability	0.17	0.30
4	$8.0 \times 10^{-5} \text{M}$ , 100% probability	0.18	0.31
5	$8.0 \times 10^{-4} \text{M}$ , 8% probability	1.0	1.0
6	$8.0 \times 10^{-3} \text{M}$ , 8% probability	1.3	1.3
7	$8.0 \times 10^{-1} \text{M}$ , 8% probability	1.3	1.3

Table 5.2. Releases for PANEL Simulations at  $10^{-3}$  Probability

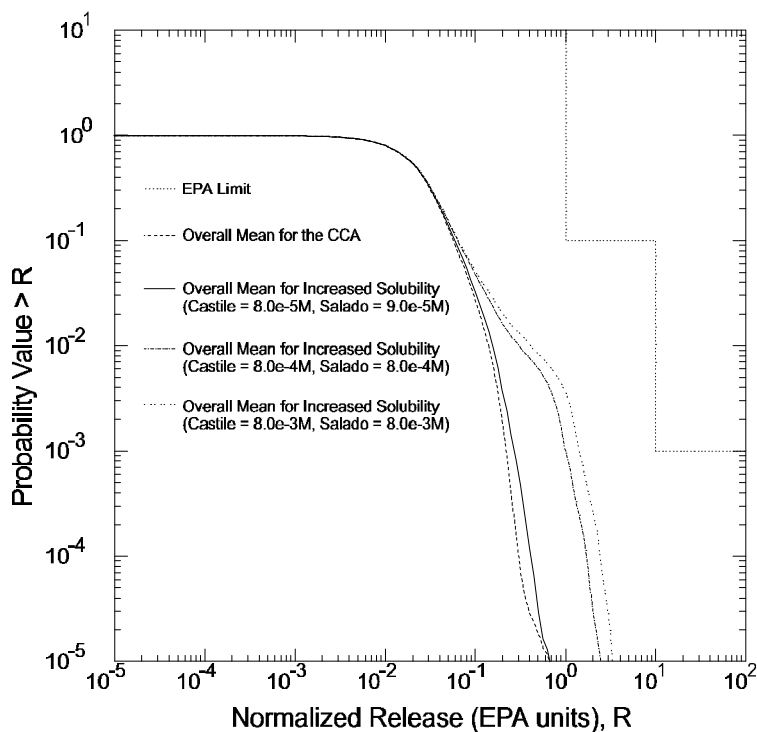


Figure 5.6. Overall Mean of Blowout Releases with Increasing Solubility

As expected, the simulations seemed to be more sensitive to the increased solubilities than the increased Castile intrusion probability. The one order of magnitude increase in solubility from  $8.0 \times 10^{-5}$  M to  $8.0 \times 10^{-4}$  M increased releases by 0.87 EPA Units, whereas the one order of magnitude increase in probability of hitting the Castile brine reservoir from 8% to 100% only increased the releases by 0.08 EPA Units. The releases continued to increase with increasing solubility to a threshold of  $8.0 \times 10^{-3}$  M. Above this solubility no additional increase was calculated, and was most likely limited by the amount of direct brine release. Also, one should note the nonconstant increases in total normalized releases compared to the blowout normalized releases of Table 5.2. The increased solubility of plutonium affects the direct brine release calculation enough to make it a dominate release mechanism for Simulation #5, for probabilities lower than  $10^{-2}$ . Lower solubilities (less than  $8 \times 10^{-4}$  M) mask the effect of the actinides in solution.

The curves represented in Figure 5.6. show the increasing total normalized releases with increasing plutonium solubility in both the Castile and Salado brine, with a maximum release of 1.3 EPA Units at  $8.0 \times 10^{-3}$  M at a  $10^{-3}$  probability. The EPA limit suggests that releases remain below 10.0 EPA Units at the probability of  $10^{-3}$ , therefore rendering all justifiable plutonium solubilities conservative with the current amount of brine release. Additional studies should be conducted in which the amount of brine volume increases with the increasing solubility.

## **6. TRANSPORT MODELING OF $K_d$ S**

### **6.1. Summary**

A modeling study was performed to investigate the roles of chemical retardation through the Culebra aquifer at the WIPP repository. The transport code SECOTP2D was used by varying the values of the partition coefficient ( $K_d$ ) from that used in the Performance Assessment of the Compliance Certification Application for several key actinides. The results show that the assumed sorption of radionuclides to the surrounding rock matrix coupled with the amount of actinides reaching the Culebra produce very low releases compared to the 40 CFR 191(U.S. EPA 1996a) containment requirements.

### **6.2. Introduction**

The concern of actinide transport through the Culebra has prompted a modeling study by the EEG that investigates the consequences of radioactive wastes to sorb onto the aquifer material through the evaluation of  $K_d$ s. The matrix partition coefficient, or  $K_d$ , is a species dependent property that varies depending on the sorbing material type, which describes the amount of waste that can be chemically bonded to the matrix adsorbed through ion exchange.

Results of various laboratory experiments to determine the  $K_d$  of plutonium, uranium, americium, thorium, and neptunium were reported by Brush and Storz (1996). However, the values obtained from the experiments and the statistical representations that are used for modeling the coefficients were questioned by the EEG (EEG 1997a; 1997c). The EEG argues that the data for  $K_d$  values are too limited to justify the current range in the CCA, the amount of organic ligands that will bind with the actinides is much higher than that assumed by the DOE, and a uniform distribution as a representation for all data is unjustified. Therefore, transport modeling of the transuranics using other  $K_d$  values were investigated to determine whether chemical retardation is needed to meet compliance standards established by the EPA.

### **6.3. Methodology**

The modeling of the partition coefficient was conducted using the Sandia transport code, SECOTP2D version 1.30. For the present study, the groundwater flow calculations were not rerun and grid velocity files were fetched from the CMS.

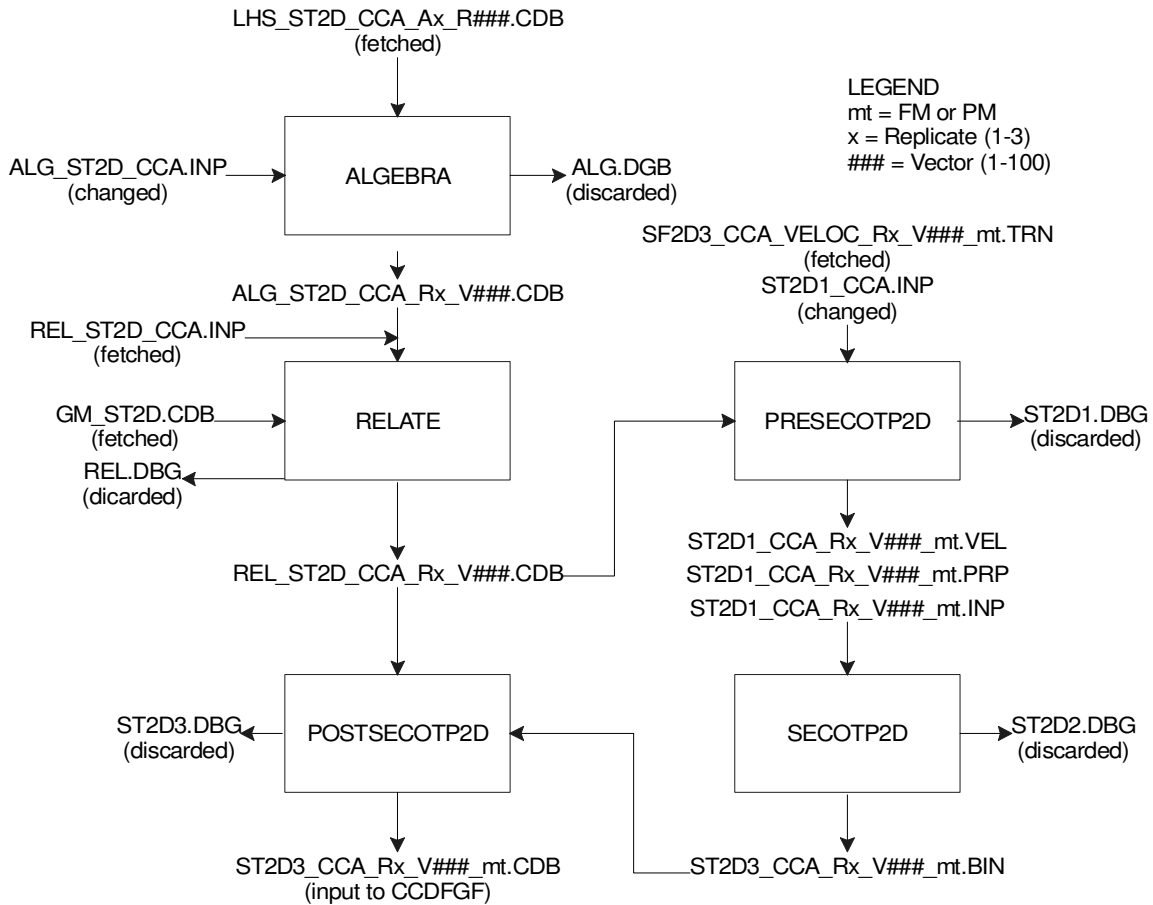


Figure 6.1. Flowchart of SECOTP2D Runs

The only files that were modified for transport simulations were the input file for the ALGEBRA code and the input file for SECOTP2D. The ALGEBRA file, ALG\_ST2D\_CCA.INP was altered by changing the way the retardation was being calculated. A new value was substituted for the partition coefficient. The input file for SECOTP2D was changed by specifying the transport of only one actinide. Figure 6.1. shows the stream of codes used in modeling with SECOTP2D.

#### 6.4. Transport Modeling Of Plutonium

The importance of the partition coefficient was investigated by Blaine (1997). The investigation found that a value of  $3 \text{ ml/g}$  was sufficient to retard plutonium through the Culebra for a “worst case” vector. The study was meant to test minimum values of  $K_d$  for violation of the EPA standards. The worst case vector included the minimum advective porosity of the Culebra matrix (0.0001), the maximum diffusive porosity of the Culebra matrix (0.25), and the largest half matrix block length (0.5) that were estimated in the CCA. The vector was also tested against

larger half matrix block lengths, of up to 1.0 m. The latter model showed that a value of  $15 \text{ ml/g}$  for  $K_d$  was needed to chemically retard the species adequately to meet EPA regulations.

The above experiment studied the phenomenon of small  $K_d$  quite thoroughly. However,  $K_d$ s smaller than  $1 \text{ ml/g}$  were never investigated. Therefore, the present study changes the CCA  $K_d$  values from that generated from a range for performance assessment calculations to a model that assumes a very small mass fraction (1%) of the radionuclides have a  $K_d$  equal to zero. This effect allows the waste to move through the aquifer unretarded.

The justification for using  $K_d$  of zero is summarized in Channell (1997). The evidence, reproduced here, that support the 1%  $K_d=0 \text{ ml/g}$ :

- (1) A fraction of the actinides is likely to be in organic complexes or chelated. Experimental evidence suggests that these conditions will drastically reduce  $K_d$  values.
- (2) Column infiltration experiments have shown that small fractions of transuranic radionuclides will move through natural rock columns at or near the speed of water. These radionuclides are not in complex or chelated form.

The first experiment simulated plutonium moving through the Culebra with a fraction of the contaminate having a zero  $K_d$ . The original PA groundwater flow calculations from SECOFL2D were used to obtain velocity and discretization (spatial and temporal) information for transport calculations. The original PA assumed that 1 kg of waste would be brought to the surface through a human intrusion borehole. The 1 kg was assumed to be a unit mass of release to the Culebra and is coupled later with the actual amount that is released from the repository through the code CCDFGF. Hence, 0.01 kg was accepted for a 1%  $K_d = 0 \text{ ml/g}$  transport simulation.

Transport simulations were conducted on 100 vectors of both full and partial mining of the first replicate. Results of the modeling efforts are presented as integrated discharge and contour plots of waste concentration. Figure 6.2. shows the partial mining scenario with integrated discharges at 10,000 years (on  $\log_{10}$  scale) as a function of vector number. The integrated discharge is the fraction of waste mass that crosses the Land Withdraw Boundary (LWB) at a given time. Hence, an integrated discharge value of 0.001 kg is equivalent to 10% of the original waste mass crossing the LWB in 10,000 years. All parameters for the present study were kept the same as that used in the CCA, except for the partition coefficient.





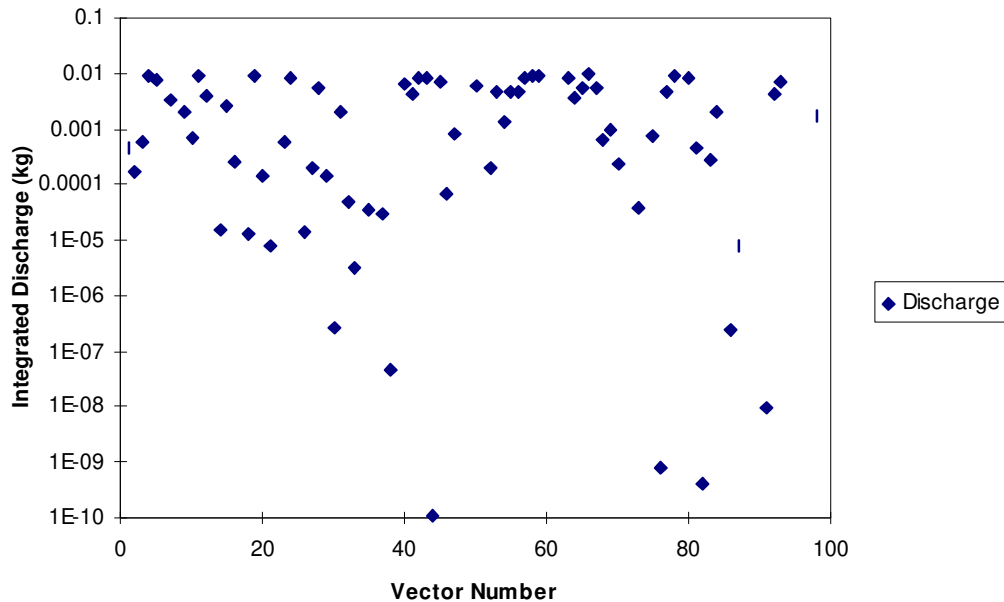


Figure 6.2. Integrated Discharge vs. Vector Number for Partial Mining Scenario at 10,000 Years

In the CCA calculations, there were no vectors with discharge across the boundary at 10,000 years for the first replicate. All actinides were retarded sufficiently and were kept from migrating any substantial distance from the intrusion borehole. Retardation values for plutonium ranged from 216 to 455492 in the PA and were calculated from a linear isotherm. Plutonium retardation for the present model was a single value of 1.0 for all vectors. As a result of lower retardation, a substantial number of vectors showed releases across the LWB.

Figure 6.3. shows a contour plot of vector 4 of replicate 1 for plutonium migration with 1% of the  $K_d=0 \text{ ml/g}$  for the partial mining scenario at 10,000 years. The isopleth concentration levels in  $\text{kg/m}^3$  are equivalent to that seen in the Analysis Package, Task 3 (Ramsey and Wallace 1997) with darker shades indicating lower concentrations. The integrated discharge for the plot is 91.9%. The areal view of the figure indicates the location of the Waste Panel Area and the Land Withdraw Boundary in relation to the plume's spread, with the ordinate and abscissa marking 1000 m distances between ticks. An asterisk around the center of the plume designates the highest concentration in  $\text{kg/m}^3$ , which is not to be confused with the centroid of the plume. The figure shows that the plutonium moves quite quickly (relative to 10,000 years) through the Culebra, and a significant amount passes through the Land Withdraw Boundary in 10,000 years.

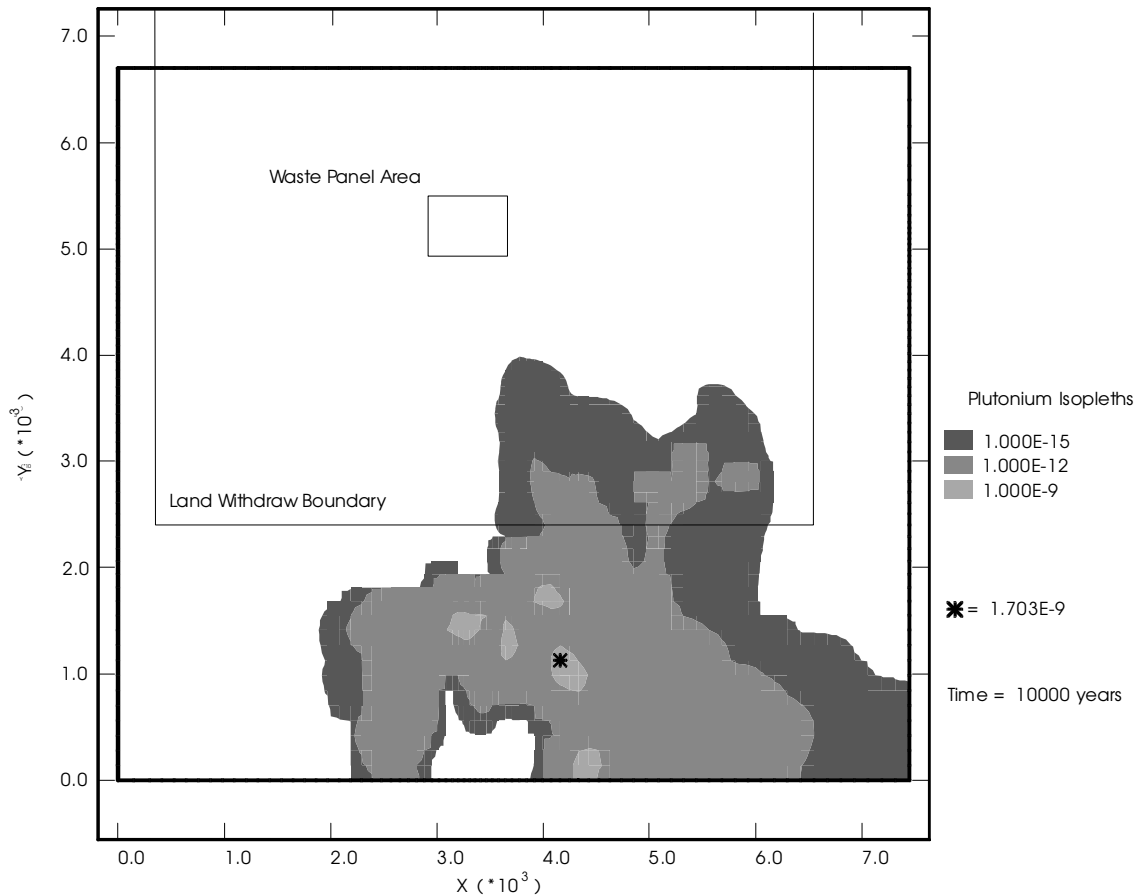


Figure 6.3. Plutonium Concentration (kg/m<sup>3</sup>) for Replicate 1, Vector 4, Partial Mining

Figure 6.4. shows the releases for the vectors of the full mining scenario of replicate 1. Again, none of the PA calculated vectors in the CCA had releases across the LWB in 10,000 years. This is a large contrast to the present model, where a substantial number of vectors crossed the LWB. Approximately half of the total vectors have at least 1% discharge across the Land Withdraw Boundary in 10,000 years in both full and partial mining scenarios.

Though many vectors seem to have a high release, one vector in particular, Vector 20, stands out as a possible error. The discharge across the LWB is 0.0135 kgs, normalized to 135% of the original mass entering the Culebra. The obvious error of the overcalculated mass could be attributed to the large mass balance error (-0.3619 kgs) associated with the calculation. These errors are documented for SECOTP2D version 1.30 by the EPA (U.S. EPA 1997) and the DOE (U.S. DOE 1997c). The EPA's request for additional information about the mass balance calculations in the PA prompted a study in (Ramsey and Treadway 1997) on the extent of the errors associated with the code. Their findings demonstrated that the major problems of mass conservation are attributed to the boundary conditions on the southern-most boundary. The total

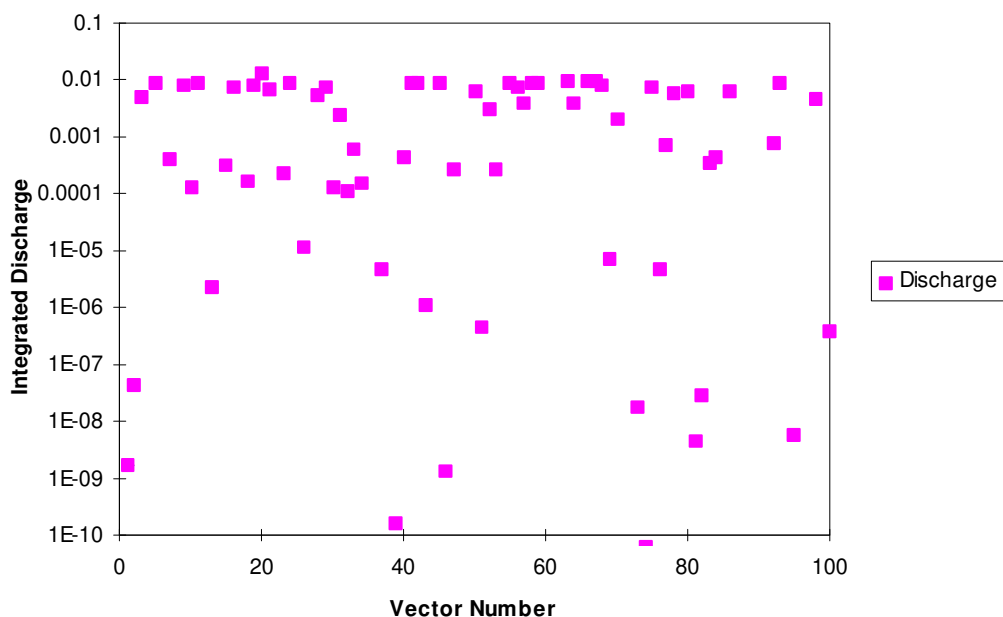


Figure 6.4. Integrated Discharge vs. Vector Number for Full Mining Scenario at 10,000 Years with 1% of Plutonium Having a  $K_d$  of Zero

variation diminishing (TVD) differencing scheme in combination with large Courant numbers were the culprit and was subsequently fixed in version 1.40. However, this version was unavailable at the time of these simulations.

The effect of the nonconservative models is uncertain. The problem lies on the southern boundary, where most of the nuclides are transported across the LWB. The mass balance error has been quantified in a single vector (EEG 1997b) for all five nuclides as approaching 100%. The error shows a large underestimation of transport decreasing in time, and yet it cannot be reasonably assumed that all vectors are underestimated, since Vector 20 in the present model shows an overestimation of 35%.

Figure 6.5. shows a similar plot to that of Figure 6.3.: plutonium concentrations for Vector 58 of the full mining scenario. The discharge across the LWB for Vectors 58 is 88.6%. The slight difference in discharge between the two figures is compensated greatly in Figure 6.5. by the areal extent of higher concentrations. The isopleths indicating  $1.0 \times 10^{-9} \text{ kg/m}^3$  has a farther and more continuous reach than seen in Figure 6.3. Conceptually, this could have a greater impact on future generations who may drill into the aquifer, especially if they were in a direct downstream pathway from the source of the highest concentration.

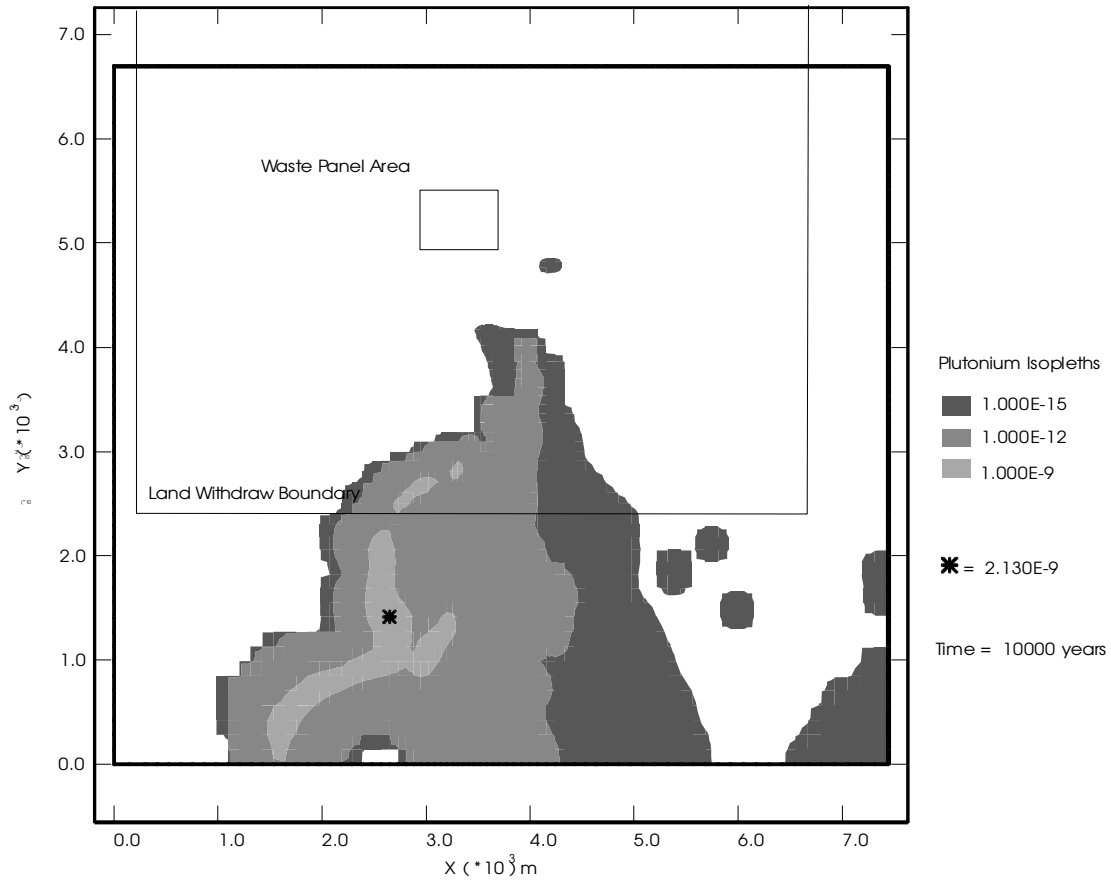


Figure 6.5. Plutonium Concentration (kg/m<sup>3</sup>) for Replicate 1, Vector 58, Full Mining

The combined effort of the partial and full mining scenario modeling with a 1%  $K_d=0 \text{ ml/g}$  can be seen in the CCDF plots of Figure 6.6. The plot demonstrates a probability associated with a release from the Culebra in EPA units. This figure shows that the consequence of a one percent, zero matrix distribution coefficient for plutonium has virtually no effect on compliance. Only 10 vectors appeared on the plot, with the mean of all vectors superimposed on the figure. At a probability level of  $10^{-3}$ , less than  $10^{-4}$  EPA units will be released from the Culebra. The EPA limit for a  $10^{-3}$  probability is 10 EPA units. The extremely low consequence is attributed to the coupling of the releases to the Culebra that were calculated through NUTS and PANEL. Table 6.1. lists the releases of plutonium-239 and the total for all actinides for scenarios 2 through 6 to the Culebra. Scenario 1 assumes no human intrusion, therefore no waste is released from the repository to reach the Culebra aquifer. The low releases seen in Table 6.1. confirms the low probabilities associated with the radionuclides reaching the assessible environment.

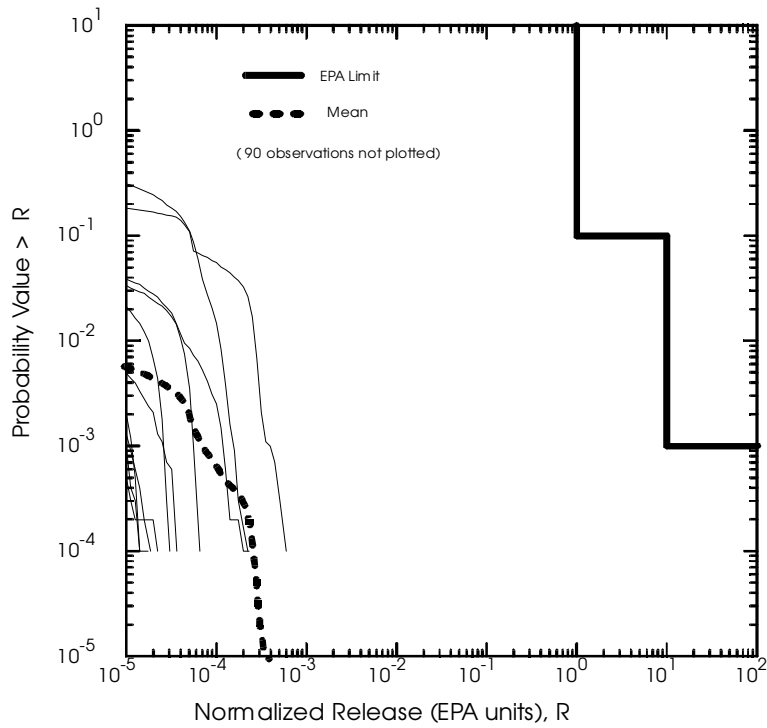


Figure 6.6. Total Normalized Releases from Culebra for 1%  $K_d=0$  ml/g for Plutonium Simulation

Scenario	Intrusion Time (yr)	Pu-239 Releases (U.S. EPA units)	Total for all Actinides (U.S. EPA units)
2	100	0.045	6.62
	350	0.044	6.04
	1000	0.044	2.19
3	3000	0.32	0.36
	5000	0.24	0.24
	7000	0.14	0.14
4	9000	0.035	0.04
	100	20.8	21.1
	350	20.1	20.4
5	1000	18.2	18.4
	3000	11.5	11.6
	5000	5.57	5.62
6	7000	1.09	1.10
	9000	0.027	0.03
	100	0.43	95.0
6	350	0.42	68.7
	1000	0.41	26.0
	2000	0.39	5.57
	4000	0.66	0.79
	6000	0.47	0.49
	9000	0.18	0.20

Table 6.1. Maximum Releases of Plutonium-239 and Total for all Actinides to the Culebra

## 6.5. Probability Modeling Of Actinides

Finally, the CCDF code was run assuming that 100% of all actinides that reached the Culebra crossed the boundary, instantaneously. This scenario can be used as an upper end bounding case for transport through the Culebra. The simulation was run for the first replicate only, and was found to fail the EPA compliance criteria at  $10^{-3}$  probability, as seen in Figure 6.7. Yet, one should not reach a conclusion that  $K_d$  could have significance from this plot. Further investigation shows that the failure is due to a single vector of high plutonium release to the Culebra. The transport coupled with the actinide source calculations from NUTS and PANEL may pose a possible threat in the 10,000 year future of the repository, but the transport alone, keeping all other parameters the same, is inconsequential.

## 6.6. Conclusions

The main focus of this study was to model the transport actinides through the Culebra Dolomite at the WIPP with a small portion of the radionuclides being nonreactive to the surrounding dolomite rock. Plutonium and uranium were simulated with a matrix partition coefficient ( $K_d$ ) equal to zero. Probability modeling was also conducted on all actinides to test the robustness

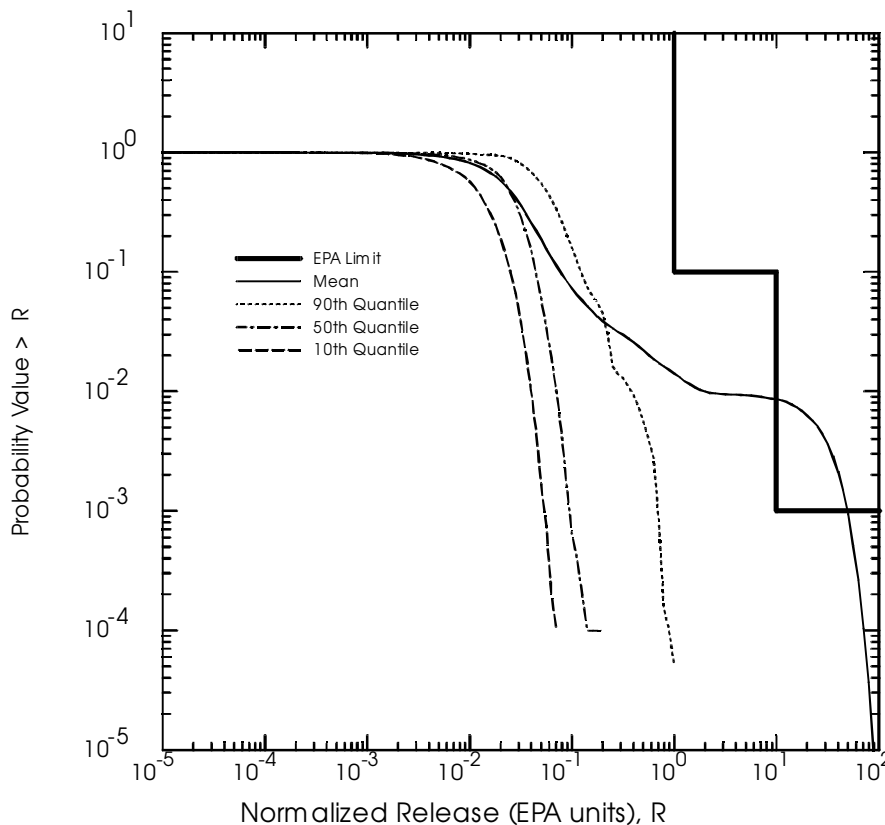


Figure 6.7. Total Normalized Releases for all Actinides Crossing the LWB

and consequences of all the actinides crossing the LWB in 10,000 years.

The plutonium simulations included 100 vectors for each partial and full mining scenarios for a single replicate. The results were summarized and incorporated into the CCDF curves of the CCA, as seen in Figure 6.6. Over half of the vectors (approximately 100 out of 200 vectors) had releases of at least 1% across the accessible boundary, which is substantial compared to the number that crossed in the CCA (zero out of 200). However, after coupling these unit releases with the actinide sources in NUTS and PANEL, the releases were shown to have negligible effect on the overall CCDF.

## **7. CASTILE BRINE RESERVOIR PARAMETERS**

### **7.1. Summary**

The results of a sensitivity analysis for several key parameters dealing with the Castile Reservoir and waste permeability are reported in this chapter. The modeling starts with flow calculations within the Salado Formation using BRAGFLO, and finishes by incorporating the results of the amount of solid waste and brine that may be ejected from an inadvertent human intrusion using CUTTINGS\_S and BRAGFLO\_DBR into a CCDF. The changed modeling parameters include Castile Reservoir volume, rock compressibility and permeability, and waste residual brine saturation and permeability. The results show that the overall mean of the CCDF does not increase above that seen in the CCA when all other performance assessment assumptions are used. The CCDF shows a trivial increase in releases when the probability of actually hitting the Castile reservoir increases from 8 to 100%.

### **7.2. Introduction**

The pressurized Castile brine reservoir that underlies the Waste Isolation Pilot Plant has been the subject of many debates on its extent and importance (EEG 1997b; 1997d; Silva 1994; U.S. DOE 1997a; Beauheim 1997). The scientists who setup the CCA performance assessment calculations recognized the fact that the brine could play a significant role in the degradation of wastes and waste container, if an inadvertent drilling intrusion were to pass through the repository to the brine reservoirs below, by assigning two of the six scenarios to calculate the effects of the breach. However, the characterization of the parameters associated with the reservoir were undermined by associating them to data that clearly lies outside of the domain of the repository. The more realistic parameter values proposed by the EEG could potentially demonstrate higher direct brine releases to the surface, affecting the compliance of EPA standards in the 40 CFR 191. Therefore, additional calculations were performed using more reasonable parameters for the simulation of Castile brine migrating into the repository. These calculations are referred to as the Castile Simulation.

### **7.3. Reservoir Parameters**

Reservoir parameters used in performance assessment calculations were derived from borehole information that lie mainly outside the domain of the WIPP repository. The distance to these boreholes ranged from 3.75 miles to over 11 miles from the repository center. Figure 7.1. shows the location of some of the boreholes used to characterize the Castile brine reservoirs. Two boreholes in particular, WIPP-12 and ERDA-6, stand out, as they were used most frequently to define Castile Reservoir parameters. The depths of these two boreholes vary significantly.



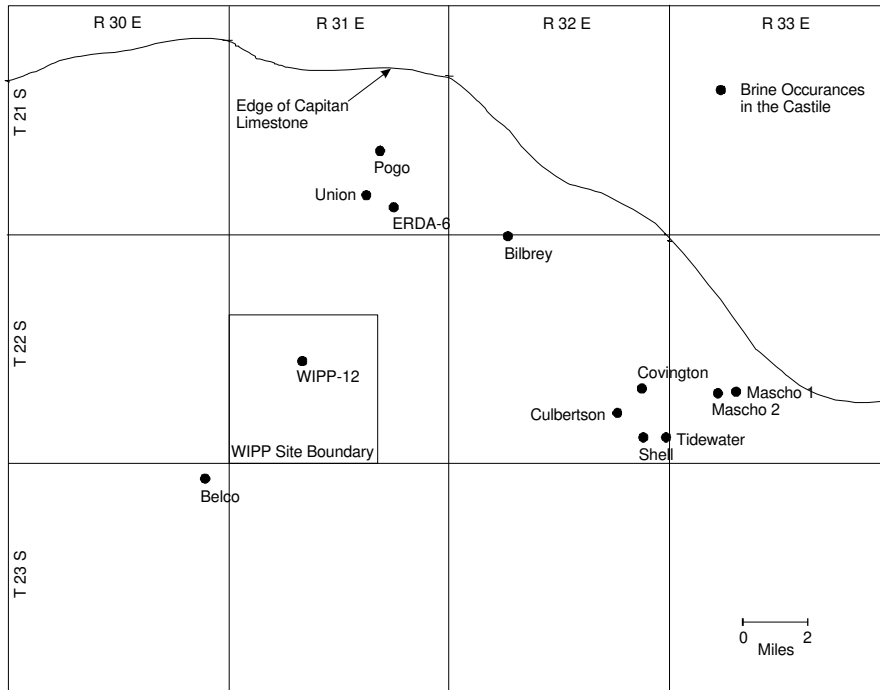


Figure 7.1. Location of Boreholes in the Castile Formation that were used to Characterize a Castile Brine Reservoir

WIPP-12 was bored into the Anhydrite I layer of the Castile to 3925 feet, whereas ERDA-6 had a total depth of 2775 feet into the Anhydrite II layer.

New values were assigned to several parameters that describe the Castile brine reservoir based on WIPP-12 data that is more closely identified to the conditions at the repository. The WIPP-12 borehole, is located within the WIPP site, one mile north of the repository. The borehole was originally drilled in 1978 and deepened in 1981 at the request of the EEG, which caused the repository to be moved south after brine was encountered at the borehole. The borehole experienced brine flow to the surface when drilling reached a depth of 3012 feet (D'Appolonia 1982). While extending the borehole to depths greater than 3,900 feet, a total of 80,000 barrels was allowed to flow from the borehole.

### 7.3.1. Productivity Ratio

The parameters associated with describing the Castile brine reservoir include reservoir volume, rock compressibility, reservoir pressure, and permeability. The correlation of volume and rock compressibility was recognized when Beauheim (1997) described a ratio based on these parameters. The productivity ratio is the product of the brine volume and rock compressibility by the porosity:

$PR = V \frac{C_r}{\theta}$ , where V is volume,  $C_r$  is rock compressibility, and  $\theta$  is porosity. This

value was identified by Beauheim (after CCA calculations were completed) to a range of 0.0007 m<sup>3</sup>/Pa to 0.04 m<sup>3</sup>/Pa. The range was based on more relevant data. The CCA calculations had a range that varied from 5.3x10<sup>-5</sup> m<sup>3</sup>/Pa to 0.06 m<sup>3</sup>/Pa.

Beauheim's new range was based on borehole data from ERDA-6 and WIPP-12. Both borehole encountered brine in the Castile formation, and it was assumed conservative that parameter values should include data from both boreholes to cover the uncertainty in a possible reservoir under the repository. However, using the lower value of the range, calculated from the ERDA-6 borehole, seems unjustified for the repository. The borehole is located approximately 6.4 km (4 miles) northeast of the site, and much less brine was encountered, compared to the WIPP-12 borehole. The upper value in the range was calculated from WIPP-12 data. Figure 7.2. shows the productivity ratios of the CCA with the new range suggested by Beauheim and where the WIPP-12 data lie.

A single productivity ratio value for WIPP-12 is the basis for additional simulations by the EEG. The value of 0.04 m<sup>3</sup>/Pa eliminates the dependence on boreholes in the far field, and places it solely on the importance of WIPP-12. The value is constructed by choosing a single value for the brine volume size and rock compressibility, and using the CCA value for porosity. The basis for the new volume and compressibility values are discussed below.

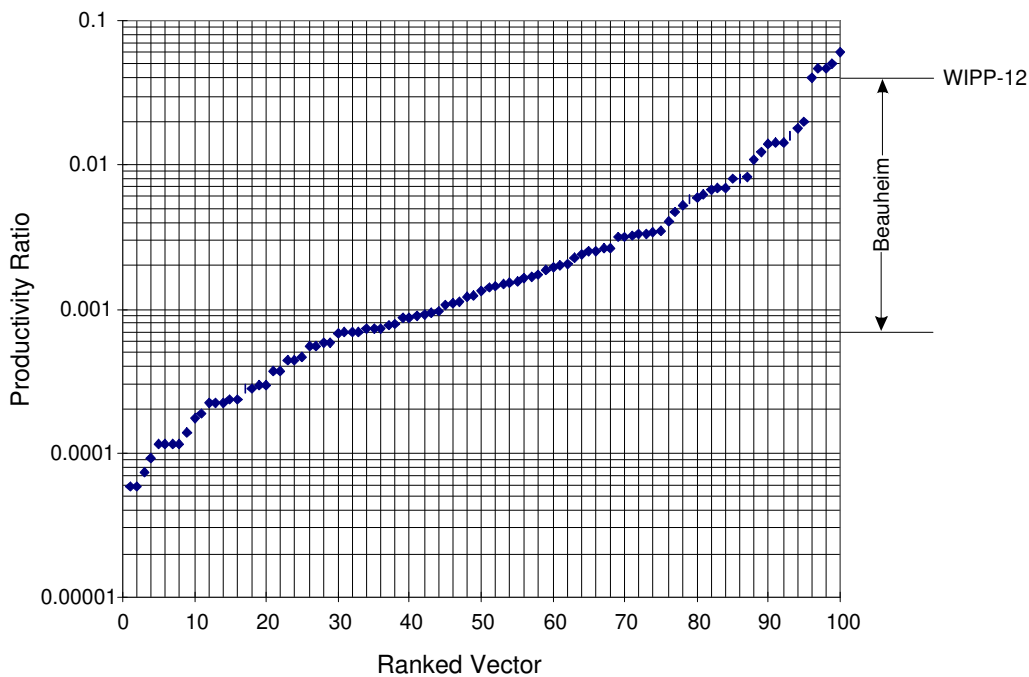


Figure 7.2. Productivity Ratio of the CCA for Replicate 1

### 7.3.1.1. Castile Brine Volume

Though unimportant as an individual concern in calculating the reservoir's function in the performance of the disposal system, the volume of the Castile brine may show the extent to which the reservoir attenuates underneath the repository. Chapter 5 of this report discusses the possibility of a higher probability associated with striking a pressurized brine reservoir. If the volume is grossly underestimated, then the likelihood of an encounter is low. The CCA values in the performance assessment used five different volumes: 32,000 m<sup>3</sup>, 64,000 m<sup>3</sup>, 96,000 m<sup>3</sup>, 128,000 m<sup>3</sup>, and 160,000 m<sup>3</sup>. The smallest of these was calculated from WIPP-12 data assuming a compressibility of  $5 \times 10^{-12} \text{ Pa}^{-1}$  and porosity of 0.008 (Larson and Freeze 1996). A maximum calculated reservoir volume of 64,000,000 m<sup>3</sup>, based on a compressibility of  $10^{-8} \text{ Pa}^{-1}$ , was rejected by assuming either that multiple intrusions into the reservoir would deplete the availability of brine, or that the brine reservoirs were not interconnected with highly conductive fractures to produce a single large combined volume. It was theorized that small, highly pressurized brine reservoirs would produce higher brine flow to the repository than large depressurized pockets.

The report describing the WIPP-12 brine reservoir data (D'Appolonia 1983) lists a calculated volume of 2,700,000 m<sup>3</sup>, based on pore compressibility values different from the CCA values (discussion below). When the range was suggested by Beauheim (1997) to be 100,000 - 1,700,000 m<sup>3</sup>, the performance assessment calculations were already complete and the change was postulated to have no effect on compliance due to the single importance of the productivity ratio. However, new calculations should be performed to include a more reasonable brine reservoir volume from more relevant data.

### 7.3.1.2. Rock Compressibility of Castile Reservoir

The rock compressibility data for the performance assessment calculations were established on laboratory measurements of an Anhydrite III core from the WIPP-12 borehole, in-situ hydraulic testing of Salado anhydrite and halite, and textbook ranges (Freeze and Cherry 1979) of fracture rock compressibility. The compressibility was calculated from Equation 6-3 in (Beauheim et al. 1990),

$$C_r = \frac{1}{K + \frac{4G}{3}},$$

where K is the grain modulus (or bulk modulus) and G is the shear modulus. The bulk modulus of the Anhydrite III core was estimated to be  $6.9 \times 10^{10} \text{ Pa}$ , but a value of shear modulus was not

known. It was determined that  $G$  was approximately  $1/3 K$  for Salado anhydrites (Beauheim et al. 1990), and again was used in calculating the compressibility for Castile anhydrite. Hence, the core data indicates  $C_r = 1 \times 10^{-11} \text{ Pa}$ . However, the range was changed based on hydraulic testing performed on Salado anhydrites and halites. The lower compressibility value in the CCA range was calculated to be  $5 \times 10^{-12} \text{ Pa}^{-1}$ , and the upper value was from the textbook value of  $1 \times 10^{-8} \text{ Pa}^{-1}$  based on the potential effects of the fracture on formation compressibility.

The compressibility was determined in an earlier report (D'Appolonia 1983) based solely on the bulk modulus and porosity from the equation,

$$C_r = \frac{1}{\phi K},$$

where  $\phi$  is the porosity and ranges from 0.001 to 0.01 in Castile anhydrites. This definition of compressibility was derived from the basic understanding of the compressibility in porous media. The values for compressibility were calculated to be  $1.45 \times 10^{-7} \text{ Pa}^{-1}$  to  $2.9 \times 10^{-9} \text{ Pa}^{-1}$  with bulk moduli ranging from  $6.9 \times 10^9 \text{ Pa}$  to  $3.45 \times 10^{10} \text{ Pa}$ . Therefore, it is possible that the range used in the CCA are too small. A larger value is suggested here, that would correlate with the volume to produce a productivity ratio of  $0.04 \text{ m}^3/\text{Pa}$ .

### 7.3.2. Castile Reservoir Pressure

The initial pressures of the Castile reservoir ranged from 11.1 MPa to 17.0 MPa in the CCA calculations based on observed data from four boreholes drilled to depths of the Castile formation. The WIPP-12 data were clearly the best measured values with a pressure at 12.7 MPa (Larson and Freeze 1996), but the range was extended to include the Covington (Figure 7.1.) and ERDA-6 data and adjusted for lithostatic pressures at the WIPP level. The adjusted range for CCA calculations should have been 11.1 MPa to 16.4 MPa, but was increased to 17.0 MPa. Although higher values are more conservative, the most reasonable value should be used. EEG used a fixed Castile reservoir pressure of 12.7 MPa.

### 7.3.3. Castile Reservoir Permeability

The permeability of the Castile reservoir ranged from  $1.6 \times 10^{-10} \text{ m}^2$  to  $2.0 \times 10^{-15} \text{ m}^2$  in the CCA calculations. The calculations performed by the EEG used slightly different values, ranging from  $5.8 \times 10^{-11} \text{ m}^2$  to  $5.8 \times 10^{-15} \text{ m}^2$ . The new values used a median of  $5.8 \times 10^{-13} \text{ m}^2$  based on Beauheim (1997) and were increased and decreased by two orders of magnitude to create the upper and lower values in the range, to cover uncertainty. The role of the Castile permeability is relatively unimportant, and does not affect the amount of brine that eventually migrates upward to the Culebra. The flow of brine up the borehole is controlled by the borehole permeability.

However, the Castile brine movement will affect the amount of brine that will reach the repository to be released through a breach. With the small changes in this parameter, it is unlikely that it would have a significant affect on the new calculations.

#### **7.3.4. Other Parameter Changes**

Since the simulations using the changed parameters as suggested by the EEG would take a considerable amount of time to complete, it was reasoned that two additional parameters would be included in the Castile Simulation. The two parameters are waste permeability and waste room residual brine saturation, and each describe different processes of the repository.

##### **7.3.4.1. Waste Permeability**

The permeability of the waste in the repository was a constant in the CCA, equal to  $1.7 \times 10^{-13} \text{ m}^2$ . This value was derived from consolidated waste made from sludge, combustibles, and metals. However, a peer review (U.S. DOE 1996-Appendix Peer 1) of the work found an error in the calculation and suggested a new value of  $2.4 \times 10^{-13} \text{ m}^2$ . The new value will allow a higher brine flow through the repository, up the borehole, and to the surface. It will directly impact the amount of direct brine releases, and a constant value of permeability is more conservative than a range of values, which would incorporate lower values.

##### **7.3.4.2. Residual Brine Saturation**

The parameter for residual brine saturation is used in calculating the relative permeability of brine in the waste and to define the capillary pressure curves for the models of partial saturation. The number is expressed as a fraction between 0 and 1, and brine is immobile when the brine saturation is below the value of the parameter. Therefore, this parameter may be very important in postulating the amount of brine that will move through the waste area up the borehole to the surface. Numbers that are too large will inhibit brine movement.

The data used in calculating the residual brine saturation in the CCA does not relate to any material from the waste or the disposal system. Instead, the data are typical values from literature for unconsolidated material, ranging from 0.0783 to 0.560. However, the largest value in the range is from a consolidated sandstone. The EEG believed that this value should be ignored, and the range reduced with an upper value of 0.318 (from fragmented sandstone). The EEG has since concluded that the original range used in the CCA was appropriate and that the calculations performed in this analysis are conservative, due to the consolidation of waste after creep closure of the rooms.

## 7.4. Methodology

The objective of the new calculations was to determine the change in the amount of radionuclide release from the repository due to the changes in the Castile reservoir and waste area parameters. This was accomplished by (1) running BRAGFLO to determine the brine saturations, pressures, and repository porosities, (2) running CUTTINGS to determine the amount of solid material that would be brought to the surface and to establish initial conditions to be used in BRAGFLO\_DBR and (3) running BRAGFLO\_DBR, which uses the data from CUTTINGS and BRAGFLO to calculate the volume of brine released from the repository. Each code required a set of separate steps to run, and are presented below.

### 7.4.1. BRAGFLO Calculations

The only changes in running the suite of codes was in BRAGFLO. Table 7.1. lists the parameters and the values that were used in the CCA, suggested ranges by Beauheim (1997),

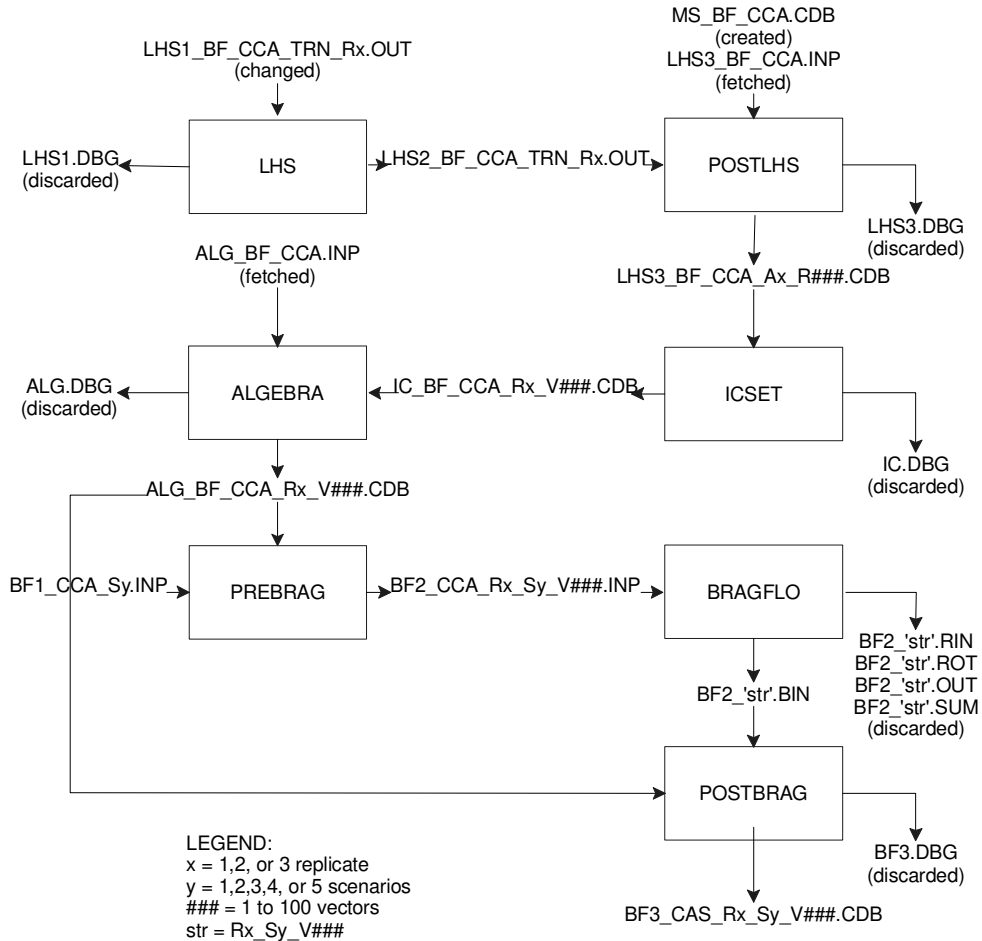


Figure 7.3. Flowchart for BRAGFLO Calculations

Simulation	Log Reservoir Permeability (log m <sup>2</sup> )	Initial Pressure (MPa)	Log Rock Compressibility (log Pa <sup>-1</sup> )	Reservoir Volume (m <sup>3</sup> )	Waste Permeability (m <sup>2</sup> )	Waste Room Residual Brine Saturation
CCA	-9.8 to -14.7	11.1 to 17.0	-8 to -11.3	32,000 to 160,000	1.7x10 <sup>-13</sup>	0 to 0.552
Beauheim (1997)	-10.2 to -14.7	11.1 to 16.5	-9 to -10.7	100,000 to 1,700,000	NA	NA
EEG <sup>*</sup>	-10.23 to -14.23	12.7	-8.66 <sup>*</sup>	160,000 <sup>*</sup>	2.4x10 <sup>-13</sup>	0 to 0.318

Table 7.1. Castile Reservoir Parameter Suggestions

<sup>\*</sup> BRAGFLO only allowed the choice of 5 volume sizes: 32,000 m<sup>3</sup>, 64,000 m<sup>3</sup>, 96,000 m<sup>3</sup>, 128,000 m<sup>3</sup>, and 160,000 m<sup>3</sup>. The largest volume size available was chosen and the compressibility was calculated based on a productivity ratio of 0.04 m<sup>3</sup>/Pa. The porosity for the calculation remained at 0.0087. If the recommended volume of 2,700,000 m<sup>3</sup> could have been chosen as the measured size, then the log compressibility value would be -9.88 log Pa<sup>-1</sup> (1.28x10<sup>-10</sup> Pa<sup>-1</sup>).

and the new range for the present EEG calculations.

The changes in the simulations started at the LHS files. The values and ranges were modified to reflect the new selected parameters. Figure 7.3. shows the flowchart of the BRAGFLO suite of codes and where the changes were made. The massive amount of files created from the

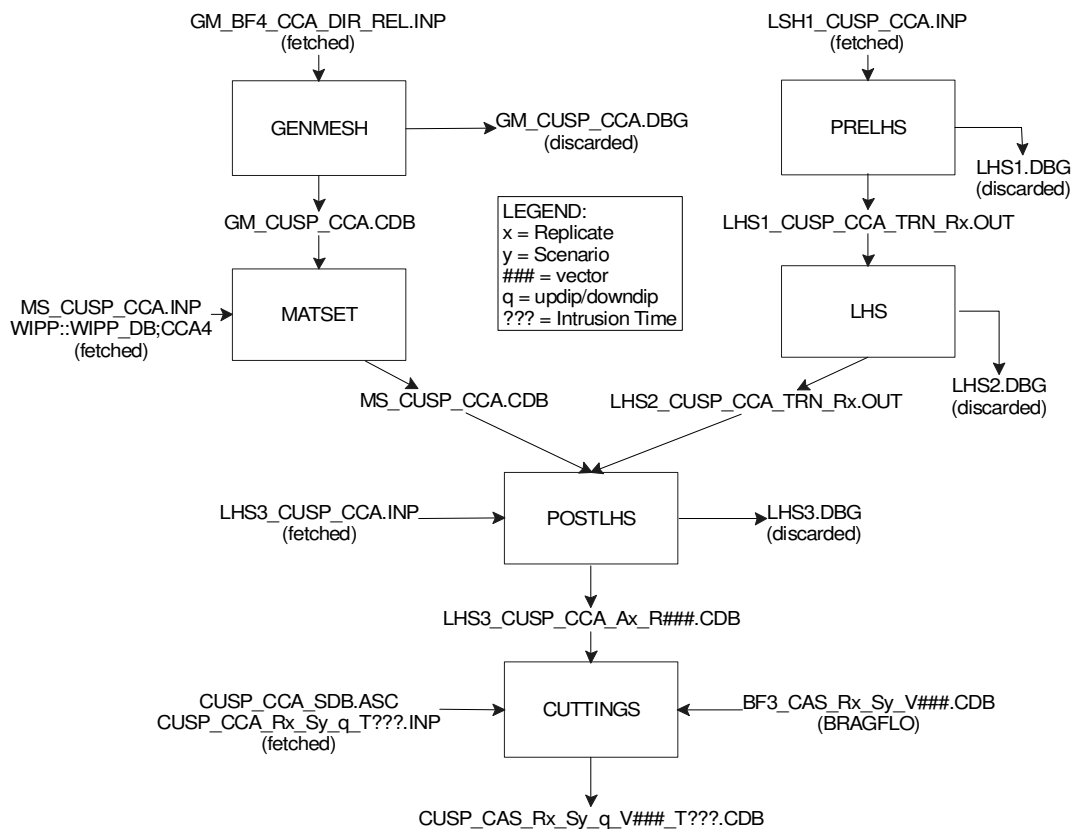


Figure 7.4. Flowchart of CUTTINGS\_S Simulations

simulation allowed only two files from each vector to be retained, the postprocessed BRAGFLO file, BF3\_CAS\_R1\_Sy\_V###.CDB and the input file for BRAGFLO, BF2\_CAS\_R1\_Sy\_V###.INP, where 'y' is the scenario and '###' is the vector number. Both files are important to running other codes.

Due to time and disk space constraints, only two scenarios of one replicate could be simulated. The two scenarios, S2 and S3, deal with an E1 intrusion. The E1 intrusion describes the possibility of a drill intrusion through the repository to the pressurized brine pockets below. The remaining four scenarios would be unaffected by the changes in Castile brine reservoir parameters, but would show slightly different releases due to the waste area parameter changes.

#### **7.4.2. CUTTINGS\_S Calculations**

The release of solid materials from a drill intrusion was calculated in CUTTINGS\_S. The code extracted information from the BRAGFLO simulation to establish the amount of material brought to the surface. Figure 7.4. shows the steps involved in running the CUTTINGS\_S suite and where the BRAGFLO output file is read.

As explained in Chapter 2, the CUTTINGS code calculates the effects of a drill intrusion at other times than specified by the scenario number. An S2 scenario assumes an E1 initial intrusion at 350 years, and uses that information to calculate an E2 intrusion at 550, 750, 2,000, 4,000, and 10,000 years. The S3 scenario assumes an E1 initial intrusion at 1,000 years, and calculates an E2 at 1,200, 1,400, 3,000, 5,000, and 10,000 years. The large number of time intrusions allow the CCDFGF code to scale the releases over the 10,000 year future of the repository.

The CUTTINGS\_S code also calculates an intrusion into two areas of the repository. The repository is on a 1° slope to the south, and is divided into updip and downdip regions. The downdip includes Panels 4 and 5, whereas the updip includes Panels 1,2,3,6,7,and 8. It is suspected that the downdip panels will fill with brine sooner than in the updip due to gravity, producing a higher activity of gas generation from corrosion and microbial activity. The gas generation will increase the pressures in that area until pressure is equilibrated with the surrounding rock. If the repository is breached, the downdip region should release more waste and brine to the surface. The updip portion of the repository remains virtually closed off from the downdip as a result of creep closure and low permeability of waste, thus prohibiting migration of brine to the area. Therefore, a totally separate calculation is performed for the two areas.



Unlike the other two codes in the sequence, CUTTINGS\_S also indirectly calculates the amount of radionuclides released to the surface. Therefore, the files are retained for input to the CCDFGF code for probability assessment.

### 7.4.3. BRAGFLO\_DBR Calculations

Lastly, the BRAGFLO\_DBR code is used to calculate the amount of brine released directly to the surface. The code uses the CUTTINGS and BRAGFLO results for initial conditions and extracts the parameters needed for calculations. Figure 7.5a. and Figure 7.5b. lists the configuration of a direct brine release calculation. The time intrusion calculations for the direct brine release are the same as for CUTTINGS.

The direct brine release calculation uses only the downdip CUTTINGS files. The downdip panels have higher pressures, producing higher saturations and releases. However, releases are not calculated for every simulation. Some vectors do not result in a release, i.e., the pressures and/or saturations in the repository may not be high enough to overcome the column of drilling

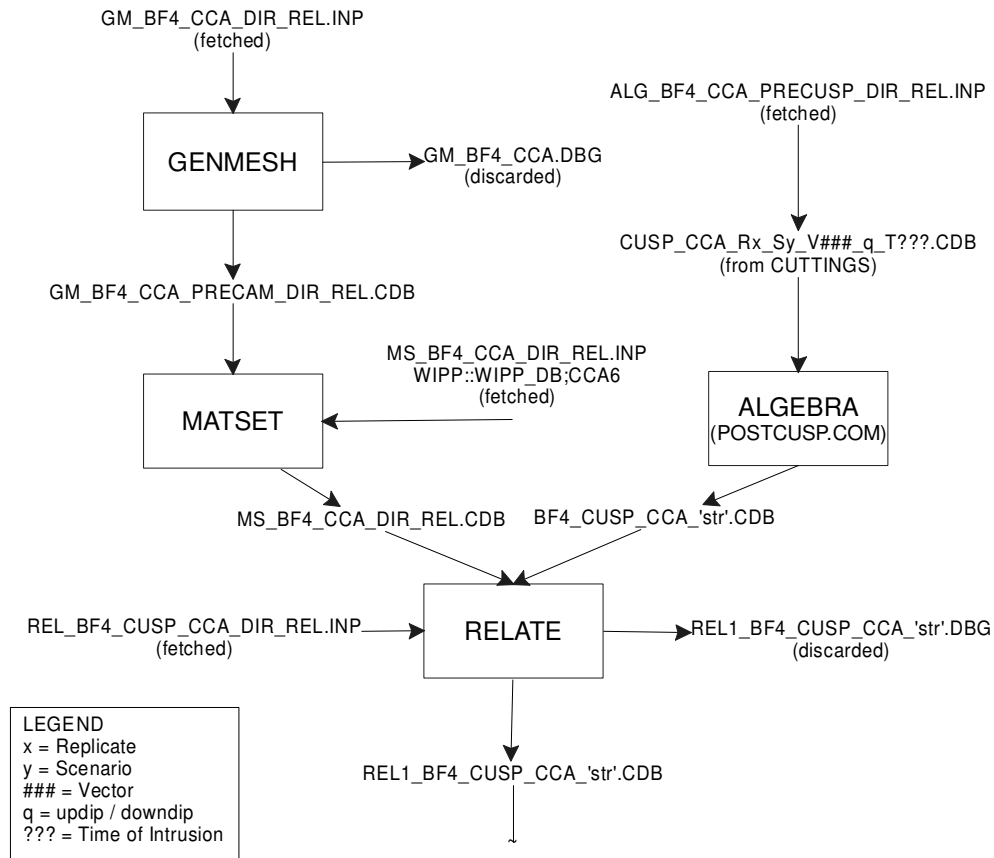


Figure 7.5a. Flowchart of BRAGFLO\_DBR

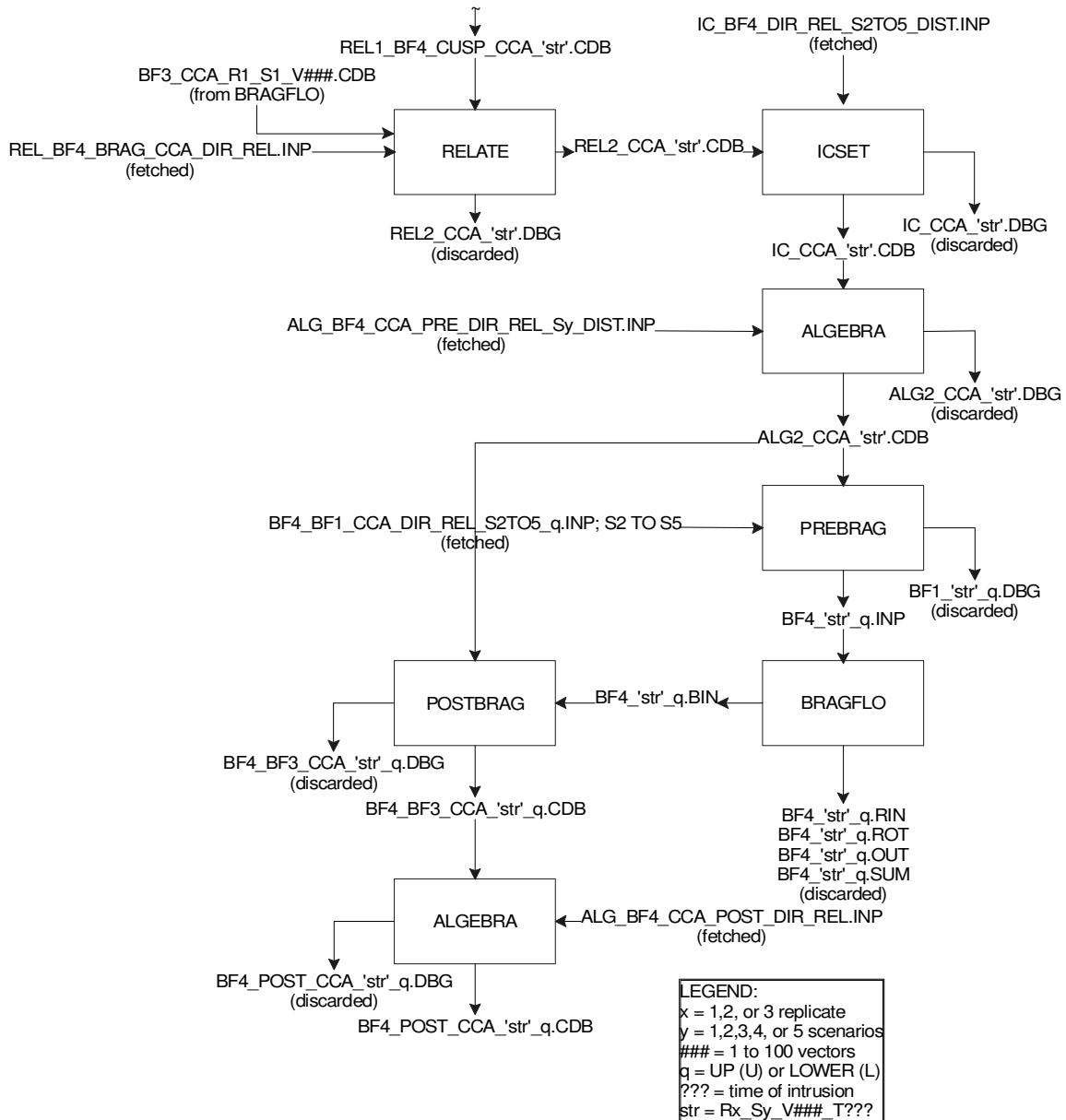


Figure 7.5b. Flowchart of BRAGFLO\_DBR (cont.)

mud or there may not be an availability of brine due to consumption from corrosion or microbial activity. Those that do qualify undergo a 50 day simulation, with blowout lasting a minimum of three days. This is the estimated time it takes to drill through the repository to the Castile reservoir and cement the casing. If there is a significant amount of gas flow from the repository, the driller may lose control and brine releases may last longer. The releases will accumulate until the gas flow rate drops below an arbitrary value, set to 100,000 ft<sup>3</sup>/d in the CCA calculations. The maximum blowout duration is 11 days, and is based on the time it took to control the South Culebra Bluff Well Unit # 1, which blew on January 1978 (Stoelzel and O'Brien 1996).

## **7.5. Results**

The results of the amount of brine released to the surface are as predicted. With an increase in productivity ratio and waste permeability, coupled with a decrease in the range for residual brine saturation, an overall increase in the volume of brine was observed to be released.

### **7.5.1. BRAGFLO Results**

#### **7.5.1.1. The Repository**

The BRAGFLO calculations performed on the two scenarios that modeled intrusion into the Castile reservoir showed higher brine pressures and higher brine volumes in the repository than what was modeled in the CCA. Higher pressures will allow more releases from spall and direct brine release. Higher brine volumes indicate more brine to (1) corrode waste containers, which will produce high pressures, and (2) be released through a direct brine release scenario. Though more brine with less gas would intuitively indicate more releases to the surface, a limit is seen, after which this is not the case because gas is needed to drive the brine up the borehole. If pressurized gas is eliminated, then no brine would reach the surface without pumping.

The results of the BRAGFLO simulations were postprocessed by codes described in the Analysis Package, Task 1 (Bean et al. 1996). The codes calculated average values in each area of the repository for elemental cells and created a total of 215 time history variables (pressure, saturation, volume of brine consumed, etc.) that were plotted in SPLAT (CMS plotting program). The results herein mainly use the average value for all vectors as comparison.

Figure 7.6. shows a comparison of repository pressures in the waste area of the Castile simulation to repository pressures of the CCA. The figure shows two plots. The left plot shows the mean results of an E1 intrusion at 350 years for both simulations, and the right shows the mean results with an intrusion at 1,000 years. The pressures are averaged over the entire volume of the waste area only, and excludes pressures from the operations and experimental regions. It is clearly evident that both plots in the figure show higher pressures for the Castile Simulation. The difference between the Castile Simulation and the CCA in average pressures at 350 years for S2 is approximately 3.25 MPa. The pressures rise sharply up to the intrusion point due to gas generation from the availability of iron in the waste and waste containers, and from the organics (cellulosics, rubber, plastic, etc.). After intrusion, the borehole is assumed to be plugged immediately, with plug lifetime lasting 200 years. Once the plug degrades, the gas in the repository is vented, until eventually creep reduces the borehole permeability at 550 years postclosure, allowing pressures to rebuild until most of the cellulosic inventory is exhausted

(around 1,500 years). A steady decline in pressure for the remaining 8,500 years is noticed, with the Castile simulation always being at least 1.8 MPa higher.

The simulation with the intrusion borehole entering the Castile Formation at 1,000 (S3) years exhibits similar behavior as the S2 scenario. The pressure builds in the repository until gas and brine is allowed to escape. The pressure declines after plug degradation, and rebuilds until all organic material is consumed. The pressures eventually decrease steadily for the remaining time of the repository history. The differences in the Castile simulation and CCA, though not as drastic as the previous S2 simulation, are still substantial. The differences are around 1.75 MPa at the time of intrusion, and decrease to 1.3 MPa around 10,000 years. The higher pressures in the repository of S3 compared to S2 would indicate higher releases to the upper layers above the repository and to the surface, and will be discussed later.

The higher pressures are a result of more brine entering the repository from the Castile brine reservoirs' below. The brine mixes with the waste and degrades the organic material, which produces gas. Figure 7.7. shows, for both scenarios, the amount of brine entering the whole repository from the Castile reservoir. The flow of brine from the Castile up the borehole to the repository is an effect of the high differential pressure between the Castile and repository. The values were calculated by subtracting the net inflow of brine from the marker beds and the brine volume consumed through corrosion and degradation. Again, both plots show a higher amount of brine entering the repository from the Castile simulation. This may be from the combination of the set constant value of 160,000 m<sup>3</sup> for Castile Reservoir volume and productivity ratio. The CCA used a range from 32,000 to 160,000 m<sup>3</sup>, with a 1/32 chance of getting the 160,000 value

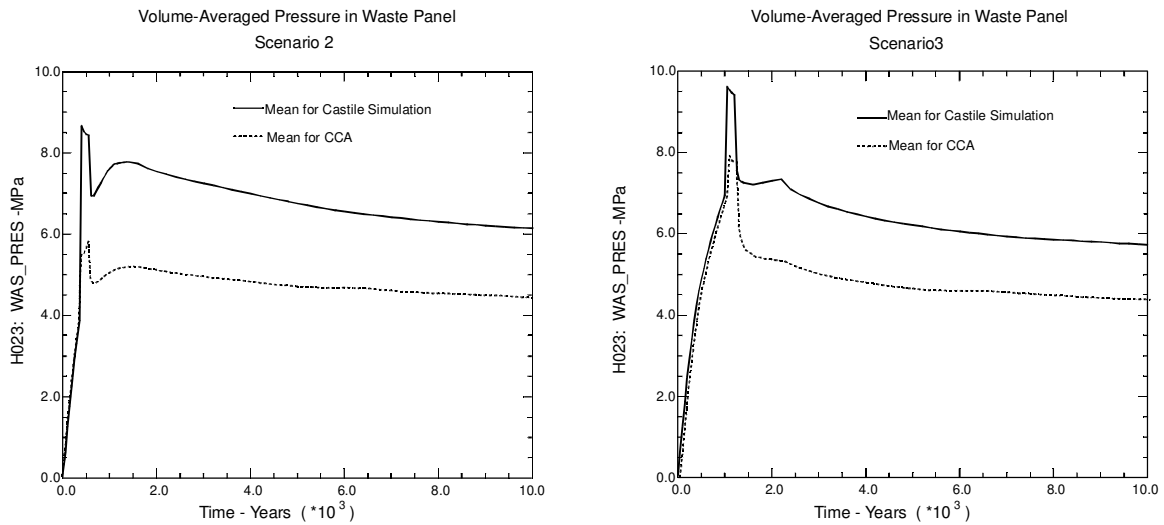


Figure 7.6. Volume Averaged Pressures of 10,000 Year Time History for Left) Scenario 2 and Right) Scenario 3

for volume and a range of 0.0007 to 0.04 m<sup>3</sup>/Pa for productivity ratio.

The differences in the two simulations are very notable, varying by as much as 20,000 m<sup>3</sup> in S2. Both simulations also follow the same pattern. For the scenario of borehole intrusion at 350 years, the repository quickly fills with brine after closure, decline linearly as brine is consumed through corrosion of iron and degradation of organics. When the intrusion borehole hits the brine pockets below the repository, it fills at a higher rate until a pressure equilibrium is reached between the repository and brine pockets. A steady decline marks the remaining future of the repository, with minor amounts of brine being consumed and the rest being leaked to the stratigraphic units that lie above the repository and minor amounts flowing back down the borehole to the reservoir.

The S3 scenario behaves slightly differently from S2 with less total brine entering the repository. After the intrusion at 1,000 years, the amount of brine does not immediately decrease, but increases slightly for approximately 1,000 years (between 1,000 and 2,000 years postclosure). The gain of almost 2,000 m<sup>3</sup> of brine in both the CCA and Castile Simulation can be attributed to the pressure recovery seen in Figure 7.6. After the intrusion, the pressure for S3 does not recover like that seen in S2, allowing more brine to enter, and pressure equilibrium is reached approximately 500 - 1,000 years after intrusion (1,500 to 2,000 years postclosure). The mean

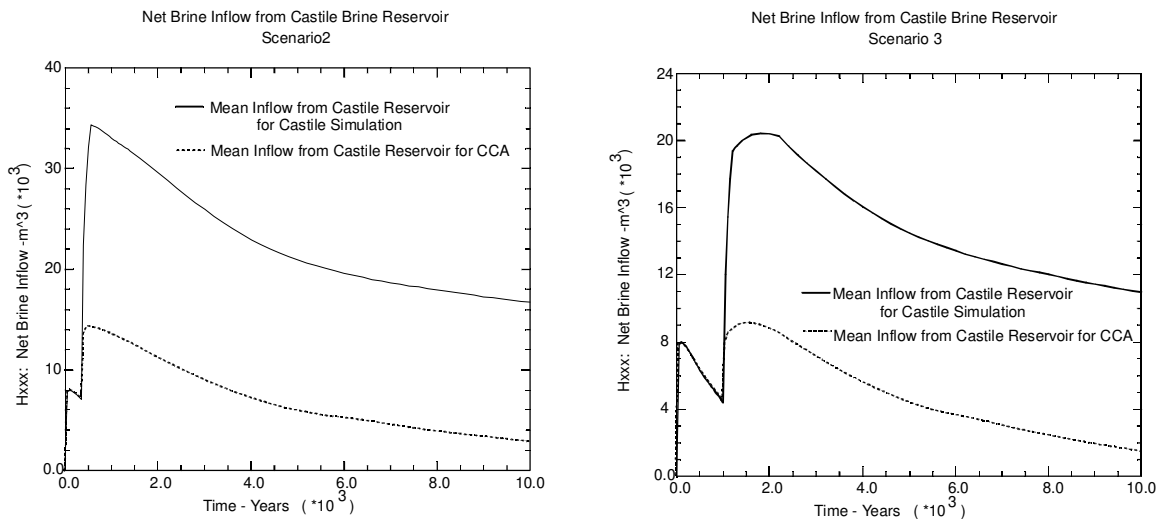


Figure 7.7. Net Inflow of Brine from Castile Reservoir for CCA and Castile Simulation for Left) Scenario 2 and Right) Scenario 3

	S 2		S 3	
	CCA	Castile	CCA	Castile
Fraction of Steel Remaining after 10000 years	55.06	42.04	57.60	50.59
Fraction of Cellulose Remaining after 10000 years	50.02	50.01	50.02	50.01

Table 7.2. Fraction of Steel and Cellulosics Remaining after 10000 Years

for CCA and Castile Simulations for S2 and S3

pressure curves of Figure 7.6. are dominated by vectors that exhibit low corrosion rates in that region.

With the inflow of brine to the repository, gas volumes also soar after intrusion. Figure 7.8. shows total mean of gas volumes generated from corrosion and microbial degradation (both humid and inundated) for the CCA and Castile simulation for Scenarios 2 and 3. The Castile simulation follows the CCA's calculated gas volumes before the intrusion, then increases significantly there after. The increase in the amount of brine reaching the repository has a direct effect on the amount of gas generated, as seen in the figure. As the Castile simulation allows more brine to enter the repository, more gas is generated. Even though microbial decay ceases for the most part after 1500 years, corrosion of the steel drums continue for the entire 10,000 years. The fraction of steel and cellulose remaining after 10,000 years can be seen in Table 7.2. The amount of steel remaining for the Castile simulation offers a good insight on the differences seen in Figure 7.8.

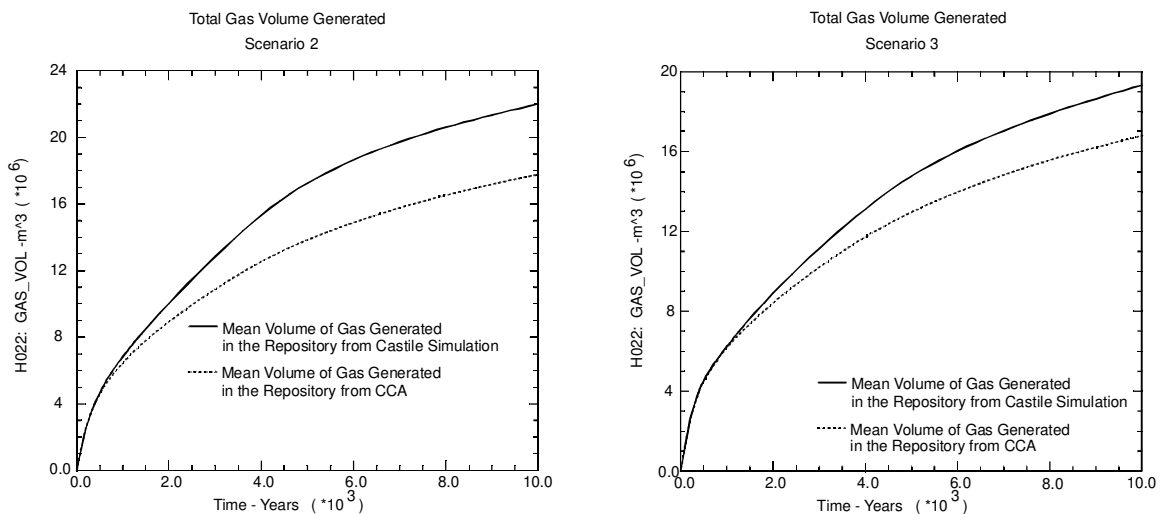


Figure 7.8. Total Gas Volumes Generated from Corrosion and Microbial Degradation for CCA and Castile Simulation for Left) Scenario 2 and Right) Scenario 3

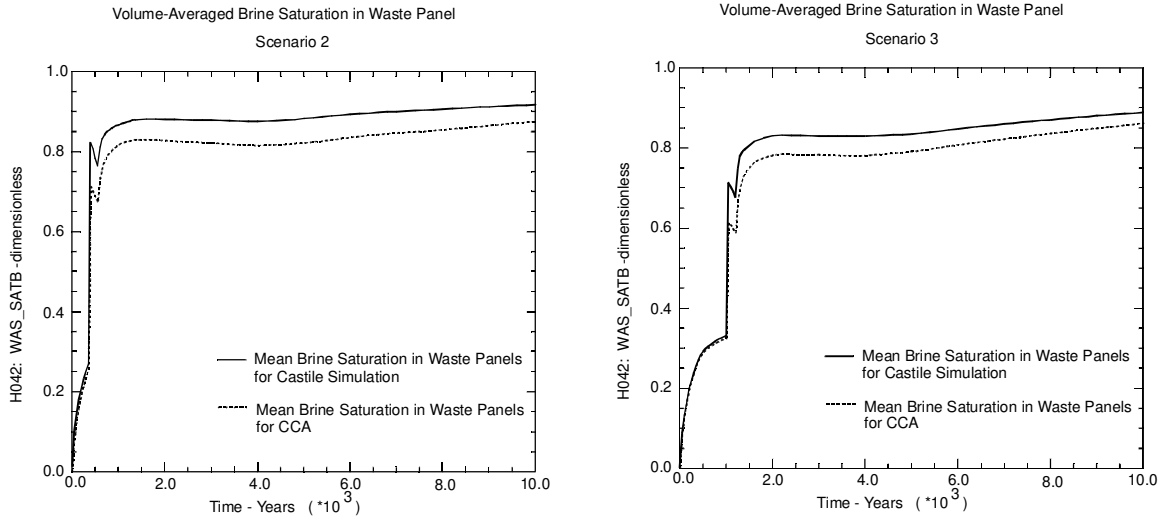


Figure 7.9. Volume Averaged Brine Saturation in Waste Panels for CCA and Castile Simulation for Left) Scenario 2 and Right) Scenario 3

Lastly, the saturation of brine plays an important role in the availability of gas as a mechanism for pushing the brine out through the borehole. Figure 7.9. shows how the fraction of brine as compared to gas increases through time, as brine enters from the Castile reservoir. The Castile simulation follows the CCA up to the time of intrusion for both scenarios, with the Castile simulation increasing in saturation after intrusion. The differences between the Castile simulation and the CCA are around 0.1 at the time of intrusion, but remain at 0.05 for the rest of the time history of the repository for both scenarios. The availability of brine to be released is definitely increased in the Castile simulation, but Figure 7.9. may indicate that the ratio of brine to gas may be too high to push the brine up the borehole.

### 7.5.1.2. Fluid Flow through the Borehole

The flow of brine and gas up the borehole to the upper stratigraphic members is linked closely to the values for permeabilities selected by the LHS code. Following the intrusion, brine and gas from the repository move up and/or down the borehole, depending on the pressures, permeabilities, and the time of occurrence. Figure 7.10. shows the cumulative brine flow up the borehole to the top of the panels. The individual vectors are represented here to demonstrate the influence of chosen parameters on the system.

The discharge of brine out through the borehole to the units above the repository for the Castile simulation is higher than what was calculated in the CCA. The CCA's maximum release was 22,500 m<sup>3</sup> for S3 with only four vectors releasing above 4,000 m<sup>3</sup>. This is about 14,000 m<sup>3</sup> less than the Castile simulation's maximum release, which had 20 vectors above 4,000 m<sup>3</sup>. The vector showing the highest release in Figure 7.10. for the Castile simulation, Vector 23, is the

same vector with the highest release in the CCA, indicating the physics of the system is roughly the same.

Scatter plots of permeability versus brine discharged up the borehole to the top of the waste panels reveal that the permeability of the degraded concrete plug, BH\_SAND, is more closely related to the discharge than any other permeability investigated, with a correlation coefficient ( $r^2$ ) of 0.846. This indicates that as the permeability of the degraded borehole plug increases, the amount of brine flowing upwards increases. Figure 7.11. shows four scatter plots, using sampled permeabilities from different regions of the disposal system with the correlation coefficient located in the lower right-hand corner of each plot. The figure shows, from upper left to lower right, 1) the plots for permeability of degraded borehole, 2) Castile reservoir, 3) surrounding undisturbed halite, and 4) Marker Bed 139. The scatter plot is for the Castile simulation, Scenario 2 only. It is interesting to note that when the vector of highest brine flow is removed (Vector 23-36,000 m<sup>3</sup>), the  $r^2$  for BH\_SAND increases to 0.912, and the other three essentially become zero.

Once the brine passes the top of the repository, it moves further up the borehole to the Culebra and eventually to the surface. However, as it moves upward, the brine loses energy through interactions with the borehole wall and overcoming the gravitational effects, and many of the vectors do not make it to the upper layers. Figure 7.12. shows the flow of brine in the borehole to the top of the Rustler Formation. Similar to Figure 7.10., this figure shows the individual vectors for S2 and S3 of the Castile simulation only. The figure reveals that little to no brine makes it this high up the borehole, with a maximum of 1.55 m<sup>3</sup> for S2 and 5.0 m<sup>3</sup> for S3. Further investigation shows that no brine reaches the surface for either scenario. Figure 7.12. shows

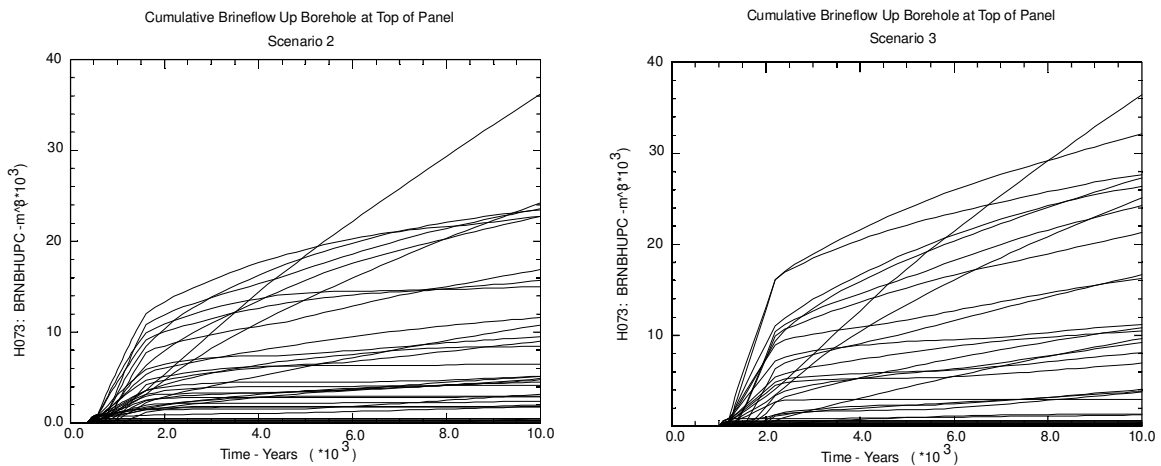


Figure 7.10. Cumulative Brine Flow up the Borehole from Waste Panels to the Top of the Panel for Castile Simulation of (Left) Scenario 2 and (Right) Scenario 3



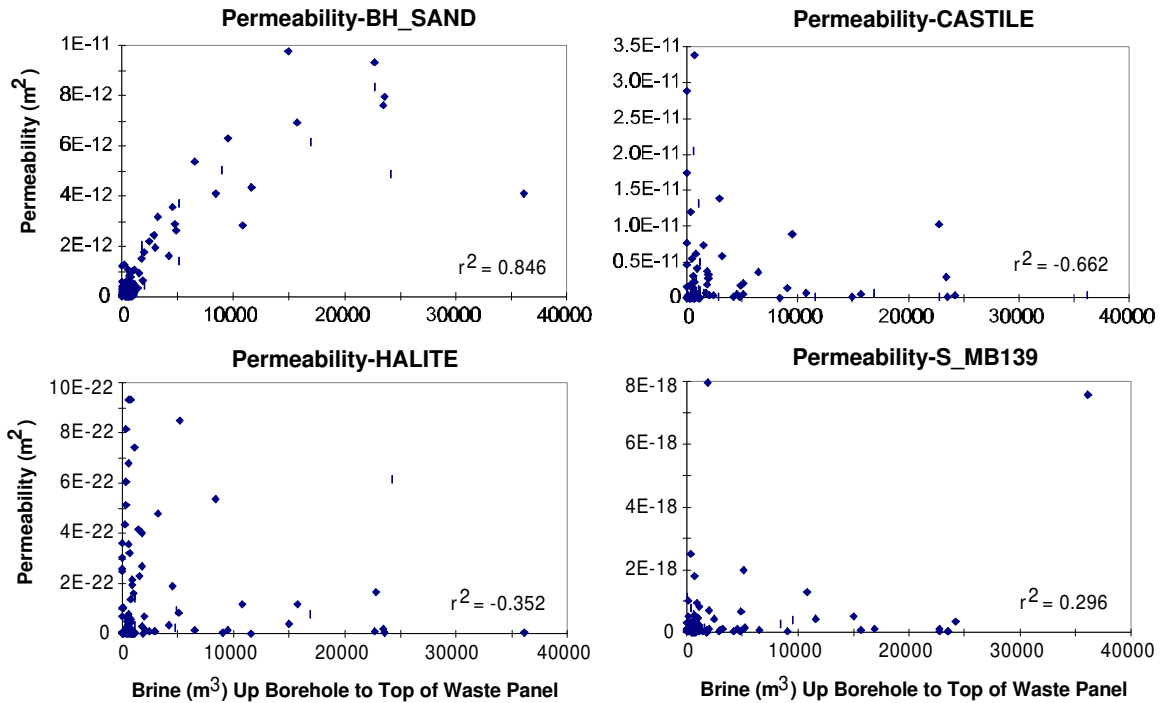


Figure 7.11. Scatter Plot for Volume of Brine Reaching the Top of The Waste Panels through an Intrusion Borehole and Permeabilities from Regions of the Disposal System with Permeabilities Described from Upper Left to Lower Right: 1) Degraded Concrete Plug (Silty-Sand), 2) Castile Reservoir, 3) Halite that does not Include the Disturbed Rock Zone (DRZ), and 4) Marker Bed 139

that if the brine can make it as far as the Dewey Lake Formation, it does so very quickly, with S3 contributing more brine than S2 due to the pressure differences in the two simulations.

The flow of brine up the exhaust shaft is considered minimal when compared to the borehole. At most  $49 \text{ m}^3$  flowed up the shaft to the Salado, with no brine reaching the Rustler Formation for the Castile simulation. This is comparable to the CCA, which only had a maximum of  $48 \text{ m}^3$  of brine up the shaft, because the assumption of pressure, borehole permeability, and the mechanisms of loss of pressure were the same.

### 7.5.2. Cuttings, Cavings, and Spallings Results

The borehole and solid waste material removal were calculated using CUTTINGS\_S, a cuttings and cavings code that also incorporates spallings. The CCA identified both mechanisms as major contributors to radionuclides reaching the accessible environment, and calculations were made to quantify the effects of both. The following discussion compares results of the CCA to those calculated by changing the Castile reservoir parameters.

### 7.5.2.1. Cuttings and Cavings

The cuttings and cavings calculations were performed at several times throughout the repository future. Section 7.4.2. lists the times that were used for borehole removal. At each time calculation, the amount of material removed through cuttings and cavings were the same for the CCA and the Castile simulation. Since the parameters for cutting rate, depth, drill bit size, and waste characteristics remained the same in both simulations, the values for this mechanism of waste removal also remained the same.

The CUTTINGS\_S code was only concerned with the actual waste from the repository that was brought to the surface, and not the cuttings or cavings from the borehole of inert stratigraphic material (uncontaminated geologic material) above the repository. Figure 7.13. shows the volume of material brought to the surface from cuttings and cavings for 100 vectors versus waste shear strength for Scenario 2, at 4,000 years after the repository is closed. However, this figure is representative of all times for both S2 and S3, and the waste shear strength will be discussed below. The cuttings volume of material was calculated by

$$V = AH(1-\phi),$$

where A is the area of the drill bit, H is the compacted repository height (calculated from BRAGFLO), and  $\phi$  is the porosity at the time of intrusion. The volume of cavings is much more complicated, involving an iterative method to find the final borehole radius from erosion of material due to turbulent flow of mud between the drill collar and the borehole wall. Total volume for both mechanisms, as seen in Figure 7.13. is 2.86 m<sup>3</sup>, with a mean volume of 0.606 m<sup>3</sup> and a median volume of 0.508 m<sup>3</sup>. For the CCA, the approximate average compacted room height was 1.3 m and waste panel porosity was 0.52. Therefore, the cavings portion contributed roughly 90% to the total volume extracted.

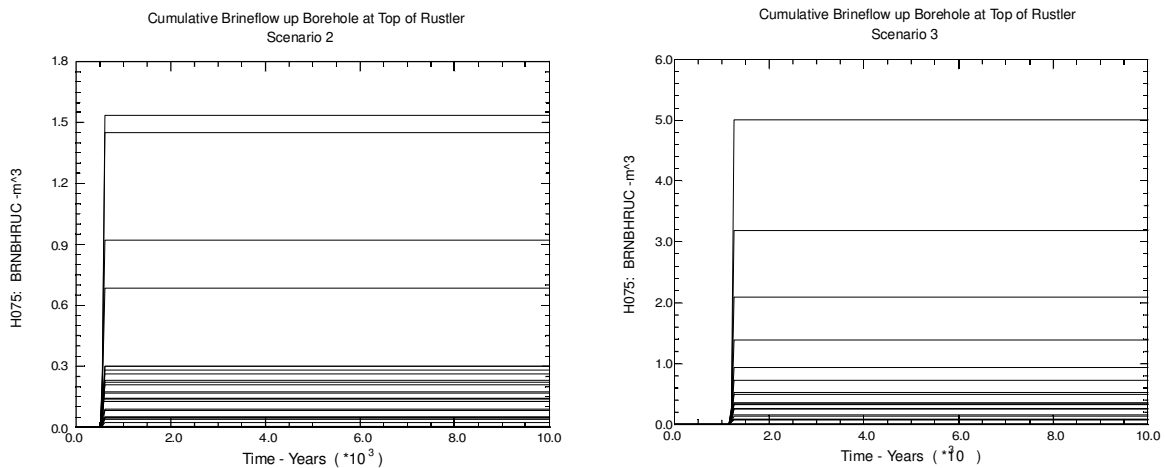


Figure 7.12. Brine Volume (m<sup>3</sup>) Reaching the Top of the Rustler Formation for Castile Simulation for Left) Scenario 2 and Right) Scenario 3

The volume of material through cavings is linked closely to waste shear strength, by the relationship,

$$R_1 = R_0 - \frac{\tau_o - \tau_{fail}}{\frac{d\tau}{dR}} \Big|_0$$

where  $R_1$  is the eroded radius,  $R_0$  is the radius of the borehole,  $\tau_o$  is the borehole wall shear stress, and  $\tau_{fail}$  is the material shear stress (Berglund 1996). Intuitively, as the waste shear stress decreases, the radius of the borehole wall increases, allowing higher volumes of waste to be brought to the surface. The CCA range, as seen in Figure 7.13, uses a uniform distribution to describe possible values of waste shear strength between 0.05 Pa and 10 Pa. Small values of shear strength are destructive to the system, with values below 1.0 Pa contributing to the major releases. Future simulations should use a loguniform distribution to describe the possible values of shear strength that vary by over an order of magnitude.

### 7.5.2.2. Spallings

The calculation of spalled material from the borehole only included the possibility of blowout, and dismissed stuck pipe and gas erosion by the estimation of a cutoff level for waste permeability in which values above the cutoff will reduce the probability of the two phenomena from happening. The cutoff permeability was  $10^{-16} \text{ m}^2$  (See CUTTINGS\_S Manual for additional information on stuck pipe and gas erosion (Berglund 1996)). The waste permeability in the CCA was  $1.7 \times 10^{-13} \text{ m}^2$ , but was calculated incorrectly and thus updated for the Castile simulation to be  $2.4 \times 10^{-13} \text{ m}^2$ . If waste permeability were to fall within the region of stuck pipe and gas erosion (below the

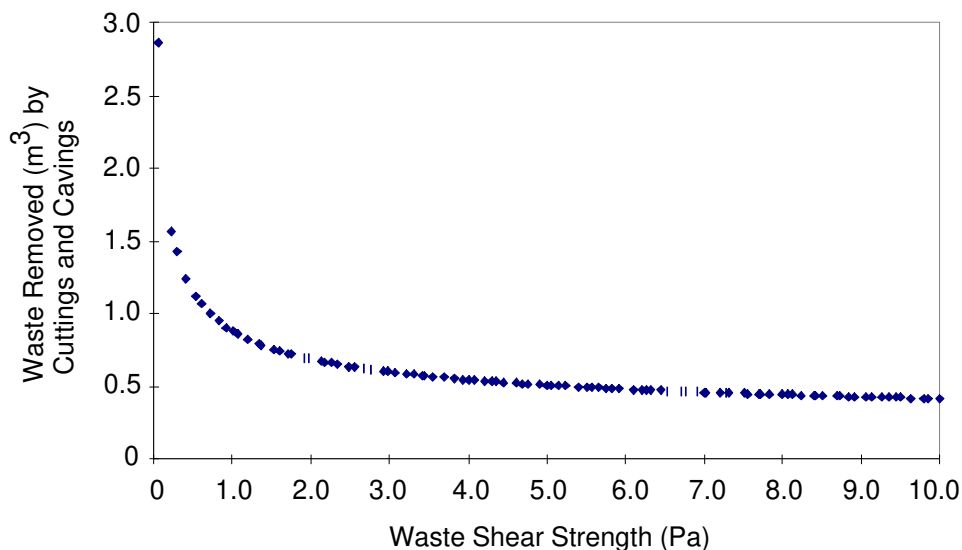


Figure 7.13. Waste Removed ( $\text{m}^3$ ) by Cuttings and Cavings vs. Waste Shear Strength, Scenario 2, at Time 4000 Years Post Closure

arbitrary limit of  $10^{-16}$  m<sup>2</sup> with pressures above hydrostatic), releases could range between 43 to 365 m<sup>3</sup> (Berglund 1996), 100 times the releases of cuttings and cavings.

The spillings calculations in the CCA were proven to be flawed, but the values of the blowout volume were accepted as being reasonable by the DOE's Conceptual Model Peer Review Group (Wilson et al. 1997). The CCA had a maximum blowout release of approximately 4 m<sup>3</sup>. The Castile simulation did not exhibit larger releases, though it did have more realizations with blowout occurring, with at least twice as many occurrences at each time intrusion calculation than in the CCA. Figure 7.14. shows a frequency distribution of the number of blowout realizations versus blowout volume. The figure is for S3 at a calculated time intrusion of 1200 years into panel 5 (downdip intrusion). The time, scenario, and borehole location was chosen to display the maximum number of releases. As the average pressure drops, the number of realizations that produce a blowout also drops, as seen in Figure 7.6.

The figure of spalled volume should not be taken as a literal interpretation of the actual spalled volume that will be ejected from the borehole. The conceptual model for the code was proven inadequate, and the calculated results do not reflect the correct volumes. It does show, however, that the Castile simulation exhibits higher pressures than calculated in the CCA, causing CUTTINGS\_S to calculate more releases. Experiments on a new code, after the submittal of the CCA, showed the spalled volume would be no more than 0.25 m<sup>3</sup> for WIPP conditions (Hansen et al. 1997). The results of Hansen et al. (1997) showed that the values obtained in the CUTTINGS\_S were higher, therefore they were believed reasonable by the Conceptual Models Peer Review Group (Wilson et al. 1997). Chapter 9 of this report explores the analysis of Hansen et al. more closely.

### **7.5.3. Direct Brine Release**

Once an intrusion breaches the repository with sufficient pressures from gas generation, the brine in the waste will move towards the cavity and be expelled out of the borehole. The pressure near the borehole or flowing bottom hole pressure (FBHP) must be above hydrostatic, in this case 8 MPa (density of brine = 1215 kg/m<sup>3</sup>, length of borehole = 655 m, and friction = ~0.2MPa). The amount of brine ejected from the waste panels range from a few thousandths of a cubic meter up to a few tens of cubic meters. Figure 7.15. shows a frequency distribution of brine released to the accessible environment for all time intrusions for both the CCA and the Castile simulation of Scenarios 2 and 3. The Castile simulation, as one might expect, has higher releases than in the CCA.

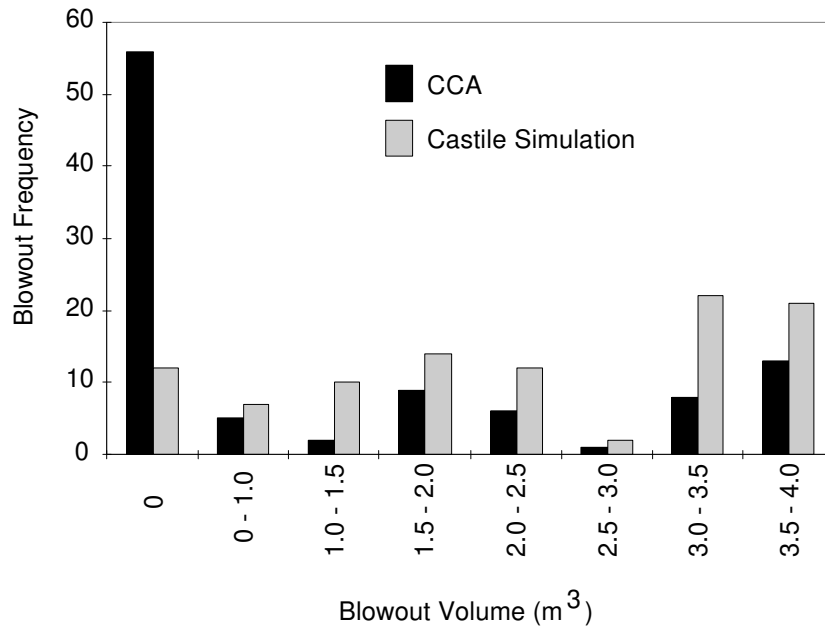


Figure 7.14. Frequency Distribution of Spalled Blowout Volume from an Initial Intrusion at 1,000 Years (Scenario 3) and a Subsequent Intrusion into Panel 5 at 1,200 Years with both CCA and Castile Simulation Values Displayed

The brine releases from an intrusion borehole is directly related to the repository pressure and brine saturation. Figure 7.16. shows the two relationships as scatter plots of brine release vs. pressure on the left and brine release vs. saturation on the right. The plots are for S3 at 1,200 years post closure of the Castile simulation. The first striking feature of the figure is the relationship between the volume of brine released and pressure. The releases are zero for pressures less than 8 MPa and increase linearly from 8 to 9 MPa. At 9 MPa, the releases sharply increase, and then decrease to nearly zero again for pressures above 9 MPa. This is a unique feature of this simulation and is only observed in early times of the repository's projected history. A similar feature is noticed at 1,400 years, but essentially dissolves at 3,000 years and beyond. A possible explanation for the phenomena is the control that the Castile reservoir pressure has on the repository in early times. Since the Castile reservoir pressure is constant in all 100 realizations, the pressure in the repository is directly affected by the amount of brine flow to the repository.

However, the pressure in the repository is affected by other key parameters as well, and not just by the amount of brine flow from the Castile reservoir. Figure 7.17. shows a scatter plot of pressure in the repository for S3 at 1,200 years post closure for the Castile simulation versus the inundated steel corrosion rate. As the corrosion rate increases, the pressure increases, and again is dependent on a third parameter. The probability of degradation of cellulose, plastics and rubbers separates the scatter plot into two regions. The parameter, PROBDEG, is the

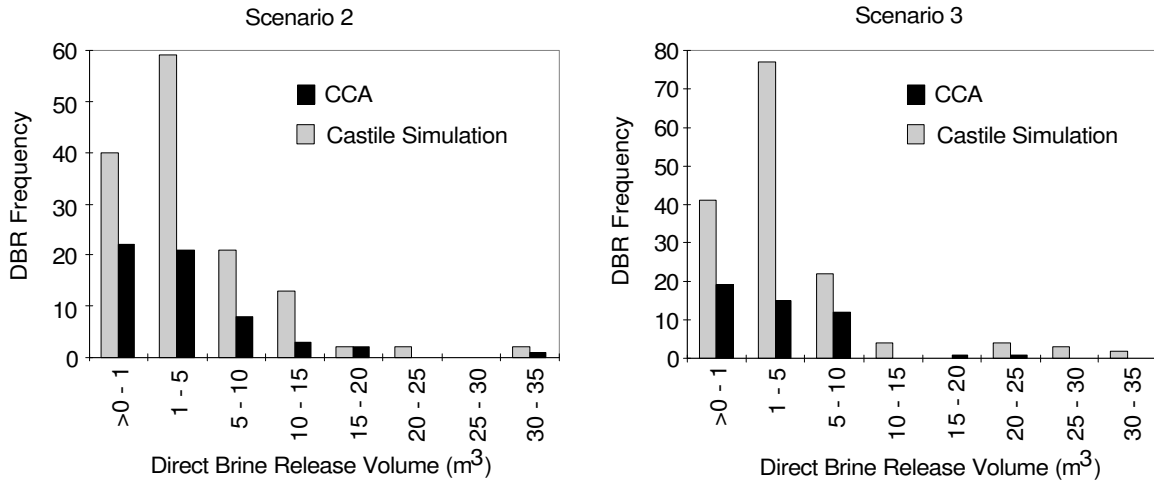


Figure 7.15. Frequency Distribution of Direct Brine Release Volumes (m<sup>3</sup>) for CCA and Castile Simulation for Left) Scenario 2 and Right) Scenario 3

second LHS sampling variable, and can have values of 0, 1, or 2. A “0” indicates no microbial degradation of organic material and has a probability of 50%. The selection of “1” means that only the cellulose will degrade, and “2” denotes cellulose, plastics and rubber will degrade, with a 25% probability each. The region of high pressure in Figure 7.17. is from a PROBDEG of 2. These diamonds are black, meaning there was no significant direct brine release. The gray diamonds indicate a notable brine release, which fall in the region of pressures seen in Figure 7.16. to have the major releases. Excluding those realizations with a PROBDEG of 2, the plot has a correlation coefficient of 0.68, and a correlation coefficient of 0.67 considering only those with a PROBDEG equal to 2. This is higher than the coefficient of 0.14 if all realizations are included.

Relating back to Figure 7.16. and the second plot with brine release versus waste panel brine saturation: the optimum brine saturation for large release is approximately 0.65 with minimal releases above 0.85 and no significant releases below 0.4. The saturation can be thought of as a brine to gas relationship. If too much gas (low saturation) is present, then the availability of brine to be ejected is limited, and is directly related to the extremely high pressures and corrosion rate of Figure 7.17. Also, if there is too much brine and not enough gas, the pressures in the repository will not be high enough to lift the brine out of the borehole. Therefore, an optimum (or detrimental) saturation is observed for the Castile simulation at early times after the intrusion.

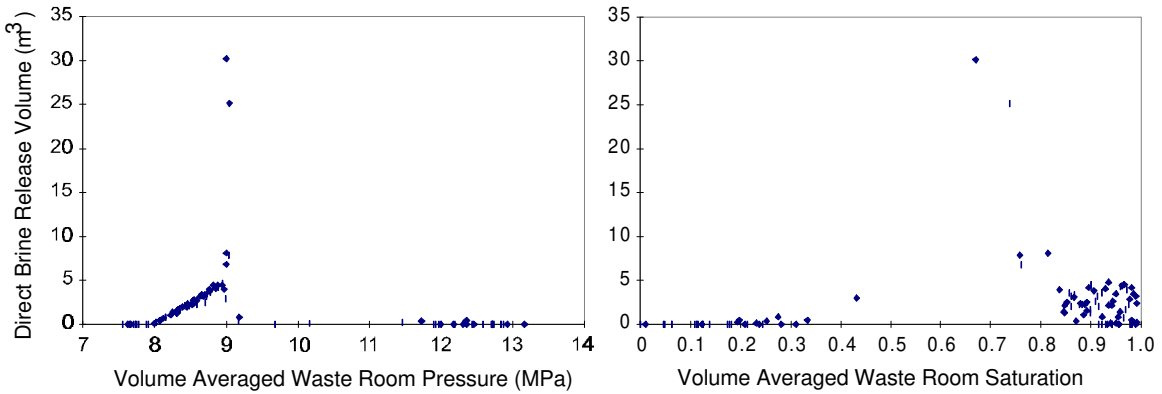


Figure 7.16. Direct Brine Release ( $\text{m}^3$ ) for Scenario 3 for Castile Simulation for the Second Intrusion at 1,200 Years for Left) Volume Averaged Waste Room Pressure (MPa) and Right) Volume Average Waste Room Saturation (Unitless)

It is stressed at this point that the above phenomenon is only for the Castile simulation, Scenario 3, at early times in the repository's projected history after the initial intrusion. Since a few of the key parameters were held constant, the predicted behavior of the disposal system was better understood. A similar response of Scenario 2 for the Castile simulation can be seen, yet differences between the two scenarios are still recognized. For example, the brine release

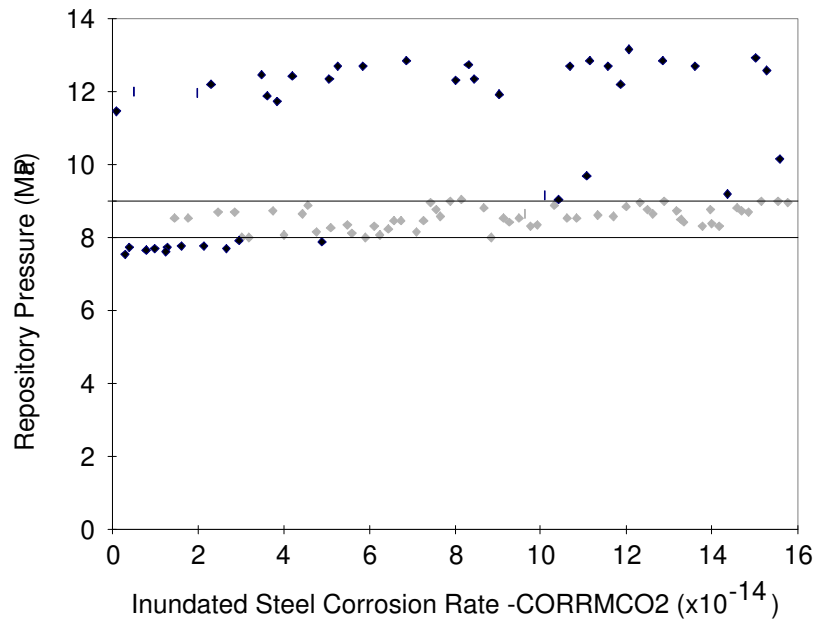


Figure 7.17. Scatter Plot of The Pressure in the Repository (MPa) for Castile Simulation, Scenario 3, 1,200 Years Post Closure Versus Inundated Steel Corrosion Rate (CORRMCO2-Parameter 1 in LHS Sampling) with Banded Region of Gray Diamonds Showing Those Vectors that had a Significant ( $>0.1 \text{ m}^3$ ) Direct Brine Release

versus brine saturation shows that brine can be ejected at saturations as low as 0.2. These are very low releases, usually less than 0.5 m<sup>3</sup> of brine. However, since the CCA has more varying parameters over large ranges, the behavior of the system is less predictable.

#### **7.5.4. Probability Modeling with Results from Castile Simulation**

The final step in assessing the results of the Castile simulation and how they will affect the overall performance of the disposal system, is to replace the results of the CCA with those of the Castile simulation in a CCDFGF calculation. The individual vectors of CUTTINGS\_S and BRAGFLO\_DBR were summarized into formats for probability modeling and modeled with the CCA results of SECOTP2D, NUTS and PANEL. Figure 7.18. shows the CCDF curves of several simulations.

The results of the Castile simulation show that Castile brine assumptions do not have a significant effect on the overall CCDF. In fact, the figure shows that the CCA may have slightly higher releases at equivalent probabilities with the same probabilistic assumptions (drilling rate, AICs, probability of hitting a Castile brine pocket, etc). Even when the probability of hitting brine is increased from 8 to 100%, the releases are not increased by any significant amount.

### **7.6. Conclusions**

A model is presented to investigate the importance of the Castile brine reservoir parameters at the WIPP. The Castile reservoir underlies the repository and is a major source of brine that may contribute to gas generation from the corrosion of metals and biodegradation of organic materials. The production of gas will increase the pressure in the repository, thus ejecting brine and waste to the accessible environment upon a breach of the repository.

The Compliance Certification Application presents data for the creation of reservoir parameters that may be extraneous. The data were derived from wells that clearly lie outside a reasonable distance for consideration of brine pockets underneath the repository. Therefore, data from a single well, one mile north of the repository, was used to simulate the effects of the reservoir. The data included reservoir volume, rock compressibility, permeability, and pressure.

In addition, two parameters describing the waste area were changed to what were considered more reasonable values. The waste permeability was increased by 41%, and has been well documented to show the error in the calculation of the original value. Also, the residual brine saturation range was decreased by reducing the upper value by 57%. This range is no longer considered to be more reasonable than the range used in the CCA calculations, due to the consolidation of waste in the repository.



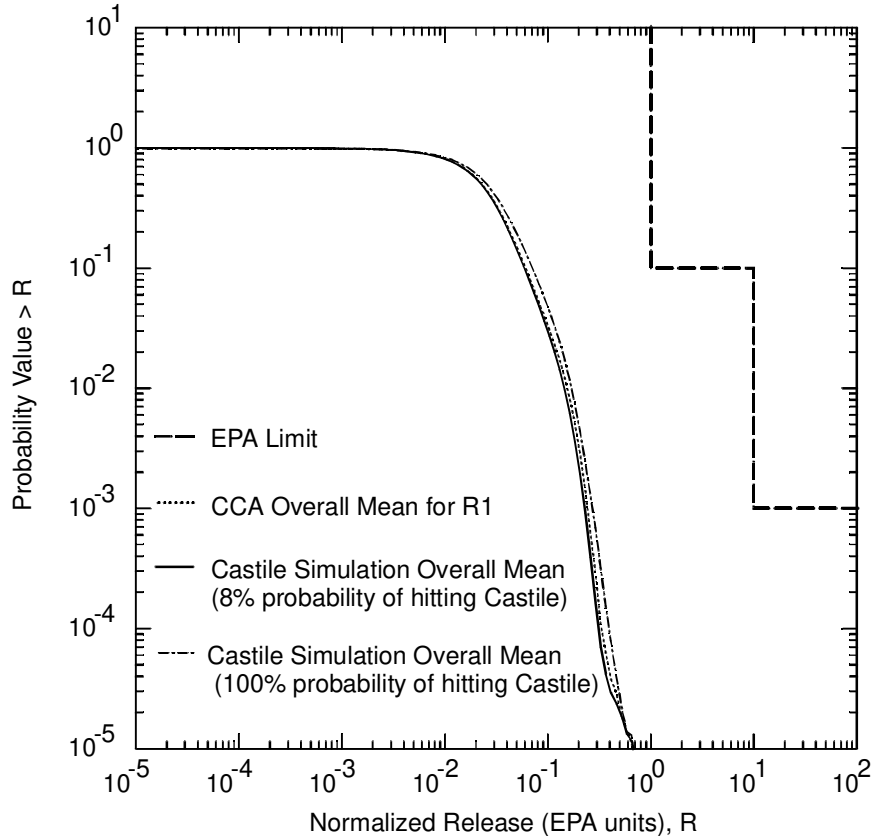


Figure 7.18. CCDF for Castile Simulation and CCA. The Castile Simulation Includes Two Probability Models: 8% and 100% Probability that the Intruding Borehole will hit the Castile Reservoir

The modeling started with two-phase flow of brine and gas through the repository using BRAGFLO. The changes in the Castile reservoir parameters affected the pressures, flow, and saturation of brine and gas through the waste. The pressures were much higher than in the CCA, with increased flow rates due to increased waste permeability.

The modeling of a human intrusion was completed by the code CUTTINGS\_S, which simulates a drill string breaching a pressurized repository and releasing solid waste up the borehole to the accessible environment. The calculations showed that the amount of waste brought to the surface would not change, but the number of realizations that possibly could result in a release would increase. The increase of a spalled events from an highly pressurized repository doubled from the CCA to the Castile simulation.

The flow of brine up an intruded borehole was calculated separately in BRAGFLO\_DBR. The results proved that the increased pressures in the repository from changing the selected parameters would result in higher and more incidents of releases to the surface.

Finally, CCDFGF modeled the probability of releases from the results of the above calculations. The outcome showed that there is no significant change in releases due to the minor addition of releases from a spalled or brine release. The releases calculated in CUTTINGS\_S and BRAGFLO\_DBR were not significantly more than those of the CCA. The constant values used for the Castile brine reservoir pressure is suspected to be the largest culprit for no change in the releases. However, the releases are subject to the concentration of radionuclides in the waste, and it is suspected that changes in the solubility, which would increase the concentrations of the radionuclides, would have a more profound effect on the Castile simulation than the CCA.

## **8. CULEBRA FLOW AND TRANSPORT USING BLM MAP FOR ECONOMIC POTASH RESOURCES OF EDDY COUNTY**

### **8.1. Summary**

A new Culebra flow and transport model with a modified extent of potash mining is presented here to demonstrate the effect of mining on the performance assessment caused by a change in flow patterns. The CCA assumes limited mining within the controlled area of the WIPP repository. A new model was justified because of the expected mining of lower grade ore due to the increase in use of fertilizers and development of more efficient mining methods. The results show that the new flow velocities in the Culebra aquifer could be important when considering lower  $K_d$ s, as the process of sorption dominates that of advection.

### **8.2. Introduction**

The possibility of mining above the WIPP repository for potash resources has been identified as a possible scenario for human disturbance of the disposal system in the EPA's criteria for the compliance standards, 40 CFR Part 194.32 (b) (U.S. EPA 1996b). The performance assessment calculations of the CCA included a mining scenario with a probability of occurrence equaling that which has transpired over the last 100 years, as stated in the guidelines. The consequences of mining would cause subsidence in the geologic units above the repository, increasing the amount of fracturing and possibly decreasing travel time of the radionuclides through those overlying units if a release occurred.

The extent of the potash reserves overlying the repository and how it affects the flow field of the Culebra Dolomite member of the Rustler Formation is investigated in this chapter. Originally, the CCA identified two possible mining scenarios: full and partial mining. These scenarios were based on studies of known potash leases and economic- and lease-grade potash reserves in the Delaware Basin. The full mining scenario includes regions outside the controlled area of the repository identified by the Bureau of Land Management (BLM 1993), excluding oil and gas well buffer zones, and regions within the controlled zones based on economic grade potash ore from the New Mexico Bureau of Mines and Mineral Resources (NMBMMR) report (U.S. DOE 1996-Appendix MASS). The partial mining zones exclude mining within the controlled area, with the exception of those areas mined before the Land Withdraw Act was established. The maps do not distinguish between the two types of ore, sylvite and langbeinite.

The future of potash mining is the limiting factor on estimating the economic extent of potash reserves. Currently, 40% of the world's agricultural production uses nitrogen based fertilizer, derived from the potash industry (Smil 1997). With the exponential increase in human

population, fertilizers usage should also increase, directly affecting potash production in the Delaware Basin. The increased demand for potash will prompt the industry to mine lower grade ore, and use methods of extraction that are more profitable.

Solution mining has been considered for the extraction of potash in the region of the Delaware Basin. The process of mineral dissolution was determined to have the lowest operational cost compared to other methods (Gruschow 1992). Therefore, the extraction of lower quality potash minerals could be economically feasible, and the extent of reserves are much greater than originally predicted. The CCA failed to recognize the possibility of solution mining around the repository, and the area affected by mining is much less than predicted. The EEG modeling of this report considers all possible potash reserves inside and outside the controlled area based solely on the BLM map (BLM 1993). The area inside the controlled area changed significantly from that in the CCA, whereas the outside was virtually unaltered. This scenario is referred to as the Modified Mining (MM) scenario.

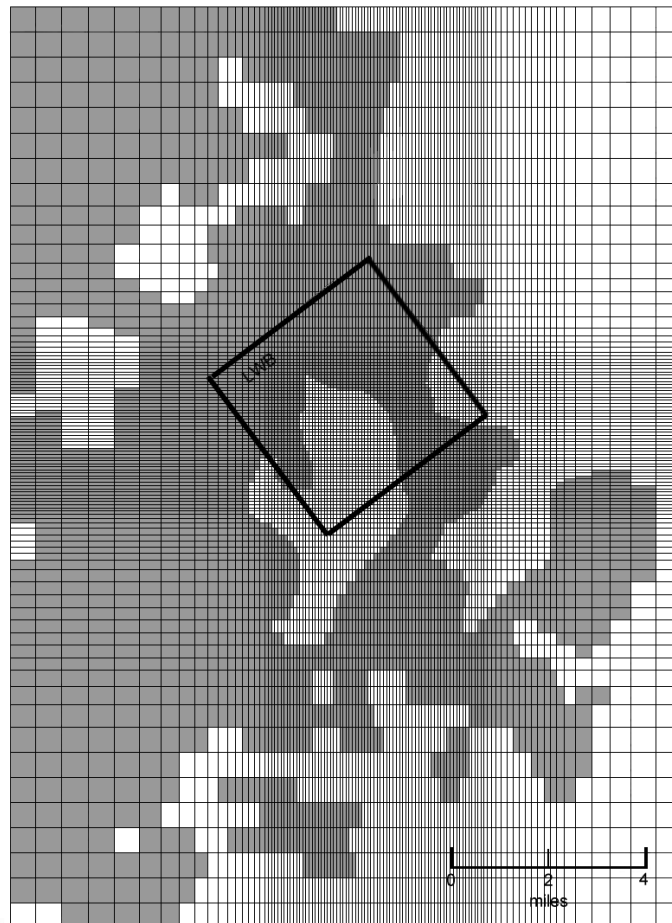


Figure 8.1. Areal Extent of Known Potash Reserves from the BLM Map (BLM 1993)

Figure 8.1. shows the new areal extent of potash reserves, superimposed on the regional modeling domain. This domain is used in the flow code for simulating flow through the Culebra. The area shows the region affected by mining, where subsidence would fracture the flow system. The EPA guidelines for subsidence are very specific about how the area is to be treated in the performance assessment. A multiplier of no more than 1000 is required to increase the transmissivity. This was a sampled parameter in the performance assessment calculations, and remained unaltered for the calculations in this report.

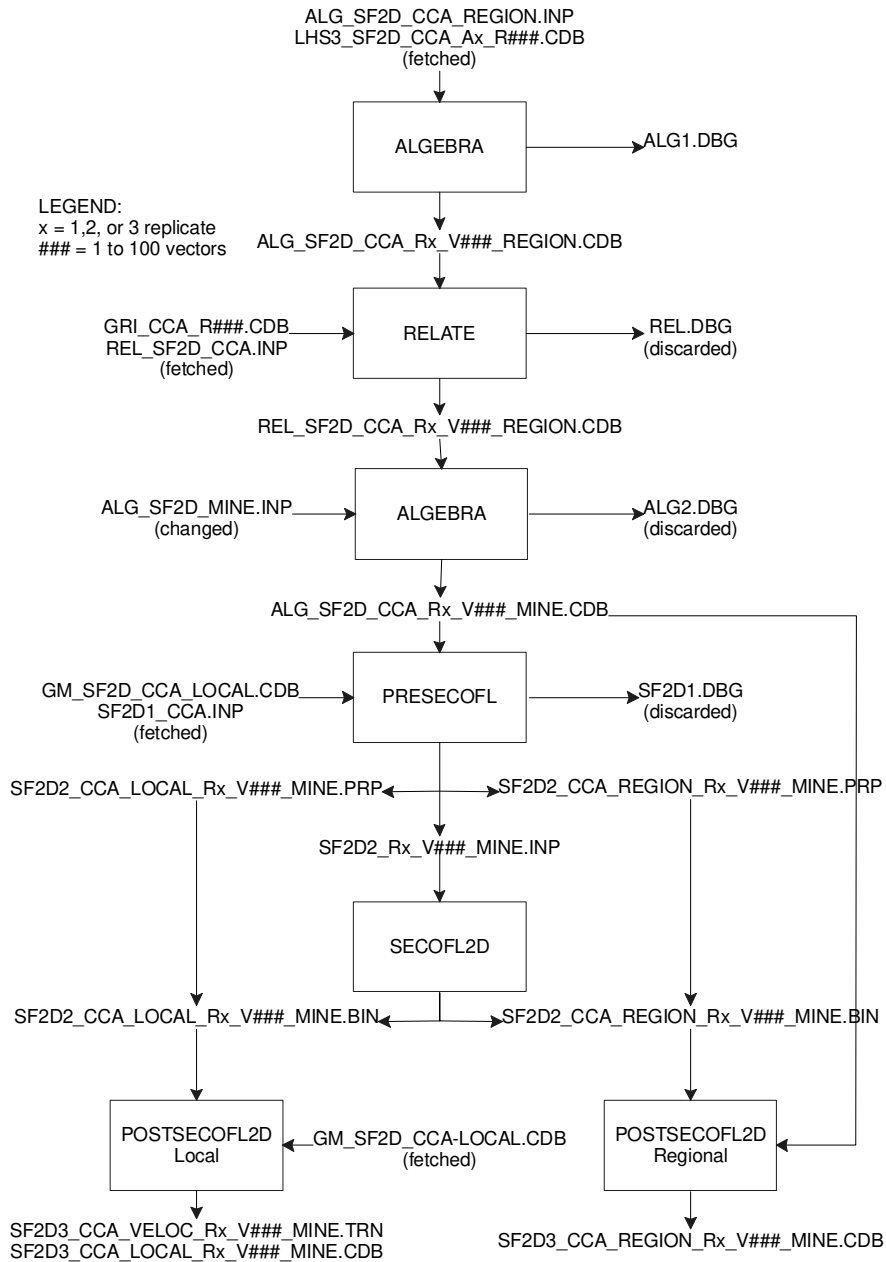


Figure 8.2. Flowchart of SECOFL2D Simulations

### **8.3. Methodology**

The purpose of this modeling experiment was to change the existing regions of the potash minable resource areas to test the effects on the flow and transport of radionuclides through the Culebra. This was accomplished by first running the flow code, SECOFL2D, a two dimensional regional flow code that solves the Darcian flow equation. The flow velocities were then used to solve the transport equation in SECOTP2D. Figure 8.2. shows the flowchart of the flow code used in modeling the mined area. The only change for modeling the new potash region was the file that controlled which transmissivity cells of the flow grid were multiplied by the increased factor for higher fracturing. All cells of the region were multiplied by the same value. The actual file is included as an attachment to this chapter for reproducibility. The transport flowchart for SECOTP2D can be found in Chapter 6.

A total of 100 vectors were completed for the flow calculations with hydraulic head being computed for both a regional and local domain. The flow field was first solved on the regional grid. The local grid acquired its boundary conditions from the regional flow characteristics. The local velocities were then used as the input to solve the transport of radionuclides on the local grid.

Two experiments were simulated with the transport equation with 100 vectors being generated for each simulation. One included plutonium with a 1%  $K_d=0$  to compare with results of Chapter 6, and the other ran uranium with  $K_d$ s generated from the LHS sampling technique to compare with CCA results. The generated  $K_d$ s were slightly different, correcting for the range as specified in Ramsey and Wallace (1997). The new range decreased the values used in the new simulations, allowing the Uranium to migrate further downstream. The complete set of vector calculations enables the results to be incorporated into the CCDFGF code.

## **8.4. Results**

### **8.4.1. Culebra Flow**

The flow field of the new mined area (MM Scenario) showed slightly different hydraulic head values than the 'fully mined' solution of the CCA calculations. Figure 8.3. compares the regional head contours of a simulation where the transmissivity multiplier (parameter MINP\_FAC) was the lowest generated value from the LHS sampling technique. Figure 8.4. also compares the regional head contours, taking the vector with the highest generated multiplier. The low and high values for MINP\_FAC are 5.1 and 996.4, respectively. Contours are in meters above sea level.

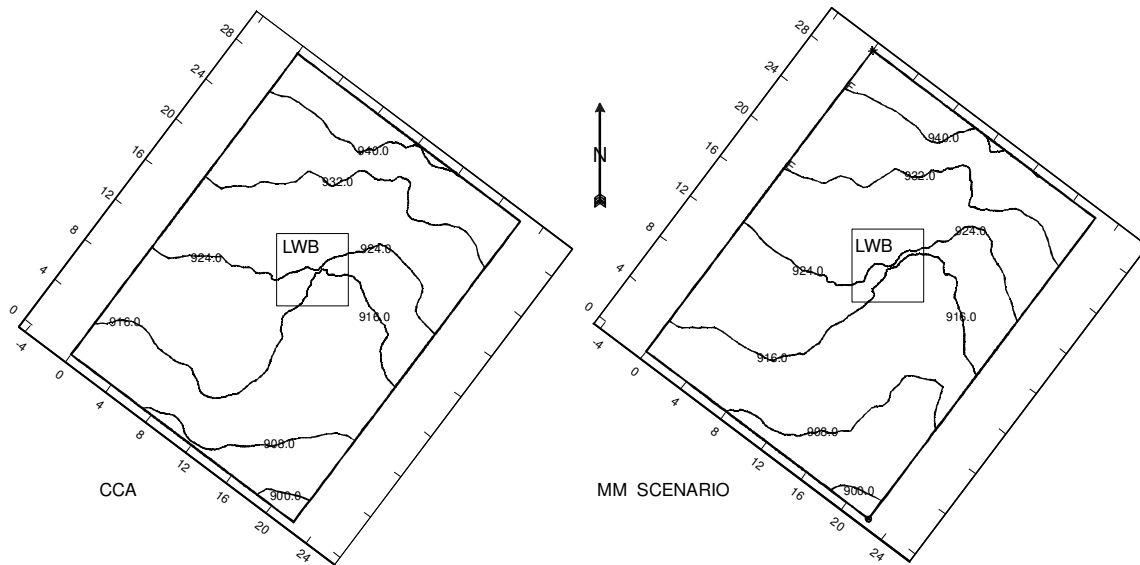


Figure 8.3. Regional Flow Contours of Vector 11. Left) CCA Right) MM Scenario

The only significant difference in head contours was in Figure 8.4., where the contour of 916 m for the MM Scenario is much further south than the CCA calculations. At first glance, this would indicate lower velocities for the MM Scenario through the controlled area, and speeding up through the south. However, due to the extreme heterogeneity of the site (as seen in Figure 8.5.), a generalization about the velocities cannot be inferred from the difference. Therefore, a velocity profile was constructed from the velocities calculated in SECOFL2D. Figure 8.6. shows the velocity vectors for both mining scenarios with correct angle and proportioned magnitude for

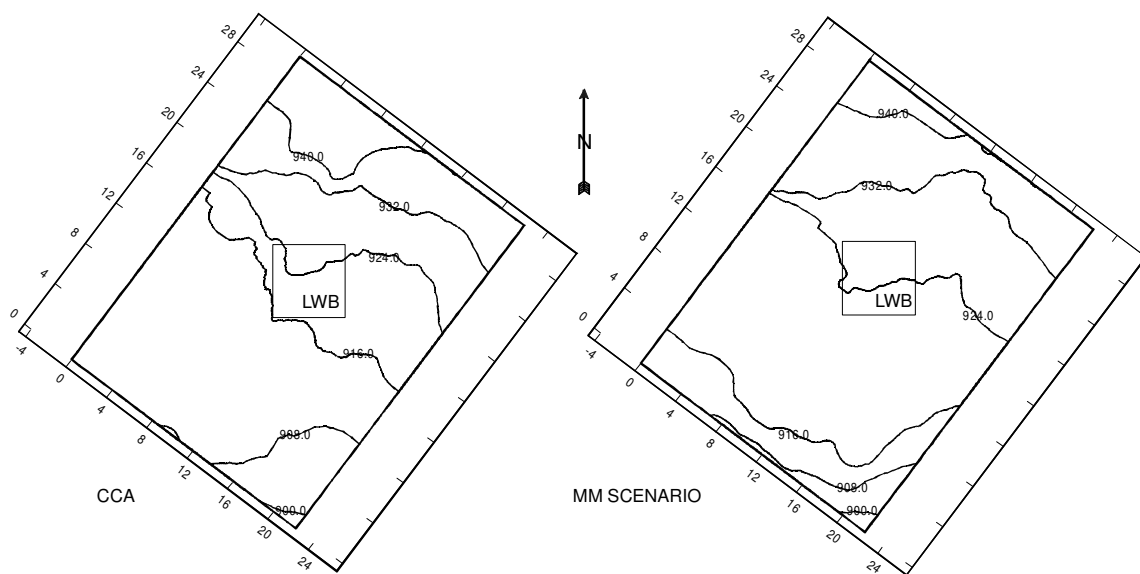


Figure 8.4. Regional Flow Contours of Vector 62. Left) CCA Right) MM Scenario

Vector 62. The velocities were extracted from the local grid to show the direction of the plume's migration in the transport calculations. The outline of the transition of small vectors and large vectors clearly shows the areas where the transmissivities were multiplied by MINP\_FAC.

The velocities of Figure 8.6. range from  $2.3 \times 10^{-14}$  m/s to  $2.9 \times 10^{-6}$  m/s for the CCA calculation, and  $2.3 \times 10^{-12}$  m/s to  $1.1 \times 10^{-5}$  m/s for the MM Scenario. Since both modeling scenarios used the same transmissivity field, the higher velocities in the MM Scenario suggest that the area to be multiplied by MINP\_FAC overlaps a region of slightly higher transmissivity than in the CCA, i.e.

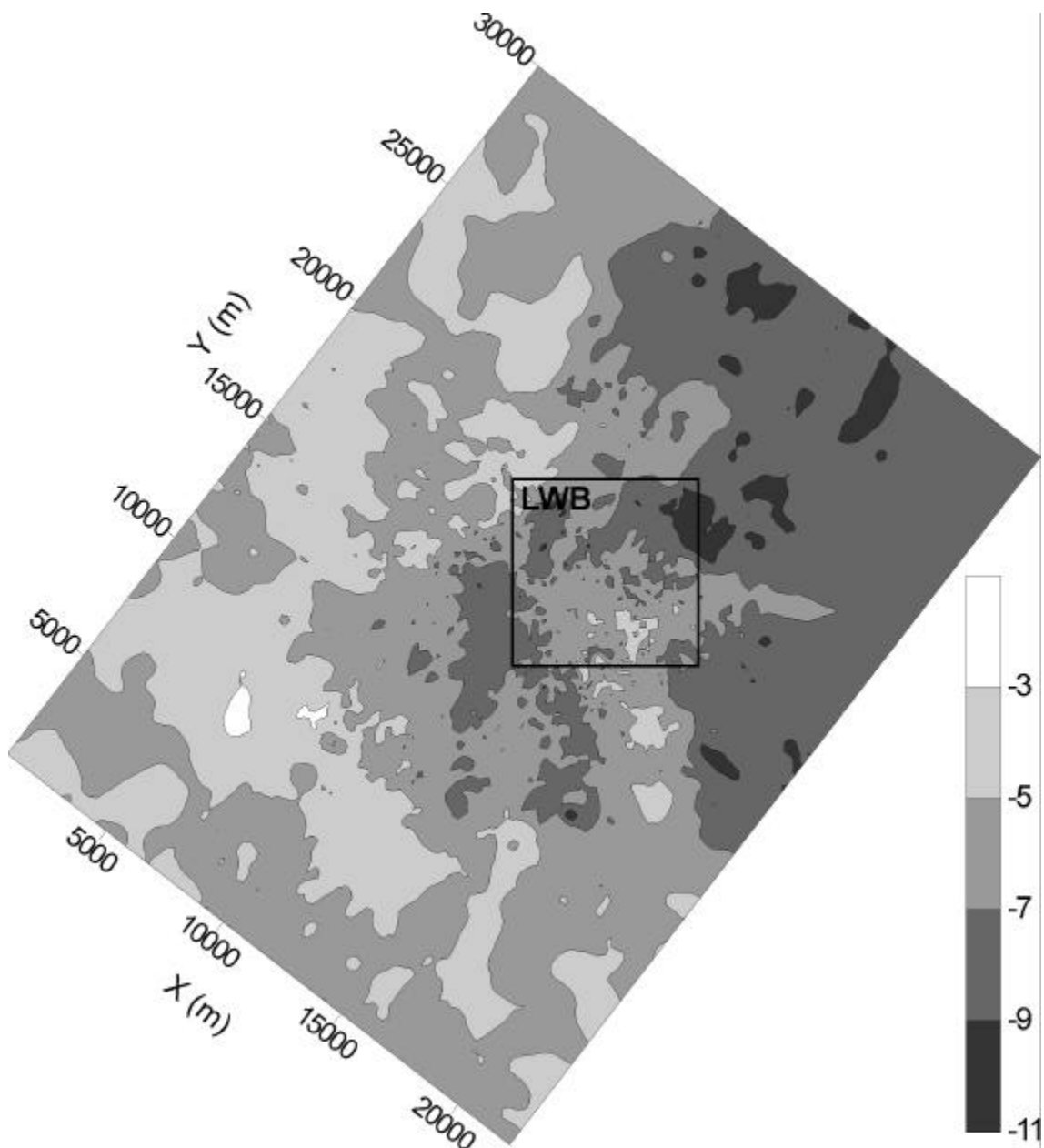


Figure 8.5. Transmissivity Field ( $\text{Log}_{10} \text{ m}^2/\text{s}$ ) of Vector 62



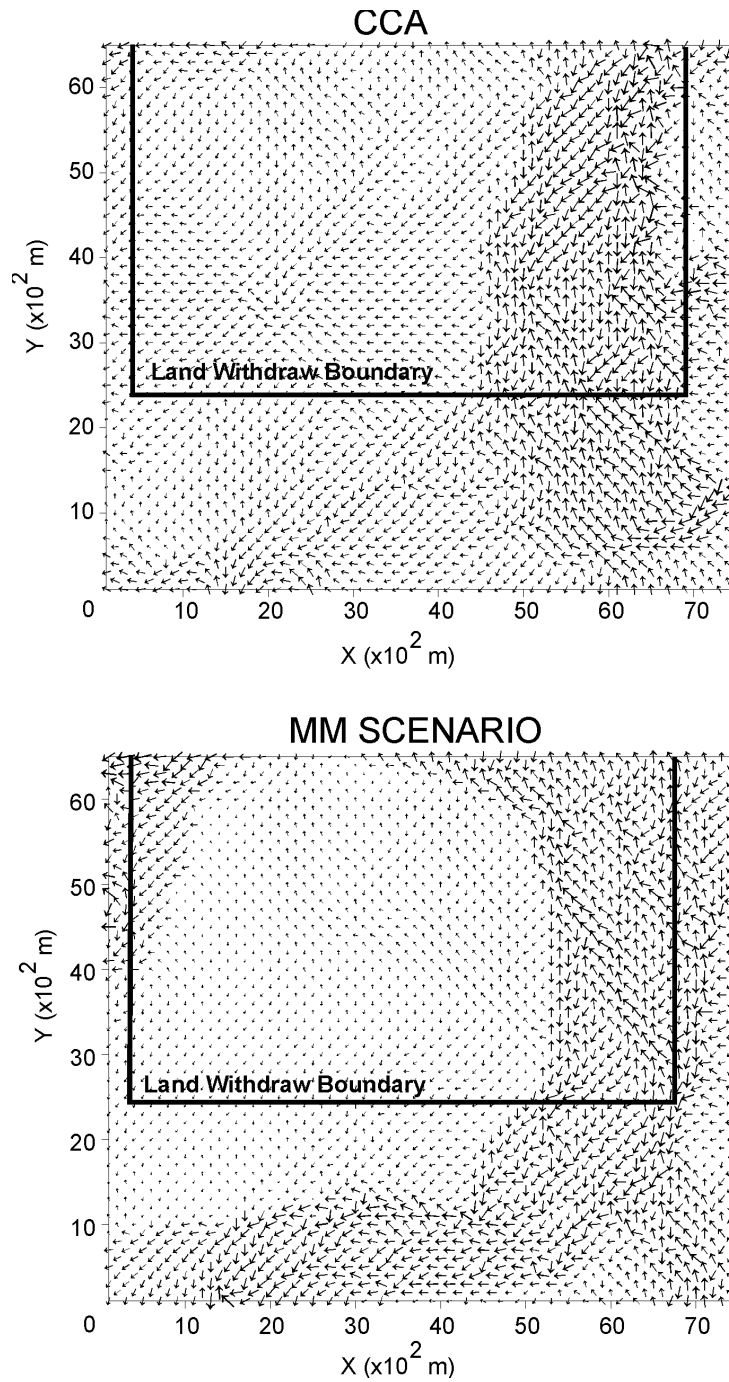


Figure 8.6. Velocity Profile of Vector 62 on Local Grid for Top) CCA and Bottom) MM Scenario

the region that is multiplied as shown in Figure 8.1. This is important, as the results of the radionuclide transport calculations will differ significantly from the outcome of the flow field functions.

## 8.4.2. Culebra Transport

### 8.4.2.1. Plutonium Transport Calculations with $K_d=0$

SECOTP2D was first used to simulate transport of plutonium with a  $K_d=0$  through the Culebra aquifer. The combination of zero sorption and higher velocities allowed higher masses of the radionuclide to migrate across the Land Withdraw Boundary (LWB). The discharge mass of the Modified Mining Scenario was compared to results from transport calculations performed in Chapter 6, which simulated changes in the  $K_d$  only. In approximately 60% of the vectors, discharges were higher for the MM Scenario than for those seen in the Chapter 6 calculations. Figure 8.7. shows vectors that discharged mass fraction higher than  $10^{-6}$  for the MM Scenario and the results of Chapter 6. The figure also displays a histogram for the frequency of vectors lying between the given ranges. The actual fractional discharge for both studies ranged from  $10^{-2}$  to less than  $10^{-15}$  (machine zero), but the limit was cut off at  $10^{-6}$ . Below this discharge, the low-consequence eliminates the vector from consideration in the complementary cumulative distribution functions (CCDFs). Both plots clearly demonstrate that the MM Mining Scenario produces faster flow fields and is more conservative in its assumptions.

During the last step of probability modeling to create the CCDF curves for comparison with the EPA limits established in 40 CFR Part 191 (U.S. EPA 1996), the fractional discharge is multiplied by the actual amount of radionuclides that reach the Culebra. In most cases, the amount is negligible, and the fact that a vector had a high fractional discharge is often eliminated by the low concentrations. To demonstrate this affect, Figure 8.8. shows the discharge across

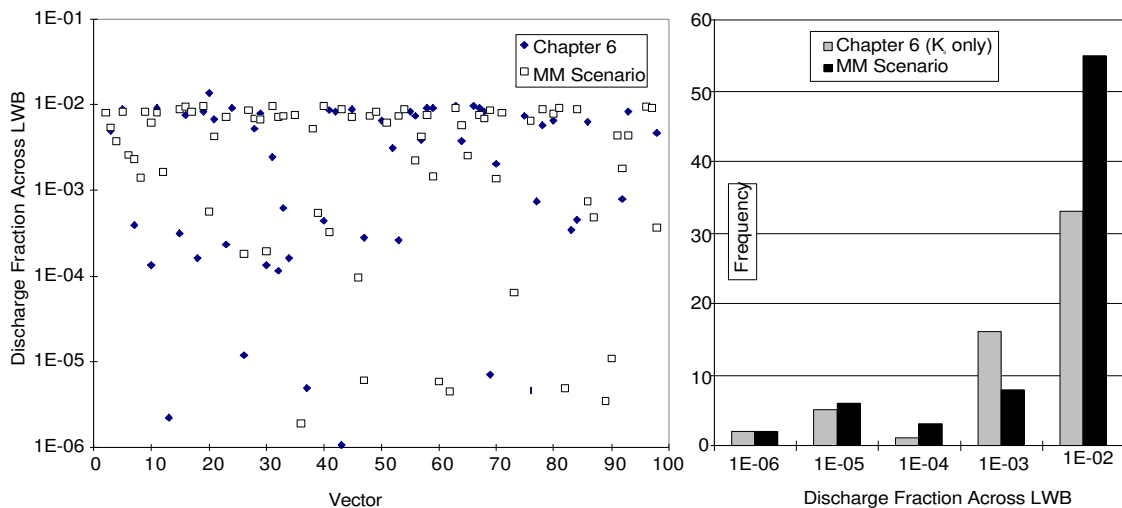


Figure 8.7. Left) Plutonium Fractional Discharge across the LWB for Chapter 6 Results (Full Mining) and MM Scenario with both having 1% of the Initial Mass with a  $K_d=0$  ml/g Right) Frequency Distribution of both Mining Scenarios for Vectors with Significant Discharge across LWB

the Land Withdraw Boundary in EPA Units. The plots in the figure show the discharge of plutonium for the S2 and S3 scenarios at 10000 years for those vectors with discharges of at least  $10^{-6}$  EPA Units. The fractional discharge is multiplied by the mass in Curies calculated from each of the scenarios, and divided by 344 to obtain the mass in EPA Units. The figure reveals that for the S2 scenario (left plot), the Modified Mining has the highest release in 10000 years with six vectors showing at least  $10^{-5}$  EPA Units crossing the LWB. The right plot of the S3 scenario also shows the highest release, however, with less vectors actually being above the  $10^{-6}$  threshold than the results of Chapter 6.

### 8.4.2.2. Uranium Transport Calculations with LHS Generated $K_d$ s

The flow velocities from the BLM Mining Scenario were also used to model uranium with higher  $K_d$ s than the plutonium simulations. The  $K_d$ s were generated from the Latin Hypercube Sampling (LHS) code. The range of values for  $K_d$ s were modified from those used in the CCA to values suggested in the Analysis Package, Task 3 (Ramsey et al. 1997). The new range for generated  $K_d$  values are lognormally distributed from  $0.03 \text{ ml/g}$  to  $20 \text{ ml/g}$ , changed from  $0.03 \text{ ml/g}$  to  $30 \text{ ml/g}$ . The new upper value, along with a lognormal distribution for the range, created smaller values of  $K_d$ s, and thus smaller retardation values. The result is more vectors with higher discharge.

In the CCA calculation only one vector from the third replicate showed any release, with an integrated discharge across the Land Withdraw Boundary equal to 0.91 kgs. The present calculations were performed on the first replicate, with no releases to compare. Figure 8.9. shows releases across the LWB only for the present model.

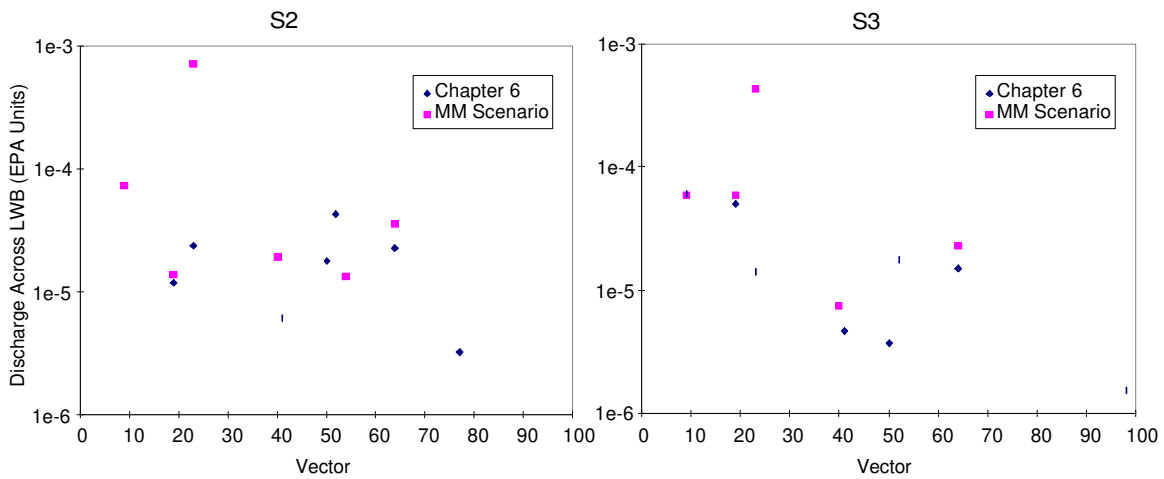


Figure 8.8. Discharge in EPA Units at 10,000 Years from CCA NUTS Concentrations for the Results Presented in Chapter 6 and the MM Scenario for Left) Scenario 2 and Right) Scenario 3

Of the 100 vectors, only six had significant releases (fractional discharge  $> 1 \times 10^{-6}$ ) across the LWB. The calculated retardation value from the generated  $K_d$ s ranged from 1.57 to 170412.2 (dimensionless), and the six vectors that showed discharge had a range of retardation values from 1.57 to 2.99. However, a strong correlation does not exist between retardation and discharge. Several vectors had no release across the LWB with retardation values less than 3. The geostatistical representation of the transmissivity field was such that it prevented any escape of uranium to the accessible environment. The CCA calculated retardation for uranium ranged from 24.8 to 431089.

The comparison for flow calculations used Vector 62, because of its high multiplier for the transmissivity field. However, the value of the newly calculated retardation coefficient for this vector was incredibly high (15763, dimensionless), and the uranium did not migrate outside of the waste panel area. To keep the comparison alive and consistent, Vector 62 was rerun with a smaller  $K_d = 0.046 \text{ ml/g}$  (retardation = 2.0). Time was also extended out to 100000 years to find when the maximum release would occur.

Figure 8.10. shows six snapshots of uranium concentration isopleths at 1875, 3875, 5250, 7150, 8650, and 10000 years after an intrusion. The isopleths range from  $1 \times 10^{-15} \text{ kg/m}^3$  to  $1 \times 10^{-6} \text{ kg/m}^3$ , dark to light. The observed behavior of the uranium plume shows it to remain in the near

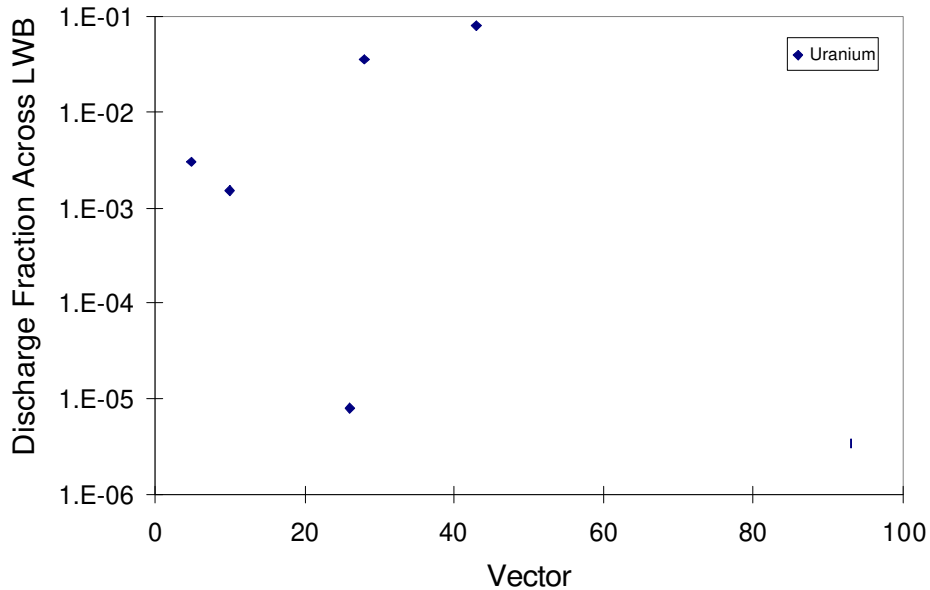


Figure 8.9. Discharge of Uranium across the LWB for MM Scenario for LHS Generated  $K_d$ s

field (near the borehole) for approximately the first 5200 years, moving slowly to the southeast. At year 7150 the plume is then noticed to enter an area of high velocities, where it shoots relatively quickly in a southwest direction. The size and location of the highest isopleth concentration of  $1 \times 10^{-6} \text{ kg/m}^3$  remains virtually unchanged through the time history of the simulation. Though bound up around the borehole for a long period of time by a low transmissivity field, the plume moves quite quickly southward, across the LWB.

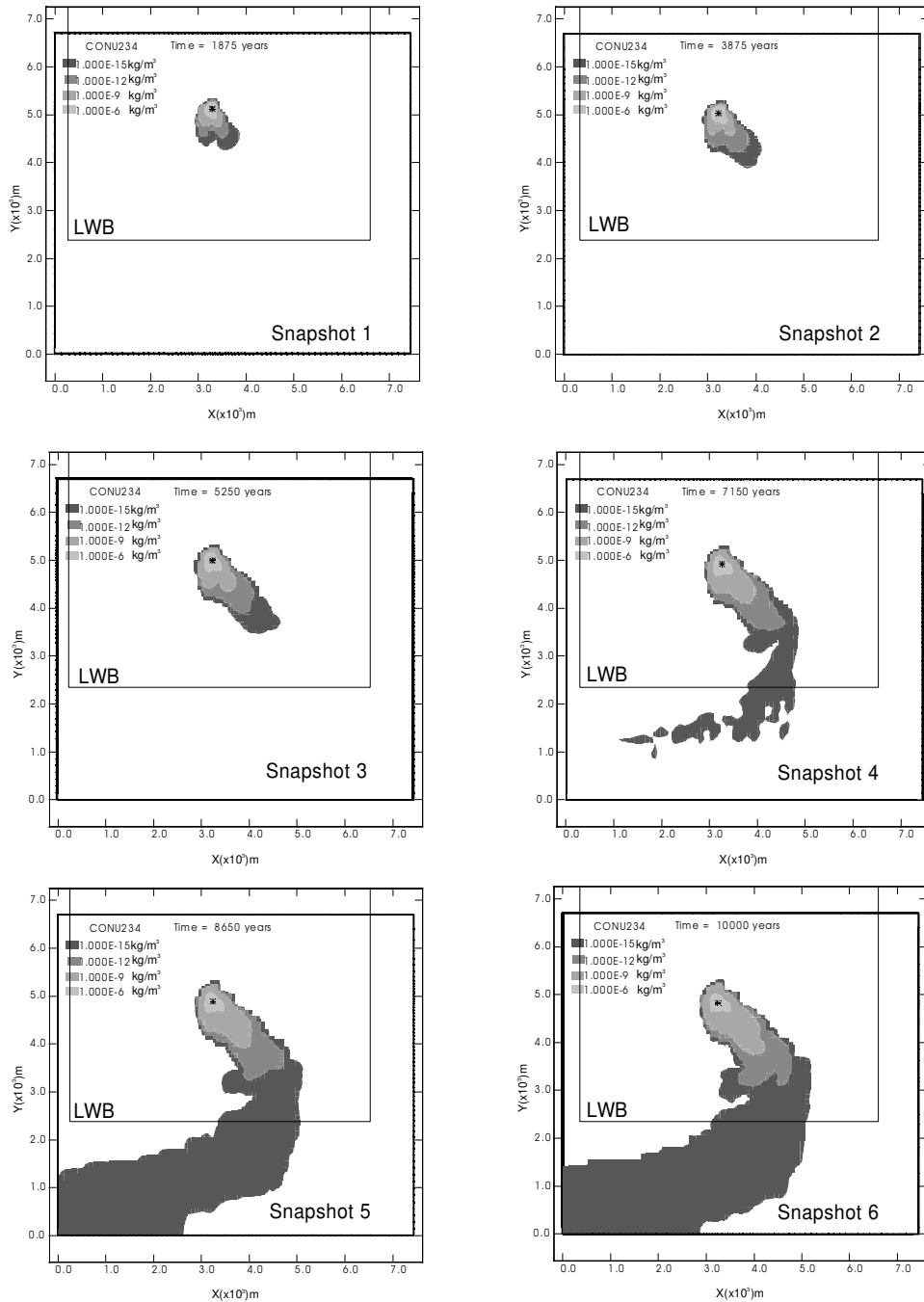


Figure 8.10. Uranium Isopleths for Vector 62 with Retardation of 2.0, MM Scenario

The discharge across the Land Withdrawal Boundary as a function of time can be seen in Figure 8.11. The simulation was extended beyond the regulatory timeframe, to 100000 years. The figure also notes the position of the snapshots from Figure 8.10. At 10000 years the fractional discharge is approximately  $1.4 \times 10^{-5}$  kgs. However, beyond the 10000 years, the discharge of uranium increases exponentially to 70000 years, where it levels off at 0.89 kgs. Regulatory compliance only requires 10000 year calculations, yet significant transport does not appear to take place until 30000 to 70000 years.

### 8.5. Probabilistic Modeling of Uranium and Plutonium

Though interesting, this chapter does not intend to discuss the regulatory timeframe in which encapsulated waste must be contained for safe disposal. It is meant to give an overall picture on the performance of the disposal system, weighting several factors not considered in the CCA. The chapter began with the formulation of a new scenario and ends with the results as compared to those submitted in the CCA. The last step in that comparison is to formulate a probabilistic model for the prediction of radionuclides reaching the accessible boundary anytime during the 10000 year future of the repository. The code CCDFGF was used to do this type of modeling.

The probabilistic model used all the results from the CCA, with the exception of transport. The new transport calculations were integrated into the CCA calculations to produce the CCDF curves, as presented in Figure 8.12. The CCDFGF code calculated curves for both plutonium with a  $K_d=0$  and uranium with newly generated  $K_d$ s, and Figure 8.12. compares the results to

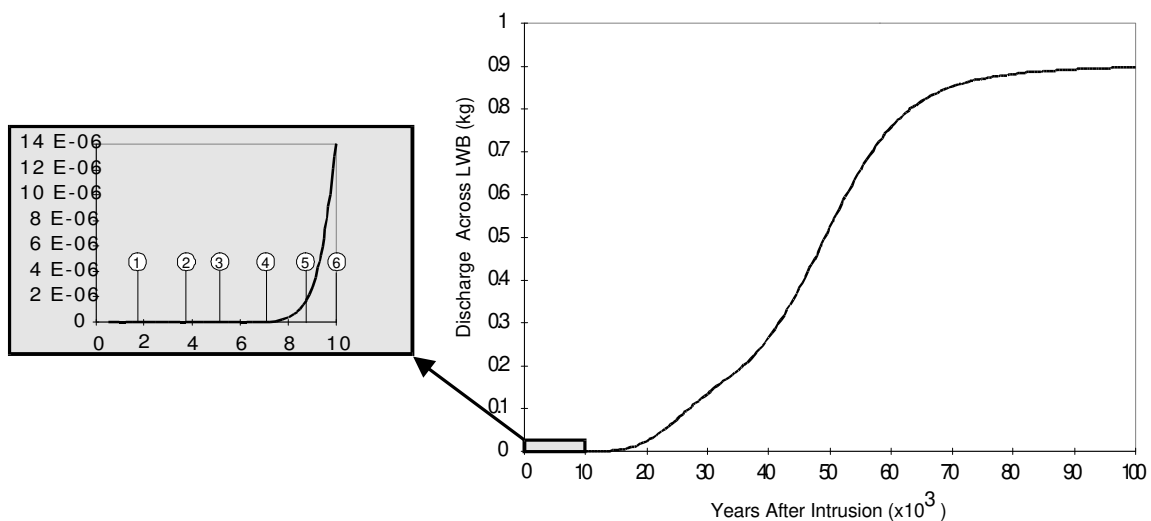


Figure 8.11. Integrated Discharge of Mass Across the LWB from 0 to 100,000 Years with Blowout Section from 0 to 10,000 Years with Snapshots from Figure 8.9. Shown as Circled Numbers in Blowout Section

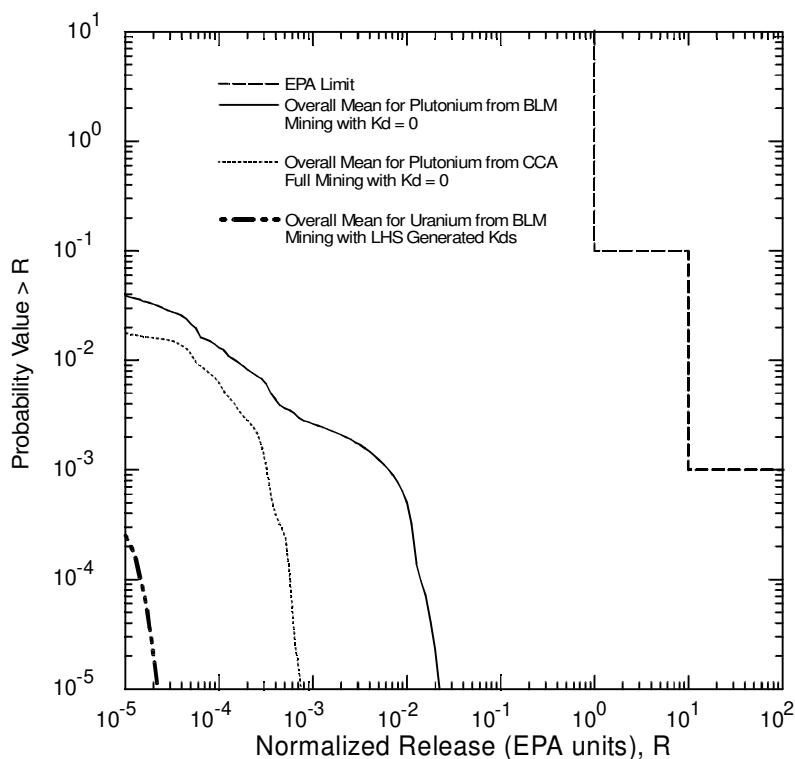


Figure 8.12. CCDF Curves for Overall Mean Releases from Culebra, Comparing Modified Mining to CCA Mining

those of the plutonium modeling with CCA Mining assumptions and 1%  $K_d=0$  (from Chapter 6). The CCA results are not presented, since no vector crossed the LWB in the first replicate.

The combination of higher velocities from the modified mining scenario and  $K_d=0$  demonstrates higher release probabilities from the Culebra than any other model, including mining or the elimination of retardation modeled separately. However, when considering the two scenarios separately, the elimination of retardation dominates the release probabilities by almost two orders of magnitude. The curves of Figure 8.12. shows plutonium with a  $K_d=0$  with the BLM Mining as the right-most curve, plutonium with CCA Mining Scenario (Full Mining only) and  $K_d=0$  in the middle, and uranium with the MM Scenario and LHS generated  $K_d$ s to the left. These results suggest that the sorption mechanism is more important than the way the velocity field behaves.

## 8.6. Conclusions

The mining of potash in the McNutt Potash Zone of the Salado formation was to be considered as a possible human intrusion scenario in the performance assessment, as stipulated in 40 CFR Part 194. The effects of such mining will change the characteristics of the overlying Culebra

Dolomite member of the Rustler Formation by increasing the fractures, and hence increasing the effective transmissivity of the region.

Modeling of mining in the CCA assumed two distinct scenarios, based on the probability of mining within the controlled area (or Land Withdraw Boundary) of the WIPP repository, namely the Full and Partial Mining scenarios. The Full Mining scenario assumes that limited mining would occur within the controlled area with consideration of present and future oil and gas wells, and the quality of present economic grade potash. The regulations of such wells mandate a 0.25 mile or 110% of the well length radius around the well to be undisturbed to insure no damage would occur to the well during mining. The Partial Mining scenario does not consider future mining in the controlled area, but only past mining conducted in the region. Outside the controlled area, both scenarios are the same, and are based primarily on the Bureau of Land Management's 1993 Map on the extent of potash in the Delaware Basin (BLM 1993).

The uncertainty of mining within the controlled area prompted an additional modeling study, which does not consider wells or the elimination of lower grade potash. The use of better extraction methods for potash, such as solution mining in combination with the increase on dependence of potash as an artificial fertilizer for world food production, has justified the present model to assume the full extent of potash mining as dictated by the BLM's 1993 map. Dubbed the BLM Mining Scenario, the new model only changes the extent of mining for flow modeling. The changes can be seen in Figure 8.1.

The transport of radionuclides through the Culebra was also modeled, with slight changes from what was assumed in the CCA performance assessment. Two experiments were conducted using the flow results of the Modified Mining Scenario to compare the results to previous modeling studies. The first experiment simulated plutonium through the Culebra unretarded, and were compared to the findings in Chapter 6. The second experiment modeled uranium with generated  $K_d$ s to compare the results with those in the performance assessment.

Figure 8.12. shows the results of the modeling conducted with the new assumed extent of potash mining within the controlled area. Modeling plutonium with no sorption to the surrounding matrix with BLM flow characteristics demonstrated to have the highest release probabilities. The experiment used a 1%  $K_d=0$  ml/g with the remaining 99% high  $K_d$ s generated from the LHS code showing no releases to the accessible environment. When compared to the 1%  $K_d=0$  ml/g with purely Full Mining of the CCA, release differences of up to 1.5 orders of magnitude are noticed. However, when comparing the Full Mining with no sorption to BLM Mining with sorption, the Full



Mining Scenario dominates the release probabilities, indicating that low sorption is much more important than high velocities.

## **9. GASOUT MODELING OF THE WIPP**

### **9.1. Summary**

The GASOUT code has been applied to the spillings scenario of the WIPP's disposal system to assess the conservatism of the results calculated in the Compliance Certification Application (CCA) (U.S. DOE 1996). A report on the application of the code (Hansen et al. 1997) states that a maximum of 0.27 m<sup>3</sup> of waste would fail in the borehole cavity from an intruding drill string and would be transported to the accessible environment through a blowout event. This calculated volume was used to verify the amount of spalled material calculated in the CCA as reasonable. However, an exercise with the code for an analysis on the sensitivity of several input assumptions shows that the code may be too sensitive, and the range of parameter values too small to judge the behavior of the disposal system accurately. It is suggested that the code be modified to allow a wide range of repository conditions to be modeled, so that an actual maximum spall can be calculated.

### **9.2. Introduction**

The blowout of spalled material reaching the accessible environment through an inadvertent human intrusion through a borehole into the WIPP repository could cause major problems with the compliance of the EPA's limit established in the 40 CFR Part 191 (U.S. EPA 1996a). EEG (1997e) has shown that spalled volume, ranging from 8 m<sup>3</sup> to 64 m<sup>3</sup> can violate these standards. DOE's published results have shown that a blowout would purge less than 4.0 m<sup>3</sup> of waste from the repository, with 0.27 m<sup>3</sup> being a more typical volume (Hansen et al. 1997). This chapter discusses the problems in using the GASOUT code as contained in Hansen et al. (1997).

Spall is waste that has been introduced into the drilling fluid due to radially channeled, highly pressurized gas flow from within the repository to a lower pressure borehole. Gas will continue to flow until the system comes to pressure equilibrium between the repository and the borehole. The high flow rates of gas will cause some of the material to fail in tension or shear, break off from the borehole cavity, and be introduced into the return stream of the drilling fluid. If gas flow is sufficiently high, it will force all the drilling fluid out of the borehole at the surface. This phenomenon is known as blowout, and is a common occurrence among drilling rigs encountering pressurized pockets of natural gas.

Spall can also occur by the mechanisms of stuck pipe and gas-induced erosion. These phenomena may dominate a spalled event if the gas flows are too low to cause blowout. Stuck pipe is a process of spall that, due to very low permeability and extremely high repository

pressures, may cause failed waste to press against the drill string sufficiently hard to prevent normal drilling. The solution of a jammed bit is to pull the drill string up and start drilling again. If the pressures remain high, the driller may have to bring the bit up several times, thus allowing significant quantities of waste to be brought to the surface through the return stream of the drilling mud. Gas erosion is spall that is eroded by the drilling mud due to high repository pressures and low waste permeability. The spall from gas erosion is slower than stuck pipe due to slightly lower pressures in the repository (just above hydrostatic), and may release waste into the drilling mud at a rate undetectable by the driller. Gas erosion would continue until the repository pressure is in equilibrium with the drilling fluid, and may also bring significant quantities of waste to the surface.

Stuck pipe and gas erosion releases will occur if the waste permeability is less than  $1 \times 10^{-16} \text{ m}^2$ , as stated in Berglund (1994), and repository pressures are greater than the pressure exerted by the drilling mud. The CCA states that the waste permeability can be represented by a constant value of  $1.7 \times 10^{-13} \text{ m}^2$ , which is much greater than the threshold for stuck pipe. Additional studies show that waste surrogates based on current understanding of waste mixtures could have a permeability of  $2.1 \times 10^{-15}$  to  $5.3 \times 10^{-15} \text{ m}^2$  (Hansen et al. 1997), and that the threshold for when blowout ceases and stuck pipe/gas erosion begins is questionable (EEG 1997e)

The DOE has made attempts at calculating the amount of material that will spall through a blowout. The code CUTTINGS\_S (U.S. DOE 1996-Appendix CUTTINGS\_S) incorporates the spallings calculations with calculations of the amount of cuttings and cavings from a drill string cutting through the repository. The calculations showed that a maximum of  $4.0 \text{ m}^3$  would fail in the borehole cavity and be forced out of the borehole to the surface. However, an independent peer review found the code to be conceptually flawed. The DOE's Conceptual Model Peer Review Group (U.S. DOE 1996-Appendix Peer 1) stated that the "Development of this [spallings] model is not sufficiently complete to determine uncertainties specific to the channel movement of waste to the existing borehole". The threshold for waste permeability and stuck pipe was also based on the findings of this code.

The spallings volume was re-calculated by using a second code, GASOUT (Shatz 1997), along with several other methods, to assess whether the results of the spalled material calculated in the CCA were reasonable. The GASOUT code was accepted by the Conceptual Model Peer Review Group (Wilson et al. 1997) based only on the conceptual model, without any independent testing or validation. Calculations with the GASOUT yielded a maximum of  $0.27 \text{ m}^3$  to reach the accessible environment upon a breach (Hansen et al. 1997). The main assumptions used in the code to derive at the calculated volume was a waste permeability of  $1.7 \times 10^{-13} \text{ m}^2$ , a repository

pressure of 14.8 MPa, and a waste tensile strength of 10 psi (0.068 MPa). Despite better understanding of the waste and measured values of the waste permeability,  $4.0 \times 10^{-15}$ , as described in Hansen et al. (1997), the CCA value of permeability ( $1.7 \times 10^{-13}$ ) was used for this investigation.

GASOUT uses a semi-analytic approach of a mechanistic conceptual model that couples the numerical calculations of a finite difference fluid flow code and a finite element rock mechanics code. This approach has been dubbed “the cavity growth method”, because it progressively calculates the region of radial tensile failure within the cavity. Hansen et al. (1997) stated that there is no tensile failure of waste below repository gas pressures of 14 MPa “under realistic but conservative assumptions”.

The conceptual model of the code during the blowout process was described as being divided into two stages. The first stage is characterized by the ejection of the drilling mud by high pressure gases, and the response of the waste to the high pressure gradients during blowout. Following the blowout, the second stage is identified by the rapid flow of gas from the repository, including the entrainment of solid waste particles. In the first stage of initial depressurization, gas velocities are small while the mud column is being expelled from the borehole. The velocities will increase during stage two, as the borehole path is clear for rapid gas movement. The larger eroded waste particles will typically be lofted to the surface during this stage.

In addition to the analysis using GASOUT, a “quasi-static” and “fully coupled” approach to solving the spillings problem was employed. The quasi-static used a spread sheet analysis to solve the porous flow equations by a sequence of steady state profiles (Hansen et al. 1997, pg. 3-24), and the conceptual model used in the quasi-static was identical to the cavity growth (GASOUT) method. The major difference in the two models is that the cavity within the quasi-static model does not change with the calculation of tensile failed waste removal. The results from the GASOUT calculation without failed material removal (removal of failed material is a toggle switch that can be turned on and off in the code), show almost perfect agreement with the quasi-static results under identical initial assumptions. Tensile failed material calculations for the quasi-static model showed  $1.17 \text{ m}^3$  of spall with initial pressure conditions of 14.7 MPa and tensile strength of 15 psi. The cavity growth model calculated an equivalent  $0.07 \text{ m}^3$  of spall.

The fully coupled approach used a purely numerical code (as opposed to the semi-analytic approach in GASOUT) to calculate the flow of gas within the waste region to the intruded borehole. The mathematical model of the fully coupled approach assumes a one-way coupling of the two-phase pressure decay following an intrusion with a decoupled two-phase pressure

response within the simulated waste region. The fluid flow and waste pressure response were solved by the code TOUGH28W with the poromechanical waste response of stress and strain invoked in the code SPECTROM-32.

Though the code did not explicitly calculate failure, it did calculate stresses within the waste. From the results using SPECTROM-32, the normal stresses show a semi-hemispherical distribution at very early times. If the initial assumptions for repository pressure are 14.8 MPa (lithostatic), and the waste tensile strength is 10 psi (0.04 MPa), then the code would indicate an elastic failure radius of 0.8 m (Hansen et al. 1997-Figure 4-9, time=0.001 s), or 2.1 m<sup>3</sup> uncompacted volume. The same figure shows a stress distribution extended out to one second, but without considering the possibility of waste removal. The removed waste would have a significant impact on the stresses in the cavity.

Though the GASOUT code was just a piece in the series of the spillings calculations performed in the investigation led by Dr. Frank Hansen, this chapter is basically restricted to the GASOUT code and will assess the performance of GASOUT for a wide variety of situations that are plausible for the WIPP disposal system. Furthermore, it will show the limitations associated with the code outside designated ranges of assumptions used for the investigation presented in Hansen et al. (1997).

### **9.3. Discussion**

GASOUT was run on a number of cases, by changing the initial permeability, the waste tensile strength, the initial repository pressure, mud density and the gas viscosity. The initial permeability refers to the permeability of the waste in the repository. Measured values of permeability from experiments on simulated waste specimens showed that the permeability is typically on the order of  $4.0 \times 10^{-15} \text{ m}^2$  (Hansen et al. 1997). However, none of the permeability experiments included the proposed backfill material, magnesium oxide, and permeability could actually decrease further with the added affect of cementation from the MgO backfill (U.S. DOE 1997b).

Waste tensile strength is the strength of the compacted waste in the repository that can withstand the flow of repository gas pressures before failing in tension. Measured values of waste tensile strength based on laboratory specimens of surrogate waste forms found a mean strength value to be 0.074 MPa with a standard deviation of 0.04 MPa (10.7 " 5.8 psi) (Hansen et al. 1997).

The repository gas pressure dictates the flow rate of gas from the internal rooms in each panel towards the borehole cavity. Higher repository pressures will result in higher gas flow rates, limited of course by the permeability of the waste matrix or the viscosity of the fluid. The maximum calculated pressure in the CCA, using the two-phase flow code, BRAGFLO, was 16.3 MPa in the waste panels for the undisturbed scenario, and 14 MPa for the disturbed scenario. The EPA's PAVT (U.S. DOE 1997d) calculated a maximum pressure of 16.8 MPa and 15.6 MPa for the undisturbed and disturbed scenarios, respectively. These maximum calculated pressures are higher than the lithostatic, since the lithostatic pressure at the depth of the repository is 14.8 MPa. Therefore, to reduce complications associated with fracturing within the repository, the highest repository pressure investigated will be 14.8 MPa.

GASOUT progressively reports the maximum tensile failed radius, and contiguous failed radius of the hemispherical cavity as the pressure gradient across the waste causes it to fail. During most simulations, these two radii will be equal. However, some simulations will report failure zones outside of the cavity, which are considered not to be spalled waste, and will not be carried out of the borehole through a blowout event. The extraneous cavities are not considered in the contiguous failed radius value.

The compacted and uncompact failed waste calculated from the failure radius are identified in Hansen et al. (1997) by the following two equations,

$$V_0 = \frac{1 - \phi}{(1 - \phi_0)} V \quad (1)$$

$$V = \frac{2}{3} \pi r^3 \quad (2)$$

where  $V_0$  is the uncompact spalling volume,  $V$  is the compacted volume,  $r$  is the radius of tensile failure,  $\phi$  is the compacted porosity of the waste (taken as 0.7) and  $\phi_0$  is the uncompact porosity of the waste (the value 0.848 was used in BRAGFLO). Simplifying, the expression yields  $V_0 = 1.97V$ , where  $V$  is dependent on the length of the failed radius.

Figure 3-12 of Hansen et al. (1997) shows the failure radius of a typical case throughout the time history of the model simulation. The effect is a "stair-step" behavior that represents failed events in the cavity. As the cavity grows from tensile failure, stress is lowered near the boundary of the cavity wall. As time ensues, the stress builds again until another failure event takes place, and the cavity grows as the result of waste breaking off.

The GASOUT results depend solely on the input assumptions provided in its evaluation. For comparison with the WIPP disposal system calculations of Hansen et al. (1997), the assumptions

remained the same for the present study with the “typical” case of the Hansen Investigation, and reasonable changes in certain parameters were conducted to test the code’s effectiveness under varying repository conditions. Through correspondence with John Schatz, the author of the code, it was noted that the code will work only for a narrow range of parameters, despite the unconditionally stable explicit solver used in the numerical (finite difference gas flow through the waste) portion of the code. Outside the designated range of values, the code calculates failure that are interpreted as meaningless, i.e., the code shows the radial failure of waste to cascade, and several “zones” of discretized waste will fail during a single timestep. Once the cascading affect starts, the stresses through the waste become discontinuous.

Table 9.1. lists the input values used as the typical case of this investigation. Table 9.1. represents the “Base” case of the present study and all analyses of sensitivity will be deviations from these assumptions.

Input Parameter	Current, EEG Investigation
Wellbore Diameter (m)	0.3111
Pipe Diameter (m)	0.2032
Outer Radius (m)	19.2
Surface Elevation (m)	1035.5
Base Elevation (m)	380.5
Base Height (m)	2.0
Initial Pressure (MPa)	14.5
Far Field Pore Pressure (MPa)	14.5
Initial Porosity	0.70
Initial Permeability (m <sup>2</sup> )	1.7E-13
Gas Base Density (kg/m <sup>3</sup> )	0.082 - reported as 11.33
Gas Viscosity (Pa*s)	10E-06 - reported as 9.2E-6
Mud Density (kg/m <sup>3</sup> )	1249.3 - reported as 1211
Mud Friction Factor	0.02
Gas Friction Factor	0.02
Far Field Stress (MPa)	14.8
Tensile Failure Velocity (m/s)	1000
Tensile Strength (psi)	15
Cohesion (psi)	18.85
Friction Angle (rad)	0.785
Max Time (s)	5
Eject Mud	True
No Flow Outer Boundary	True
Spherical	True
Allow Material Removal	True
Permeability From Porosity	False

Table 9.1. Input Assumptions for Base Case Study and from Hansen et al. (1997)

## 9.4. Base Case

The Base Case was run for the typical five second time period that was stated in Hansen et al. (1997) to be well within the first stage of the blowout process, and the amount of tensile failed material for this simulation matches the results presented in the Hansen Investigation, showing a failed radius of 0.25 m and a failed uncompacted volume of 0.05 m<sup>3</sup>. During the first five seconds, as seen in Figure 9.1., the acceleration and velocity of the mud column as well as the bottomhole pressure asymptotically reach a steady value. The left plot of Figure 9.1., shows that the acceleration of the mud column reduces significantly after the first second, when the mass flux of gas into the borehole has also significantly reduced. The figure matches quite well with Figure 3-3 of Hansen et al. (1997).

The middle plot of Figure 9.1. (below) shows velocity as a function of time for the first five seconds of blowout. Again, the plot reaches a steady value within a couple of seconds with a velocity of 6.36 m/s. This is slightly higher than presented in Hansen et al. (1997 - Figure 3-2), which reaches a steady value of approximately 5.8 m/s. The discrepancies between the two figures are slight, yet they exist. Small discrepancies are also seen for the pressure curves (Figure 9.3.-4 of Hansen et al. 1997 and the pressure plot of Figure 9.1., below). However, after running GASOUT at a lower initial repository pressure of 14.3 MPa, the velocity and pressure plots of Hansen et al. (1997) resemble the lower initial repository pressure distributions more closely.

The amount of uncompacted failed material volumes as a function of initial repository pressure and waste tensile strength presented from the Hansen Investigation (Table 1-1) are from a five second blowout simulation, and it is questionable as to what the length of time the code can run for meaningful results. The code simulates a compressible gas flow through porous media to the borehole cavity. From the flow calculation, pressure in the cavity is calculated, and is used to

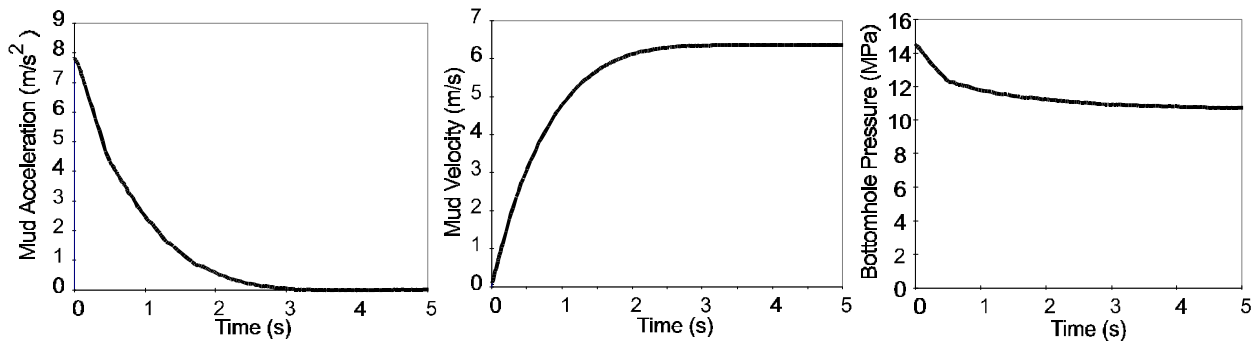


Figure 9.1. Verification of Typical Case Presented in Hansen et al. (1997) for Left) Mud Column Acceleration; Middle) Mud Column Velocity; and Right) Bottomhole Pressure



calculate the force required to push the mud column up, and out of the borehole annulus. The driving pressure of the gas for mud motion does not assume compressible flow, and is valid only when the gas pressures are high, and the mud column has moved a negligible distance. However, when the mud column has moved a considerable distance, the physics of the gas changes, and compressible flow will be an important consideration at later times of blowout.

It is suggested here that the five second results may be misleading. Though the code is questionable beyond the initial 5-10 second simulation, the Base Case shows a larger blowout release when the code is extended to 20 seconds and further to 50 seconds. By 20 seconds, the mud column has only reached 133 m, or 20% of the total borehole length, and the velocity of the mud moving up the borehole has increased from 6.36 m/s to 7.73 m/s. The tensile failed radial increased from 0.25 m (0.05 m<sup>3</sup> uncompacted volume) for a five second simulation to 0.27 m (0.066 m<sup>3</sup> uncompacted volume) for 20 seconds, and to 0.44 m (0.36 m<sup>3</sup> uncompacted volume) for 50 seconds.

Figure 9.2. shows the contiguous tensile radial failure, and mud motion velocity through time, of the Base Case simulation for an extended time of 50 seconds. It is clear that the two curves on the figure correlate, and as the velocity of the mud motion increases, the radial failure increases. However, it is unclear where the interpretation of reasonable radial failure should stop. Field conditions indicate that blowout is almost never ceased within a minute, if blowout preventers are not invoked. Therefore, it is reasonable to assume that spill would continue as long as the pressure gradient in the waste would cause failure.

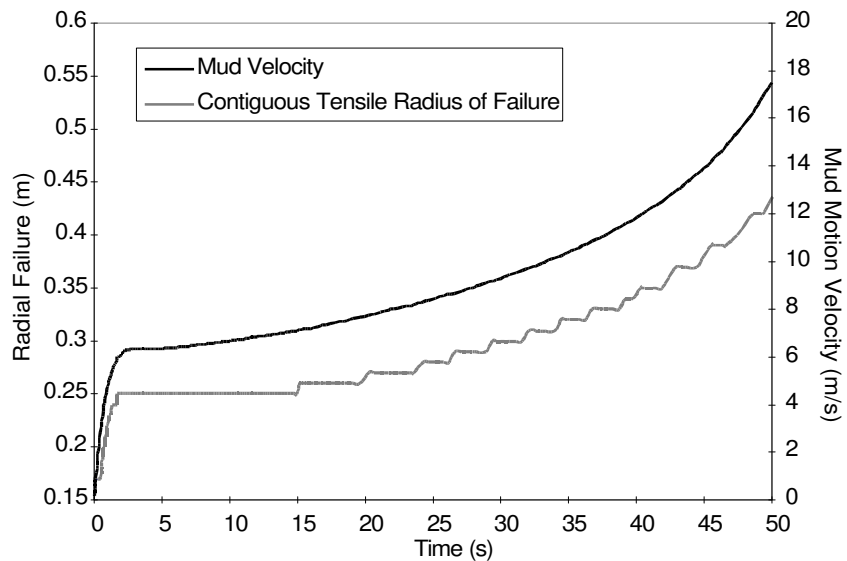


Figure 9.2. Contiguous Tensile Radial Failure and Mud Motion Velocity vs. Time for Base Case at Late Times

The duration of spall at later times would depend on the pressure gradient across the waste form, and its ability to remain high to cause failure. Figure 9.3. shows several pressure curves versus radial distance from the borehole, at 0.5, 5, 20, and 50 seconds during the Base Case simulation. The figure reveals that the pressure drop within 1 meter of the borehole center (the borehole center is marked as 0 on the abscissa) is high from 0.5 seconds to 5 seconds, much lower from 5 to 20 seconds, and becomes quite substantial from 20 to 50 seconds with a maximum drop of 2.5 MPa at 0.45 m from the borehole center. Though the pressure in the borehole cavity is low at 50 seconds (9.37 MPa), the pressure gradient across the waste at 0.5 meters from the cavity wall is higher than at 0.5 seconds. At 50 seconds, the pressure increases 3.4 MPa from the cavity wall at 0.44 m from the borehole center to 0.94 m from borehole center. The same distance of 0.5 meters from the borehole cavity at 0.5 seconds is 2 MPa. Furthermore, the radial and tangential (shear) stress distributions through the waste show smooth transitions during the time stepping and radial failure, and the simulation up to 50 seconds did not cascade waste at high rates. The only noticeable problem with the extended time simulation was the incompressible gas flow up the borehole. It is theorized that at later times when the gas expands from the lower compressive forces of the lighter mud column, the pressure in the borehole cavity will be even smaller. This will create an even higher pressure gradient across the waste, and more spall.

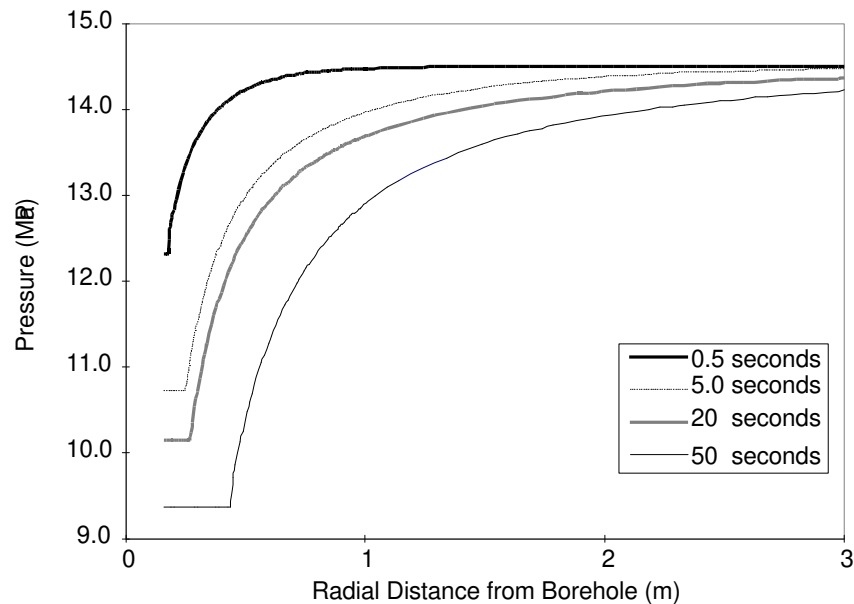


Figure 9.3. Pressure Distribution through the Repository after Intrusion with the Datum on the Abscissa Representing the Center of the Borehole, which has a Radius of 0.156 m.

## 9.5. Sensitivity to Permeability and Initial Repository Pressure

The GASOUT code was seen to be very insensitive to the initial permeability value chosen in this study. However, the code's use of a small number of parameters kept the sensitivity analysis to a minimum, and true sensitivity could not be established. The range of values narrowed as the initial repository pressure increased, and waste tensile strength decreased.

Initially, the permeability value that was used in the CCA ( $1.7 \times 10^{-13} \text{ m}^2$ ) was assumed in the present study to allow comparisons with the results in Hansen et al. (1997), despite a better understanding of permeability investigated in that report, and the value used in the CCA is under question here. The single value questioned was calculated from assumed future waste conditions.

Butcher (1990) ran permeability experiments on different and separate waste types to determine the overall waste permeability of the repository, looking for a value that could represent conditions for performance assessment calculations. These types included metals, combustibles (plastic, rubber, and wood), and sludges. Each waste type exhibited a range of permeabilities, with minimum, median, and maximum values presented in Table 9.2.

The values obtained in Table 9.2. are questionable. First, the representative materials for each type of waste do not cover the possibility of materials that will exist in the repository in the future. The combustibles, for example, used 1" pine cubes, which were to represent wood chips and sawdust (Butcher 1989). In 1,500 years, most (<90%) of the wood will be degraded, and the compaction of degraded wood would cause a lower permeability. Degraded metals would be another example, in which 50% magnetite and 50% 1" metal chips represent the average of degraded steel, aluminum, nails, and lead sheeting.

The volumes of each type of material were also considered in calculating the effective permeability of a drum. For the CCA, 40% combustibles, 40% metals, and 20% sludges were assumed from an average waste drum (U.S. DOE 1996-Appendix Peer 1). These values also varied from drum samples, and from each generating site. The Los Alamos National Laboratory volume (by percentage) of combustibles had an averaged value of 20, whereas the Savannah River Plant averaged 70 (Butcher 1989-Table 2.). These variances in volume could cause the expected value of  $1.7 \times 10^{-13}$  to decrease significantly.

The calculated value for waste permeability did not consider the effect of the proposed backfill (magnesium oxide) that will be placed around the waste to decrease gas generation, lower pH,

and help in the cementation of waste to increase waste strength. It is suspected that MgO precipitation will decrease the permeability by providing material for interstitial cementation, which was concluded by the Particle Size Expert Elicitation Panel (U.S. DOE 1997b) to be a major contributor to increased waste strength. The volume of the emplaced backfill will be approximately 25% of the total repository volume, and the permeability of cemented MgO, called Sorel cement, is much like Portland cement (Zheng et al. 1991), with values around  $1 \times 10^{-16} \text{ m}^2$ .

Lastly, a measured value of permeability on waste surrogates were reported in Hansen et al. (1997). The permeability of typical specimens were approximately  $4 \times 10^{-15} \text{ m}^2$ . It is, therefore, reasonable to assume that waste permeability could vary significantly from the single value of  $1.7 \times 10^{-13} \text{ m}^2$ , and simulations using smaller values of permeability in GASOUT are quite substantiated.

The results of spalled material failing in a borehole cavity using GASOUT over a wide range of permeabilities were not meaningful, and the code was simulated using a very narrow range. For the Base Case simulation for example, the waste permeability could only range from  $0.8 \times 10^{-13}$  to  $4.4 \times 10^{-13} \text{ m}^2$ . Above and below these permeabilities, the code predicted extremely large failed volumes. The results of the failed volume for a five second simulation can be seen in Figure 9.4. The figure shows failed volume versus the permeability range that was applicable. The reported failed volume is the maximum contiguous failed volume, calculated from Equations 1 and 2 above. The figure also shows results of varying waste tensile strength, from 10 to 20 psi. The three curves represented in the figure give the upper and lower bounds of the permeability that result in meaningful values.

The reported failed volumes outside the range for the Base Case are extremely high, resulting in as much as  $22.5 \text{ m}^3$  for a permeability of  $0.5 \times 10^{-13} \text{ m}^2$  due to the cascading affect of multiple zone failure. The geometry of the borehole cavity was discretized and solved on a hemispherical coordinate system. The layers of the hemisphere were kept to a minimum (0.01 meters) to avoid instability. When the waste in the borehole fails, it is assumed that the whole layer fails, and peels off like an onion skin. When the code calculates a large failed volume, as in the case with  $0.5 \times 10^{-13} \text{ m}^2$  permeability, the effect is several layers peeling off in one time

	Min	Med	Max
Combustibles ( $\text{m}^2$ )	2.00E-15	1.70E-14	2.00E-13
Metals ( $\text{m}^2$ )	4.00E-15	5.00E-13	1.20E-12
Sludge ( $\text{m}^2$ )	1.10E-17	1.20E-16	1.70E-16

Table 9.2. Permeability Values Used to Calculate the Waste Permeability in the CCA

step, cascading until an equilibrium is reached with the high pressure gradient that existed at a longer time period. It is assumed that when the cascading effect is exhibited, the results become meaningless.

Figure 9.4. shows some interesting results as the waste permeability increases. All the waste strengths tested showed an exponentially decreasing failed volume, up to a permeability of  $2.5 \times 10^{-13} \text{ m}^2$ . Permeabilities above this value caused larger failed volumes than values below it within the range where cascading waste is not a factor in failed volume. The upper limit on permeability shows that the code is reliable to  $2.5 \times 10^{-15} \text{ m}^2$  for waste strengths that were measured in the report by Hansen et al. (1997) and initial repository pressure of 14.5 MPa. The lower permeability limit is  $1.0 \times 10^{-13} \text{ m}^2$  for 10 psi waste strength, and decreases to  $0.8 \times 10^{-13} \text{ m}^2$  for waste strengths of 15 and 20 psi.

When the initial pressure is increased to its maximum of 14.8 MPa, the range is more narrow than discussed above. For all waste strengths investigated, confidence was only in waste permeabilities between  $1.7 \times 10^{-13} \text{ m}^2$  and  $2.0 \times 10^{-13} \text{ m}^2$ . The narrow range that the code is applicable decreases the likelihood that the code can represent the disposal system accurately. The code should be modified to allow more representative values to be modeled.

The simulation of the repository with a homogeneous waste in GASOUT is an over simplification

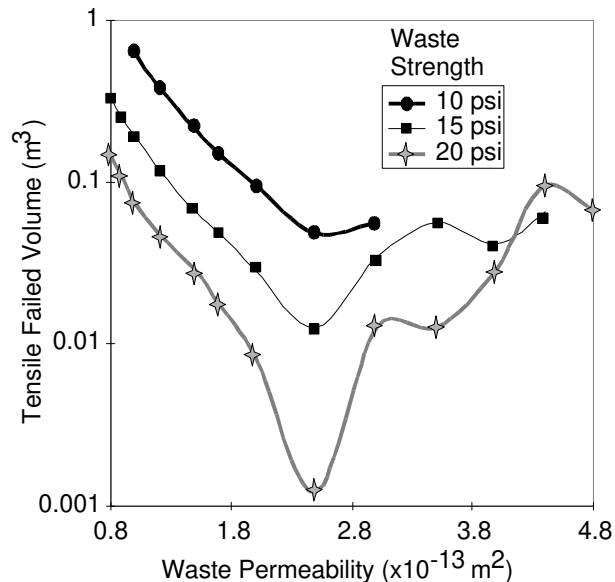


Figure 9.4. Contiguous Failed Volume as a Function of Increasing Waste Permeability for Different Waste Strengths with an Initial Repository Pressure of 14.5 MPa

of the repository model. It is likely that the waste permeability will actually be lower than that assumed in the CCA. The representation of a random permeability was explored in Hansen et al. (1997) using a fully coupled numerical code to solve the flow of gas through the repository. TOUGH28W did not calculate the amount of waste failure, but could calculate the pressure distribution through the waste for varying conditions. The code showed that a lower permeability, with values ranging from  $1 \times 10^{-12}$  to  $1 \times 10^{-16}$   $\text{m}^2$  would have a much higher pressure gradient near the borehole, than the permeability assumed in the CCA. It also showed that homogeneous waste with lower permeabilities will have higher pressure gradients. This further strengthens the argument for modifying GASOUT to represent the repository more accurately.

### 9.6. Sensitivity of Gas Viscosity

The gas viscosity parameter, along with porosity and permeability, is used to calculate the hydraulic conductivity of gas through porous media,  $K$ , by the relationship of

$$K = \frac{k}{2\phi\mu} \quad (3)$$

where  $k$  is permeability,  $\phi$  is porosity, and  $\mu$  is gas viscosity. The original equation for the flow of gas through porous media can be found in Chan et al. (1993), and is equivalent to the non-linear diffusion equation. The viscosity of Equation 3 is indirectly proportional to the gas conductivity, and as viscosity increases, conductivity decreases. The relationship also shows that a constant ratio of permeability to viscosity will yield the same conductivity.

The experiment with permeability demonstrated that values less than  $1 \times 10^{-13}$   $\text{m}^2$  for an initial pressure of 14.5 MPa would render the results meaningless. The viscosity used in the experiments was  $10 \times 10^{-6}$  Pa\*s, and the ratio of permeability to viscosity yields  $1 \times 10^{-8}$ . Values less than this ratio causes the code to predict cascading failure of waste. With the original permeability of  $1.7 \times 10^{-13}$   $\text{m}^2$ , viscosity values greater than  $17 \times 10^{-6}$  Pa\*s causes the code to give erroneous results. The ratio for failure criterion increases to  $1.7 \times 10^{-8}$  for an initial repository pressure of 14.8 MPa and waste tensile strength of 10 psi. A simulation with the ratio of  $1 \times 10^{-8}$   $\text{m}^2/\text{Pa/s}$ , an initial pressure of 14.5 MPa, and tensile waste strength of 10 psi yields a failed volume of  $0.63 \text{ m}^3$ .

The possibility of larger viscosity values is not ill conceived. The viscosity value obtained for hydrogen gas was the standard temperature and pressure value (STP), and viscosity increases moderately as pressure or temperature increases.

The components of the repository gas will also increase the viscosity. Through microbial degradation of plastics, rubbers, and other combustible material, O<sub>2</sub>, CO<sub>2</sub>, CH<sub>4</sub>, N<sub>2</sub>, N<sub>2</sub>O and H<sub>2</sub>S will be created. Francis et al. (1996) conducted experiments of microbial gas generation under expected WIPP repository conditions and found that the percentage of N<sub>2</sub> varied between 61.9% to 91.4%, CO<sub>2</sub> varied between 0.4% and 34.3%, and H<sub>2</sub> varied between 0% and 12.8%. These other constituents have a much higher viscosity than H<sub>2</sub>, with N<sub>2</sub> being as high as 19.2x10<sup>-6</sup> Pa\*s (STP), which will undoubtedly increase with an increased repository pressure.

Even though microbial degradation may create higher quantities of CO<sub>2</sub>, and N<sub>2</sub> than H<sub>2</sub>, the process itself will be limited. It is uncertain whether the colonies of microbes can exist under repository conditions, and was therefore assigned a 50% chance in the CCA. Iron corrosion on the other hand will produce massive quantities of H<sub>2</sub> and it is certain that iron will corrode when brine fills the repository. Approximately 2x10<sup>9</sup> moles of H<sub>2</sub> (Telander and Westerman 1996) will be produced from the iron in WIPP. However, the other gaseous constituents could play a small role if microbial degradation does produce gas. Figure MASS-1 (U.S. DOE 1996-Appendix MASS) shows that at lithostatic pressure, if the mole fraction of H<sub>2</sub> to CO<sub>2</sub> is reduced from 100% to 90%, then the viscosity would increase from 9x10<sup>-6</sup> Pa\*s to 16x10<sup>-6</sup> Pa\*s. Therefore, it is suggested that the code be modified to allow a larger spectrum of values to be modeled.

### **9.7. Sensitivity to Mud Column Density**

The density of the mud column in the borehole is dependent on the type of drilling mud used. For the WIPP, it is most likely that the drilling mud will come from the Salado Formation with additives to increase the average mud density to 10 - 11 lb/gal (1200-1320 kg/m<sup>3</sup>). The GASOUT code used a density of 1249.3 kg/m<sup>3</sup> in the Hansen Investigation, and it is possible that this value could vary over the range mentioned above.

Figure 9.5. shows the results of varying the parameter from 1200 to 1320 kg/m<sup>3</sup> for a 10 second simulation and an initial repository pressure of 14.8 MPa. The figure shows three curves of different waste strength, with all other parameters remaining the same as used in the Base Case simulation. The most outstanding feature of Figure 9.5. is the disjointed curve of failed waste (left) and mud motion (right) of the 10 psi tensile waste strength simulation. The code had trouble calculating failed waste for mud densities below 1228 kg/m<sup>3</sup>, resulting in the cascading affect described above. The code also had trouble at 1240 and 1250 kg/m<sup>3</sup>, and if results were plotted for these densities (failed waste and mud motion), sharp spikes would exist in the curve.

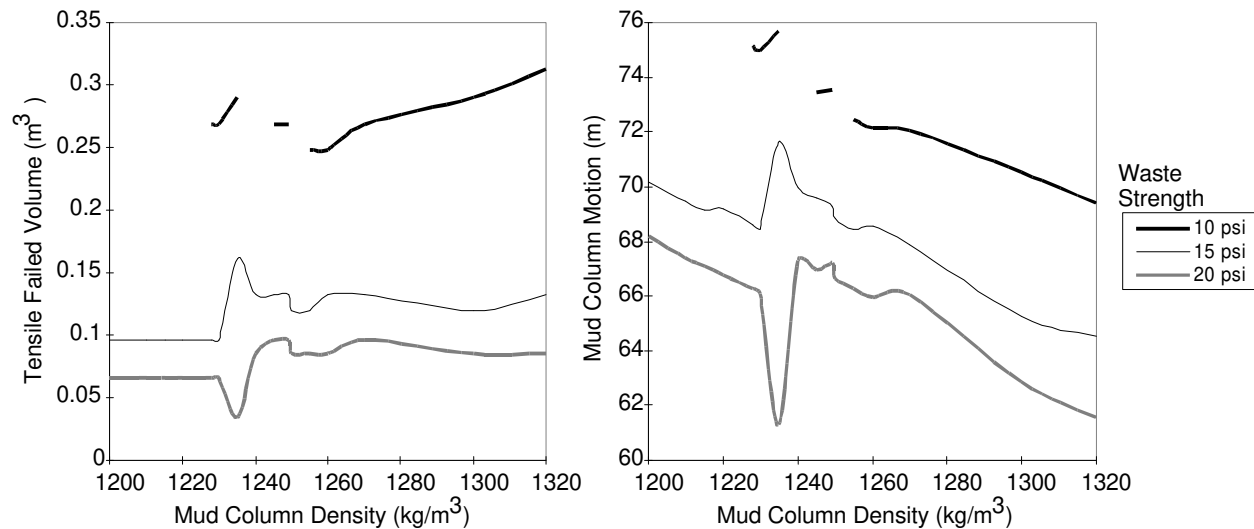


Figure 9.5. Left) Tensile Failed Volume as a Function of Mud Column Density for Several Waste Strengths and Right) Mud Column Motion as a Function of Mud Column Density

For the higher waste strengths (and subsequently lower repository pressures) of 15 and 20 psi, the mud density simulations were able to calculate failed volumes for all density values investigated. However, the results seemed almost as unreliable as the lower waste strength. Though a trend can be seen in the failed volume and mud motion, variances from those trends are high. Both graphs in Figure 9.5. show trouble with the code when densities are between 1230 and 1270  $\text{kg/m}^3$ .

### 9.8. Sensitivity to Waste Porosity

Lastly, the code was investigated to test the effect of waste failure with changing (decreasing) porosity. If the porosity is lower, then the velocity of the gas moving through the repository to a borehole intrusion is higher. Hansen et al. (1997) report a porosity of 0.7, which was said to be typical of waste porosity when the pressure reached over 14.8 MPa. However, after investigating the relationship between pressure and porosity, it was found that porosity during the long-term performance of the repository was approximately 0.2 for high pressures, and less for lower pressures. Figure 9.6. shows the relationship of porosity to pressure for the undisturbed scenario of the performance assessment for the CCA. The figure shows two separate times, at 5,000 and 10,000 years postclosure using the results of BRAGFLO.

Porosity from the two-phase calculations of brine and gas flow through the repository clearly show the porosity will be quite low. The response of the code to lower repository porosities show slightly higher releases. For a porosity of 0.2, with initial conditions of 14.8 MPa repository pressure, and 10 psi waste strength, the uncompacted spalled volume is  $0.47 \text{ m}^3$ , and decreases



smoothly up to the original porosity of 0.7 and a calculated failed volume of 0.27 m<sup>3</sup>. However, porosities above 0.7 and below 0.2 caused the calculated waste to cascade. Additional experiments using a variety of repository pressures and their expected porosities from Figure 9.6., does not show any further problems within the code.

### 9.9. Conclusions

A sensitivity analysis has been performed on the spillings code, GASOUT. GASOUT along with several other codes were used by the DOE to prove that the spalled volume calculated in the Compliance Certification Application (CCA) were reasonable, because the GASOUT calculated a much smaller spalled volume than those calculated in the CCA. The results of the experiment were documented in Hansen et al. (1997), which showed that a maximum of 0.27 m<sup>3</sup> would spall through blowout upon breach of the repository. The volume of spalled material calculated in the CCA ranged from 0.5 to 4.0 m<sup>3</sup>.

The simulated blowout in the Hansen et al. simulations only lasted for five seconds. Blowout usually takes several minutes to control, and it is believed that much higher volumes of failed material would be derived if the simulations were run for longer periods of time. Sensitivity analysis in this chapter showed that as much as six times the volume would fail, if the experiments were extended in the GASOUT code from five seconds to approximately 50 seconds. Discounting the late time effect of spall when the velocities are allowed to flow faster from the waste underestimates the total amount of failed material that will reach the surface.

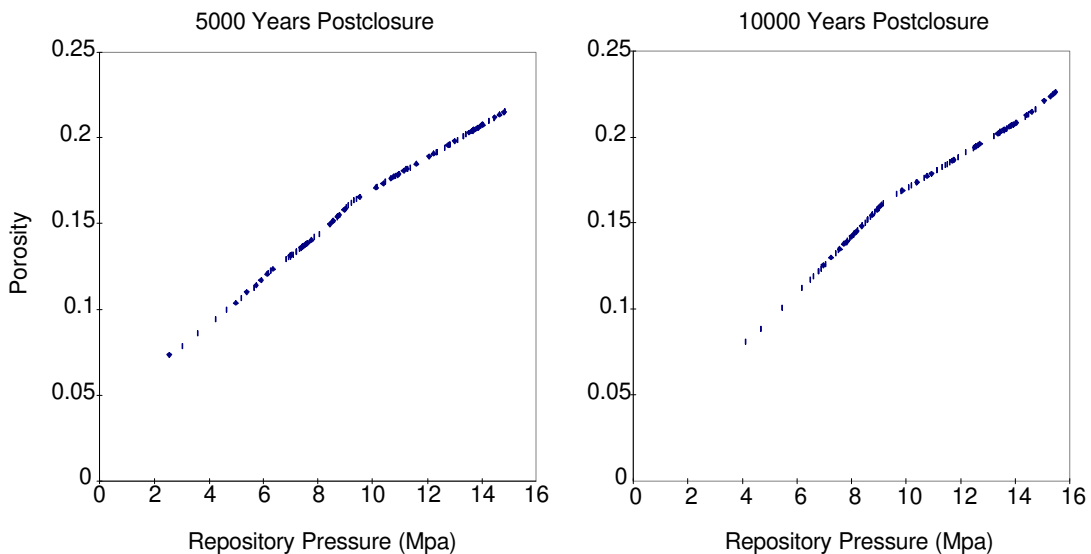


Figure 9.6. Porosity Versus Pressure Profiles for Undisturbed Scenarios of the CCA

GASOUT was also tested for its response to a range of waste permeabilities. The permeability of the waste used in the CCA was  $1.7 \times 10^{-13} \text{ m}^2$ , and thus was carried over to the analysis in Hansen et al. (1997). However, the same report also measures a new value of permeability, based on a better understanding of simulated waste forms. These surrogates for the WIPP waste exhibited a permeability on the order of  $4 \times 10^{-15} \text{ m}^2$  for “typical” specimens. None of the surrogates that measured permeability contained magnesium oxide, the proposed backfill material that is said to occupy 25% of the repository’s volume, and precipitation is expected to decrease the permeability of the waste.

An analysis of permeability with GASOUT showed that the code can only be applied to a small range of parameter values. For the most extreme case, using an initial pressure of 14.8 MPa and waste strength of 10 psi, the range is  $1.7 \times 10^{-13}$  to  $2.0 \times 10^{-13} \text{ m}^2$ . The range is extended when waste strength is increased and pressure is decreased. The small range of permeabilities prohibits the use of the code under varying repository conditions. Hansen et al. (1997) shows that lower permeabilities will have high pressure gradients through the waste, thus inducing more spall.

The code also showed sensitivity to gas viscosity. Viscosity, along with permeability and porosity are used to calculate an effective gas conductivity for the flow of gas through the repository upon an inadvertent human intrusion. It is reasonable to assume that viscosity will be higher than the ideal value for hydrogen at standard temperature and pressure. It will also be higher if other gas constituents are added to the repository. Yet, as viscosity increases to values that are reasonable and defensible, the code calculates a very high failed volume due to the cascading effect noticed from low permeabilities.

Lastly, a sensitivity of the mud column density showed that the code does not promote a strong confidence in the results obtained from GASOUT. The analysis varied the parameter over a range of expected values at the WIPP, and found the code to behave erratically to small changes in values. Figure 9.5. shows the results of the experiment, and demonstrates the problems associated with using a wide range of values. The figure represents a high initial pressure using several different waste strengths, which proves that the code can only work well under non-extreme conditions. The maximum reported spalled volume in Hansen et al. (1997) is only the maximum for a narrow set of repository conditions, and the code is shown to fail otherwise.

Hansen et al. (1997) claim conservatism in the approach to modeling the WIPP waste under a spall scenario. First, the waste form was considered homogeneous in GASOUT. Arguments

have been made to explain that homogeneity is very conservative, and heterogeneous waste will decrease spall. Yet it can be seen in the fully coupled numerical code that heterogeneity will increase the pressure gradient, and possibly the amount of spalled material. Hansen et al. (1997) show that inelastic behavior of the waste will increase tensile strength, and reduce the amount of waste failing in tension. However, inelastic behavior is attributed to saturated (wet) waste, which is ductile and will have a lower strength than dry waste. Dry waste forms will most likely be brittle, and will fail elastically. They also claim that tensile failure will induce fracturing within the waste, increasing the permeability of the cracked region, causing the system to stabilize more quickly. However, this too can be detrimental; the turbulent flow of gas will impose additional forces (e.g., drag forces) on the waste that may erode the waste and cause more spall. In short, the claimed conservatisms applied to the models for calculating the release of spalled material are actually simplifications, which are necessary in order to construct reasonable mathematical and numerical models; they are not conservative assumptions.

This analysis does not question these mathematical and numerical models used to design the GASOUT code; it addresses the working of the code itself. The code responds erratically to small changes in the input assumptions, and sometimes gives misleading results. It is suggested that the code be examined more closely, before judging the results of Hansen et al. (1997) as the maximum amount of failed material that will reach the surface, and the spalled volumes calculated in the CCA as reasonable.

## **10. SOLUBILITY MODELING ASSUMING NO MgO BACKFILL AND WITH THE MgO MINERAL PHASE OF NESQUEHONITE**

### **10.1. Summary**

A modeling study was conducted to accommodate DOE's reported observation that nesquehonite was the only identified observed product from the MgO-carbon dioxide study. The modeling study parallels the EPA requested PAVT calculations in that the magnesium compound was assumed to persist throughout the 10,000 year regulatory period. There is a difference, however, as the PAVT calculations recommended by the EPA assumed the presence of hydromagnesite, which was not observed in the DOE experiments. The study assumed the presence of nesquehonite, which was observed in the DOE experiments. Moreover, this study also calculated releases using the modeled solubilities in the case of no backfill.

As shown, these higher solubilities have a dramatic impact on the cumulative release of radionuclides to the accessible environment for the 10,000 year period. Assuming the results of the FMT calculations for solubility are correct, the calculated release for a system without backfill or a system with backfill induced nesquehonite is very close to the EPA containment requirement. While these calculations, based on DOE's own solubility values, do not violate the containment requirements, they also show that there is little margin for error.

### **10.2. Introduction**

Chapter 5 explained EEG's concern's about assuming the oxidation of plutonium to states III and IV. To determine the sensitivity of the release calculations to solubility, the solubility was increased, assuming all plutonium was in oxidation state V. The results showed that as solubility increased, the releases increased, but was limited by the amount of brine in the repository. This chapter further investigates the relevance and consequence of brucite speciation to magnesite and its effects on solubility.

The idea of adding MgO as backfill around the waste in the WIPP repository began shortly before the CCA was issued to the EPA, and consequently no analysis was performed in the Baseline Inventory Report (U.S. DOE 1996-Appendix BIR). In response, the DOE Peer Review Committee had to reconvene several times to be convinced of its effects, with the main issue being the effectiveness of  $Mg(OH)_2$  to react with  $CO_2$  to act as a buffer to increase to pH of the brine and reduce the  $fCO_2$  for reaction with the brine. Experiments had not been performed by the time of application submittal, and it was unclear how effective the backfill would be.

It was anticipated that large quantities of CO<sub>2</sub> would be generated in the repository (U.S. DOE 1996-Appendix Peer 1). The CO<sub>2</sub> would react with the brine, forming carbonic acid. The acid would decrease the pH of the Salado brine from 9.4 to approximately 4-5. Under acidic conditions (pH lower than 4), the solubility of actinides could increase by 5 orders of magnitude in brine, causing problems in the inadvertent human intrusion scenario. The higher solubilities would allow a higher mass of actinides to go into solution, and hence higher releases to the accessible environment upon breach. The original intent of the MgO was to maintain a high brine pH.

The concern was not the chemical reaction pathway however, it was the effectiveness of the design in the placement of the MgO around the waste to allow reaction with the large amounts of CO<sub>2</sub>. The DOE needed to perform experiments to demonstrate the effectiveness of MgO in increasing the pH and reducing the fCO<sub>2</sub>. The results were presented to the Third Supplemental Peer Review on April 25, 1997. It was the intention of that Peer Review for DOE to prove that the MgO will act quickly and completely with the CO<sub>2</sub> to reduce carbonate ligands from solution and to decrease gas pressures and rate of gas pressurization by the removal of CO<sub>2</sub>. The subsequent report (Papenguth et al. 1997) showed the results of the experimentation, which were used for modeling data in the FMT code to establish solubilities for the various actinides under those chemical conditions (Novak 1997).

Recently, several issues were brought to light about the inherent problems and conclusions of that study (Neill et al. 1998). First, it was assumed that by 1000 years after the formation of CO<sub>2</sub>, that the precipitates from the reactions would form magnesite. This conclusion was extrapolated (linearly) from literature data at different temperatures. Yet, the extrapolation seemed to be a poor justification that the reaction would go to completion (to magnesite) within the time frame of the WIPP projected history. If the extrapolation were assumed to be another function, then the time could extend to the order of 10<sup>5</sup> - 10<sup>6</sup> years. Secondly, the intermediate phases between brucite (Mg(OH)<sub>2</sub>) and magnesite (MgCO<sub>3</sub>) were unclearly defined in their function, length of time, and composition. It was concluded that nesquehonite (MgCO<sub>3</sub> • 3H<sub>2</sub>O) would exist for a very short time before going to hydromagnesite [(MgCO<sub>3</sub>)<sub>4</sub> • Mg(OH)<sub>2</sub> • 4H<sub>2</sub>O]. Yet, hydromagnesite was never positively identified, and a mineral species, that was noted to be hydromagnesite-like, existed instead. The composition [MgCO<sub>3</sub> • 3H<sub>2</sub>O • MgCl(OH)] looked closer to nesquehonite than hydromagnesite.

Lastly, the results from FMT were questioned for solubilities of actinides in the presence of the various mineral species and the use of the oxidation state analogy for actinides in the same

oxidation state. For example, the concentration of  $\text{Th}(\text{SO}_4)_2$  in Castile ERDA-6 brine was  $1.35 \times 10^{-5}$  mol/kg. When  $\text{Mg}^{++}$  was added to the solution, to increase it from 0.021 to 0.039 mol/kg, the concentration of  $\text{Th}(\text{SO}_4)_2$  reduced to  $9 \times 10^{-22}$  mol/kg. Nothing in the chemistry of the brine would contribute to such a large discrepancy in the values given for thorium sulfate.

Though sulfate complexes were assumed to be minor, the same problems were carried over to the carbonate species of thorium. Thorium is an important consideration in these experiments, because by the oxidation state analogy thorium was used to establish all IV actinides (Pu, U, and Th). It was seen that the errors of one actinide carried through to the other major actinides.

Novak (1997) provided projected actinide solubilities in the presence of nesquehonite and also without the presence of MgO backfill (no backfill), in addition to magnesite and hydromagnesite values. Due to the uncertainties associated in the model and laboratory experiments, it was decided to use these higher solubilities from species that were not considered in either the CCA or the EPA's verification calculations, called the Performance Assessment Verification Test (PAVT), in a new set of calculations using PANEL and NUTS. The results were then used to compare the CCDFs from the CCA (DOE) and PAVT (EPA) to acquire a better understanding of long-term performance.

The median model solubility values used for the CCA, PAVT, and for other species of brucite-magnesite complexes can be seen in Table 10.1. (reproduced from Novak 1997). The CCA used magnesite as the interactive species and the PAVT used hydromagnesite. Neither used nesquehonite, the only identified observed species. Hence, nesquehonite and No Backfill solubilities are used here. One outstanding feature of Table 10.1. is the difference in solubility of +4 actinides in Castile brine between No Backfill and nesquehonite. The experimental model values show that the +4 state is more soluble in the presence of nesquehonite than without any addition of MgO.

### 10.3. Methodology

In the CCA, the model (median) values from FMT were given an uncertainty range of -2 and

Brine Type	Salado				Castile			
	+3 (M)	+4 (M)	+5 (M)	+6 (M)	+3 (M)	+4 (M)	+5 (M)	+6 (M)
magnesite (CCA)	5.8e-7	4.4e-6	2.3e-6	8.7e-6	6.5e-8	6.0e-9	2.2e-6	8.7e-6
No Backfill	4.0e-3	5.0e-4	2.0e-4	8.0e-5	2.0e-3	7.0e-5	6.0e-4	8.0e-5
hydromagnesite (PAVT)	9.4e-8	1.2e-8	1.2e-7	8.7e-6	1.3e-8	4.1e-8	4.6e-7	8.7e-7
nesquehonite	3.2e-7	6.3e-4	1.2e-7	8.7e-6	2.1e-6	1.0e-3	7.8e-7	8.7e-6

Table 10.1. Median Solubility Values Used in Various Performance Assessment Calculations

	nesquehonite		No Backfill	
	SOLCIM	SOLSIM	SOLCIM	SOLSIM
SOLAM3	1.51616	-.27709	4.48678	3.83714
SOLPU3	1.51616	-.27709	4.48678	3.83714
SOLPU4	5.23242	2.15588	4.06695	2.05552
SOLU4	N/A	2.15588	N/A	2.05552
SOLU6	0.95861	0.96357	0.95861	0.96357
SOLTH4	5.23242	2.15588	4.06695	2.05552

Table 10.2. Solubility Factors for SOLCIM and SOLSIM

+1.4 orders of magnitude. Incidentally, the 1992 PA (Sandia 1992) had many of the parameter ranges of the actinides span 13 orders of magnitude to capture the uncertainty. The range in the CCA was given a constructed distribution, where the majority of the values (59%) fell -1.0 and 0.0 orders of magnitude from the values of Table 10.1. For the present study, the ranges have been eliminated, with each realization having the same constant value.

Running the new values for solubility of various actinides began at the Source Term files. These files contained the multiplication factors from which the median values would be modified. For example, the solubility of <sup>241</sup>Am in Castile brine was given a range, as explained above. This range was sampled in LHS, and a number was identified in each realization (vector). If the

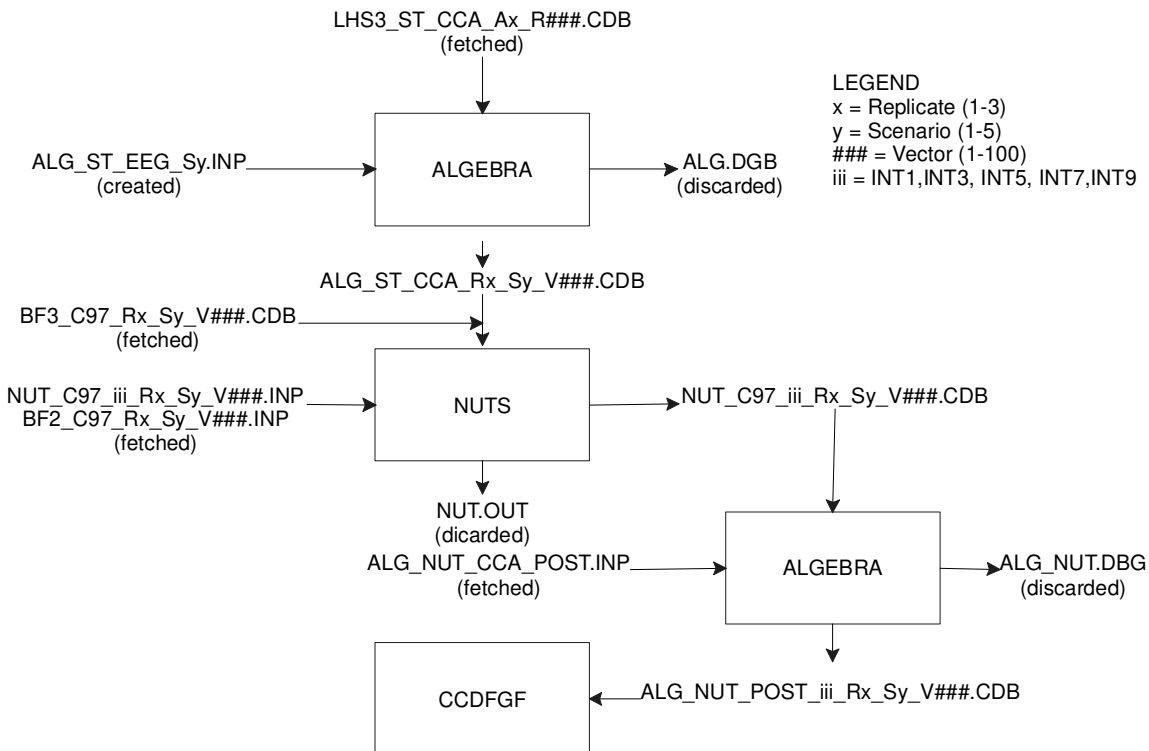


Figure 10.1. Flowchart for NUTS Time Intrusion Calculations

sampled value in LHS was -1.0, then the median value was multiplied by  $10^{-1.0}$ . In the transport experiments of this study, these values were replaced by the values in Table 10.2. for every realization. The parameter names are retained from CCA nomenclature.

After modifying the Source Term files, PANEL and NUTS were run with the new files. For this study, the BRAGFLO files from the PAVT study were used, since this would give the maximum effect for the changes. The PAVT, compared to the CCA, calculated much higher releases to the surface due to the higher pressures in the repository.

The flowchart of PANEL execution can be seen in Figure 5.1., and the flowchart for NUTS execution can be seen in Figure 10.1. The flow chart only represents one set of NUTS calculations, but represents the processes of all three sets. These sets include SRC, ISO, and INT calculations, and are further explained in Chapter 2. Figure 10.1. shows the detailed steps involved in running the INT (Time Intrusion) calculations.

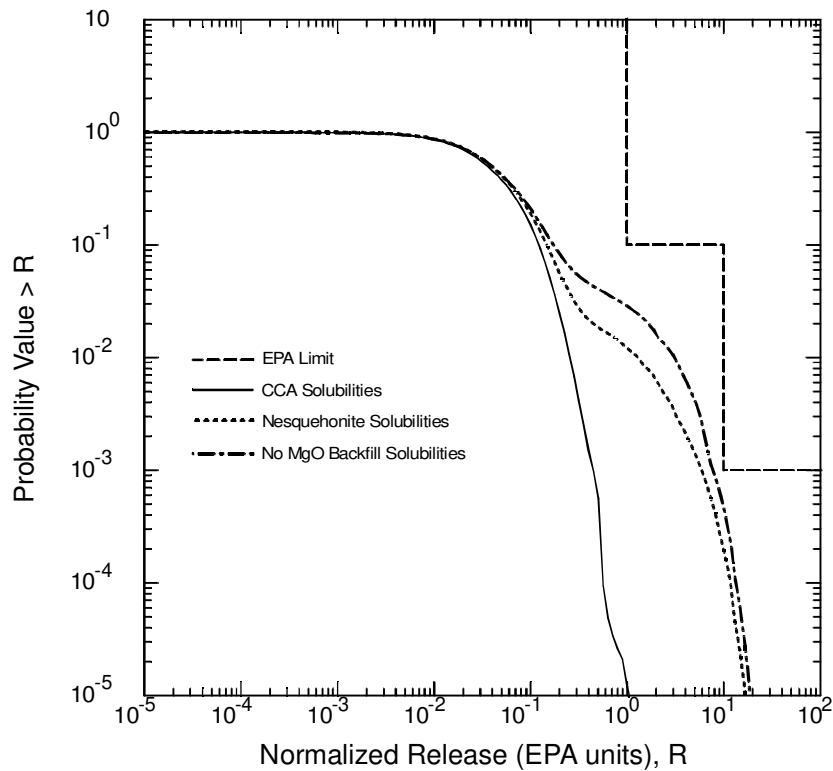


Figure 10.2. Overall Mean of Normalized Releases for Modeling of Increased Solubilities Using Nesquehonite and 'No Backfill' Values Compared to CCA Values



## 10.4. Results

The results of running the new set of solubility calculations can be seen in Figure 10.2. The figure shows the overall mean from all combined release mechanisms for No Backfill and nesquehonite solubilities from Table 10.1. In addition, the PAVT direct brine releases were combined with the CCA solubilities from CCA NUTS calculations to give another perspective of calculated solubility values. The curves show that neither release scenarios cross the EPA compliance standard, indicating that even the highest reported solubilities do not violate these standards, with all other parameters remaining the same.

The effects of increasing the solubility values for the new calculations show a substantial increase below the  $10^{-1}$  probability. The increase, in the form of a shoulder, is attributed to the increased effect of the direct brine release mechanism. Figure 10.3. shows the breakdown of all mechanisms to form the total release. The figure presents each mechanism as the overall mean from all realizations of one replicate from the nesquehonite solubility calculation. Clearly, the direct brine release calculations stand out as the largest mechanism for release at the  $10^{-3}$  probability.

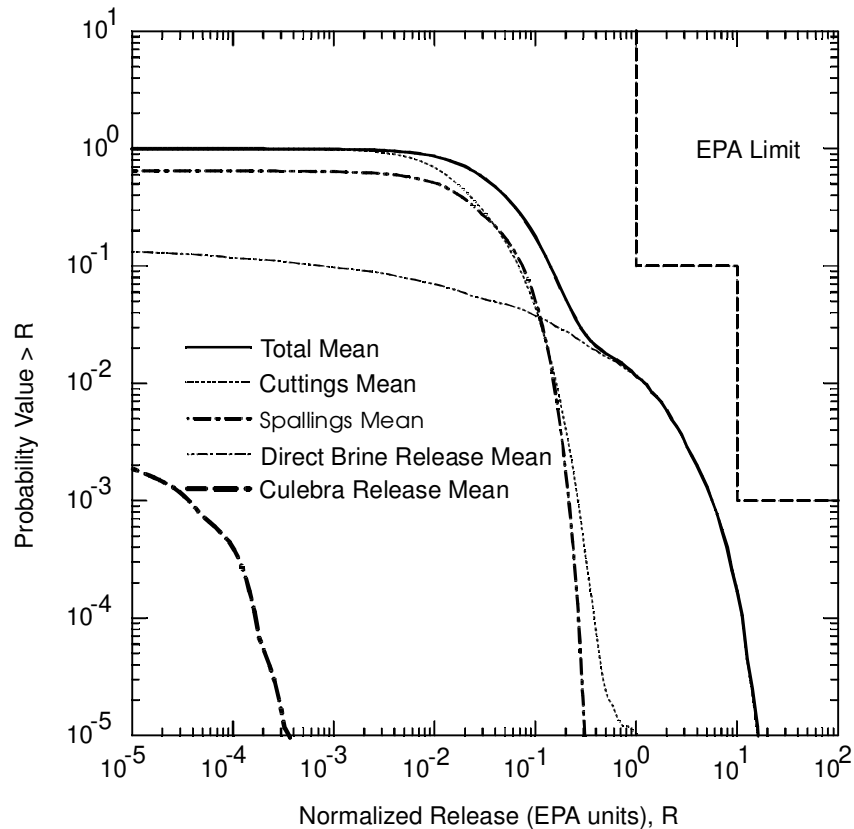


Figure 10.3. Overall Mean from all Release Mechanisms for Solubility Modeling With Nesquehonite

In addition to the results of the PAVT, the solubility modeling of nesquehonite and No Backfill was combined with other chapters of this report, namely the Culebra Transport Modeling, to assess the effects of higher initial masses injected into the Culebra. Conclusions from previous chapters stated the limitation of the Culebra releases due to the amount that would initially reach the Culebra from transport out of the repository. The combination from previous results with the present study was a simple task, since all mechanisms are calculated separately and combined in the end through the code CCDFGF.

Figure 10.4. shows the Culebra releases from Chapters 6 and 8 with the nesquehonite solubilities of Chapter 10. The conclusions of the two earlier chapters that the releases are mass limited is verified here. If the initial amount of mass that reaches the Culebra are increased, such as with increased solubility, then the effect will be quite strong on the Culebra releases, as seen by the increases in releases in the CCDF curves of plutonium at 1%  $K_d=0$  ml/g. However, in itself, solubility has little effect, and must be coupled with large fractional discharges calculated with 1%  $K_d=0$ . This can be seen when comparing the two curves in Figure 10.4., which come from the Chapter 8 analysis on increased mining. The uranium releases are very small and the

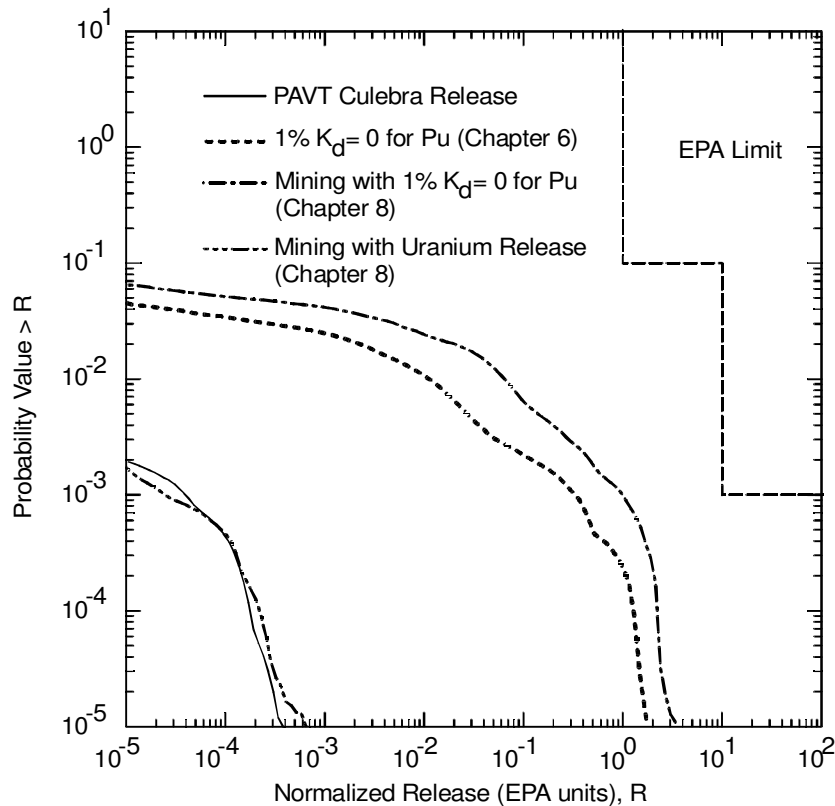


Figure 10.4. Nesquehonite Solubility Calculations Combined with Culebra Transport Calculations from Chapters 6 and 8

plutonium releases are quite large, even though both have an increase in initial mass. It is clear then that high solubilities and low  $K_d$ s will cause quite a threat to the integrity of the disposal system.

## 10.5. Conclusions

A modeling study has been presented in which the solubilities of actinides from the CCA and PAVT are questioned. New values are presented in Table 10.1. with the assumption of the persistence of an intermediate phase between brucite and magnesite to exist for the entire 10,000 year proposed history of the WIPP repository. The modeling of the intermediate phase, nesquehonite, is much like the modeling of the PAVT, in which hydromagnesite was assumed to persist throughout the 10,000 years. In addition, No MgO Backfill model solubilities were studied.

The consequence of higher solubilities, as seen in Figure 10.2. are quite high. The overall mean release for the CCA and PAVT were 0.2 and 0.4 EPA Units at  $10^{-3}$  probability, respectively. The overall mean for the increased solubilities of nesquehonite and 'No Backfill' are 6.0 and 8.0 EPA Units at the  $10^{-3}$  probability, respectively. The limit for compliance, according to 40 CFR Part 194 is 10 EPA Units. Therefore, it readily appears that even high solubility values do not cause the disposal to be out of compliance with EPA regulations. However, the large consequences of small changes of solubility values raises an important question: Are we certain that the solubility of plutonium or uranium, in any oxidation state, is less than the values presented in the CCA or the PAVT? How did we arrive at these numbers? Is there experimental evidence to back up the claims made in the CCA that deals with the oxidation state analogy between Am+3 and Pu+3? Once one really delves into the reasoning behind many of the fixed numbers associated with these actinides, many drawbacks appear in the reasoning, and confidence in the values used to show compliance is shaken.

## References

- Bean, J. E., M. E. Lord, D. A. McArthur, R. J. MacKinnon, J. D. Miller, and J. D. Schreiber. 1996. Analysis Package for the BRAGFLO Direct Release Calculations (Task 1) of the Performance Assessment Analysis Supporting the Compliance Certification Application. Sandia National Laboratories, WPO#40514.
- Beauheim, R. L., G. J. Saulnier, and J. D. Avis. 1990. Interpretation of Brine-Permeability Tests of the Salado Formation at the Waste Isolation Pilot Plant Site: First Interim Report. Sandia National Laboratories, SAND 90-0083.
- Beauheim, R. L. 1997. January 16 memo to Palmer Vaughn on ARevisions to Castile Brine Reservoir Parameter Packages, Sandia National Laboratories, WPO# 9882.
- Berglund, J. W. 1994. August 31 memorandum to Record AThe Direct Removal of Waste Caused by a Drilling Intrusion Into a WIPP Panel-A Position Paper, Sandia National Laboratories, WPO# 9882.
- Berglund, J. W. 1996. Analysis Package for the BRAGFLO Direct Release Calculations (Tasks 5 and 6) of the Performance Assessment Analysis Supporting the Compliance Certification Application. Sandia National Laboratories, WPO#40521.
- Biddle, P., D. McGahan, J. H. Rees, and P. E. Rushbrook. 1987. Gas Generation in Repositories. Oxfordshire, England: United Kingdom Atomic Energy Authority, Harwell Laboratory, AERE-R-12291.
- Blaine, R. L. 1997. Evaluation of Minimum  $K_d$  Parameter Values for Culebra Transport. Sandia National Laboratories, WPO# 41944.
- Bredehoeft, J. D. 1997a. Hartman Scenario Implications for WIPP. La Honda, CA: Hydrodynamics Group.
- Bredehoeft, J. D. 1997b. July 28 memorandum, Rebuttal: Technical Review of The Hartman Scenario Implications for WIPP (Bredehoeft, 1997) by Swift, Stoelzel, Beauhiem, and Vaughn - June 13, 1997, Hydrodynamics Group, La Honda, CA.
- Brush, L. H. 1995. Systems Prioritization Method - Iteration 2 Baseline Position Paper: Gas Generation in the Waste Isolation Pilot Plant. Sandia National Laboratories, SAND95-1140.
- Brush, L. H., and L. J. Storz. 1996. July 24 memo to M.S. Tierney, ARevised Ranges and Probability Distributions for Dissolved Pu, Am, U, Th, and Np in the Culebra for the PA Calculations to Support the WIPP CCA, Sandia National Laboratories.
- Bureau of Land Management, Roswell District. 1993. *Preliminary Map Showing Distribution Of Potash Resources, Carlsbad Mining District, Eddy And Lea Counties, New Mexico*
- Butcher, B. M. 1989. Waste Isolation Pilot Plant Simulated Waste Compositions and Mechanical Properties. Sandia National Laboratories, SAND89-0372.
- Butcher, B. M. 1990. July 24 memorandum from B. M. Butcher to M. G. Marietta, on disposal room porosity and permeability values for disposal room performance assessment, Sandia National Laboratories.
- Butcher, B. M. 1997. Waste Isolation Pilot Plant Disposal Room Model. Sandia National Laboratories, SAND97-0794.

- Chan, D. Y., B. D. Hughes, and L. Paterson. 1993. ATransient gas flow around boreholes.®  
Transport in Porous Media 10: 137-152.
- Channell, J. K. 1997. July 14 internal memorandum to EEG, ARationale for Assuming the 1% of  
the Actinides Will Be Transmitted with a  $K_d > 0$ ,® Environmental Evaluation Group.
- Chaturvedi, L., T. M. Clemo, M. K. Silva, W. W.-L. Lee. 1996. AConceptual Models Difficulties  
in the WIPP Compliance Certification Application,® in Proceedings of the Sixth  
International Conference on Radioactive Waste Management and Environmental  
Remediation, ICEM A97, Singapore, October 12-16, 1997. New York, NY: American  
Society of Mechanical Engineers, 423-7.
- Chaturvedi, L., W. W.-L. Lee, M. K. Silva, T. M. Clemo, and R. H. Neill. 1997. AEvaluation of  
the Long-Term Integrity of WIPP,® in WM-97 Proceedings: HLW, LLW, Mixed Wastes and  
Environmental Restoration - Working Towards a Cleaner Environment, March 2-6, 1997,  
Tucson, Arizona. Tucson, AZ: WM Symposia, Inc., 10-4.
- Clemo, T. M., L. Chaturvedi, and W. W.-L. Lee. 1996. AProblems with Data used in the WIPP  
Certification Application Performance Assessment,® in Proceedings of the Sixth  
International Conference on Radioactive Waste Management and Environmental  
Remediation, ICEM A97, Singapore, October 12-16, 1997. New York, NY: American  
Society of Mechanical Engineers, 1009-1012.
- D-Appolonia Consulting Engineers, Inc. 1982. Data File Report: ERDA-6 and WIPP-12 Testing.  
Albuquerque, NM: Westinghouse Electric Corporation.
- D-Appolonia Consulting Engineers, Inc. 1983. Brine Reservoirs in the Castile Formation Waste  
Isolation Pilot Plant [WIPP] Project Southeastern New Mexico. Albuquerque, NM: U.S.  
Department of Energy, TME 3153.
- Environmental Evaluation Group. 1996. September 11 letter from EEG to George Dials,  
Manager, DOE/CAO on the sensitivity to WIPP performance assessment results.
- Environmental Evaluation Group. 1997a. February 7 letter from EEG to Frank Marcinowski,  
Director, Center for the Waste Isolation Pilot Program, U.S. EPA on performance  
assessment issues.
- Environmental Evaluation Group. 1997b. March 14 letter from EEG to Frank Marcinowski,  
Director, Center for the Waste Isolation Pilot Program, U.S. EPA, on performance  
assessment issues.
- Environmental Evaluation Group. 1997c. May 23 letter from EEG to Jennifer A. Salisbury,  
Cabinet Secretary and Chair of the New Mexico Radioactive Waste Consultation Task  
Force on the distribution coefficient of actinides in the Culebra.
- Environmental Evaluation Group. 1997d. April 9 letter from EEG to Dr. Charles Wilson,  
Chairman of WIPP Conceptual Model-s Peer Review on misreading of EEG-55 in review of  
the Castile Brine Reservoir.
- Environmental Evaluation Group. 1997e. December 31 letter from EEG to Frank Marcinowski,  
Director, Center for the Waste Isolation Pilot Program, U.S. EPA, on performance  
assessment issues.
- Francis, A. J., J. B. Gillow, and M. R. Giles. 1996. Microbial Gas Generation Under Expected  
Waste Isolation Pilot Plant Conditions. Sandia National Laboratories, SAND96-2582.

- Freeze, R. A., and J. A. Cherry. 1979. Groundwater. Englewood Cliffs, NJ: Prentice-Hall, Inc.
- Gruschow, N. 1992. ASolution Mining of Potash Ore,® meeting paper, presented at the SMRI Meeting in Houston, Texas, Oct 18-23, 1992. Woodstock, IL: Solution Mining Research Institute.
- Hansen, F. D., M. K. Knowles, T. W. Thompson, M. Gross, J. D. McLennan, and J. F. Schatz. 1997. Description and Evaluation of a Mechanistically Based Conceptual Model for Spall. Sandia National Laboratories, SAND97-1369.
- Helton, J. 1996. December 23 Memo: Preliminary summary of uncertainty and sensitivity analysis results obtained in support of the 1996 Compliance Certification Application for the Waste Isolation Pilot Plant, Sandia National Laboratories.
- Larson, K. and G. Freeze. 1996. May 27 Memorandum to Record on ACastile Reservoir Volume Revision,® Sandia National Laboratories, WPO#37971.
- LaVenue, A. M., T. L. Cauffmann, and J. F. Pickens. 1990. Groundwater Flow Modeling of the Culebra. Sandia National Laboratories, SAND89-7068/1.
- Neill, R. H., L. Chaturvedi, D. F. Rucker, M. K. Silva, B. A. Walker, J. K. Channell, and T. M. Clemo. 1998. Evaluation of the WIPP Project-s Compliance with the EPA Radiation Protection Standards for Disposal of Transuranic Waste. Albuquerque, NM: Environmental Evaluation Group, EEG-68.
- Novak, C. F. 1997. Memorandum from Craig F. Novak to R. Vann Bynum ACalculation of Actinide Solubilities in WIPP SPC and ERDA6 Brines Under MgO Backfill Scenarios Containing Nesquehonite or Hydromagnesite as the MgO-CO<sub>3</sub> Solubility-limiting Phase,® Sandia National Laboratories, WPO# 46124.
- Papenguth, H. W., J. L. Krumhansel, R. V. Bynum, E. J. Nowak, Y. Wang, J. W. Kelly, and N. J. Linarez-Royce. 1997. Chemical Conditions Model: Results of the MgO Backfill Efficacy Investigation, EPA Docket A-93-02, II-A-39.
- Ramsey, J. and A. H. Treadway. 1997. Test of Mass Balance of SECOTP2D. Sandia National Laboratories, WPO# 44700.
- Ramsey, J. and M. G. Wallace. 1997. Analysis Package for the Culebra Flow and Transport Calculations (Task 3) of the Performance Assessment Supporting the Compliance Certification Application. Sandia National Laboratories, WPO#40516.
- Rao, L. F. 1996. December 18 letter from L. F. Rao, PNNL/Battelle to W. W.-L. Lee, EEG answering Lee-s December 2, 1996.
- Reed, D. T., S. Okajima, and M. K. Richmann. 1994. Stability of plutonium (VI) in selected WIPP brines. Radiochemica Acta 66/67: 105-111.
- Reed, D. T., D. G. Wygmans, and M. K. Richmann. 1996. Actinide Stability/Solubility in Simulated WIPP Brines Project: Stability of Pu(VI), Np(VI), and U(VI) in simulated WIPP Brine. Interim Report. Argonne, IL: Argonne National Laboratory.
- Sandia National Laboratories. 1992. Preliminary Performance Assessment for the Waste Isolation Pilot Plant. Sandia National Laboratories, SAND92-0700/1-5.

- Sandia National Laboratories. 1996. Waste Isolation Pilot Plant Shaft Sealing System Compliance Submittal Report, Volume 1: Main Report and Appendices A,B,C, and D. Sandia National Laboratories, SAND96-1326/1.
- Shatz, J. F. 1997. Waste Spallings Calculations, technical report. Del Mar, CA: John F. Shatz Research & Consulting, Inc.
- Silva, M. K. 1994. Implications of the Presence of Petroleum Resources on the Integrity of the WIPP. Albuquerque, NM: Environmental Evaluation Group, EEG-55.
- Silva, M. K. 1996. Fluid Injection for Salt Water Disposal and Enhanced Oil Recovery as a Potential Problem for the WIPP: Proceedings of a June 1995 Workshop and Analysis. Albuquerque, NM: Environmental Evaluation Group, EEG-62.
- Smil, V. 1997. Global Population and the Nitrogen Cycle. Scientific American (July) : 76-81.
- Stockman, C., A. Shinta, and J. Garner. 1997. Analysis Package for the Salado Transport Calculations (Task 2) of the Performance Assessment Analysis Supporting the Compliance Certification Application. Sandia National Laboratories, WPO # 40515.
- Stoelzel, D. M. and D. G. O'Brien. 1996. Analysis Package for the BRAGFLO Direct Release Calculations (Task 4) of the Performance Assessment Analysis Supporting the Compliance Certification Application. Sandia National Laboratories, WPO#40520.
- Telander, M. R., and R. E. Westerman. 1996. Hydrogen Generation by Metal Corrosion in Simulated Waste Isolation Pilot Plant Environments. Sandia National Laboratories, SAND96-2538.
- U.S. Department of Energy. 1990. Final Safety Analysis Report: Waste Isolation Pilot Plant, Carlsbad, New Mexico. WP 02-9, Rev. 0.
- U.S. Department of Energy, Carlsbad Area Office. 1996. Title 40 CFR Part 191 Compliance Certification Application for the Waste Isolation Pilot Plant, Final. DOE/CAO-1996-2184 (21 vols.).
- U.S. Department of Energy, Carlsbad Area Office. 1997a. March 12 letter from DOE/CAO to Ramona Travato, Director, Office of Radiation Programs, U.S. EPA, on DOE-s response to comments made on the CCA by the New Mexico Environmental Evaluation Group.
- U.S. Department of Energy, Carlsbad Area Office. 1997b. Expert Elicitation on WIPP Waste Particle Size Distribution(s) During the 10,000 Year Regulatory Post-Closure Period. Final Report. Carlsbad, NM: U.S. Department of Energy, Carlsbad Area Office Technical Assistance Contractor.
- U.S. Department of Energy, Carlsbad Area Office. 1997c. May 14 letter from DOE/CAO to Ramona Travato, Director, Office of Radiation Programs, U.S. EPA, on DOE-s response to EPA-s request in the March 19, 1997, etter on the WIPP CCA.
- U.S. Department of Energy, Carlsbad Area Office. 1997d. Summary of the EPA-Mandated Performance Assessment Verification Test (Replicate 1) and Comparison with the Compliance Certification Application Calculations, EPA Docket A-93-02, II-G-26.
- U.S. Environmental Protection Agency, Office of Radiation and Indoor Air. 1996a. Criteria for the Certification and Recertification of the Waste Isolation Pilot Plant-s Compliance with the 40 CFR Part 191 Disposal Regulations; Final Rule. Federal Register (February 9) vol. 61, no. 28, pp. 5224-5245.

- U.S. Environmental Protection Agency, Office of Radiation and Indoor Air. 1996b. Compliance Application Guidance for 40 CFR Part 194. EPA 402-R-95-014.
- U.S. Environmental Protection Agency, Office of Radiation and Indoor Air. 1997. March 19 letter from Ramona Travato to Alvin Alm on Additional Support or Documentation for the Compliance Certification Application, EPA Docket A-93-02, II-I-10.
- Wilson, C., D. Porter, J. Gibbons, R. Oswald, G. Sjoblom, and F. Caporuscio. 1997. Waste Isolation Pilot Plant Conceptual Models Peer Review: Final Report. U.S. Department of Energy, Carlsbad Area Office.
- Zheng, L., C. Xuehua and T. Mingshu. 1991. MgO-type delayed expansive cement. Cement and Concrete Research 21 (6) : 1049-1057.



## Acronyms

AIC	Active Institutional Control
BLM	Bureau of Land Management
CCA	Compliance Certification Application
CCDF	Complementary Cumulative Distribution Functions
CH	Contact Handled
DBR	Direct Brine Release
DOE	U.S. Department of Energy
DRZ	Disturbed Rock Zone
EEG	Environmental Evaluation Group
EPA	U.S. Environmental Protection Agency
ERDA	Energy Resource and Development Administration
FBHP	Flowing Bottomhole Pressure
FEP	Features, Events, Processes
LHS	Latin Hypercube Sampling
LWB	Land Withdrawal Boundary
NMBMMR	New Mexico Bureau of Mines and Mineral Resources
PA	Performance Assessment
PAVT	Performance Assessment Verification Test
PIC	Passive Institutional Control
PSI	Pounds per Square Inch
RH	Remote Handled
SAR	Safety Analysis Report
STP	Standard Temperature and Pressure
TRU	Transuranic Waste
TVD	Total Variation Diminishing
WIPP	Waste Isolation Pilot Plant

## LIST OF EEG REPORTS

- EEG-1 Goad, Donna, A Compilation of Site Selection Criteria Considerations and Concerns Appearing in the Literature on the Deep Disposal of Radioactive Wastes, June 1979.
- EEG-2 Review Comments on Geological Characterization Report, Waste Isolation Pilot Plant (WIPP) Site, Southeastern New Mexico SAND 78-1596, Volumes I and II, December 1978.
- EEG-3 Neill, Robert H., James K. Channell, Carla Wofsy and Moses A. Greenfield, Radiological Health Review of the Draft Environmental Impact Statement (DOE/EIS-0026-D) Waste Isolation Pilot Plant, U. S. Department of Energy, August 1979.
- EEG-4 Little, Marshall S., Review Comments on the Report of the Steering Committee on Waste Acceptance Criteria for the Waste Isolation Pilot Plant, February 1980.
- EEG-5 Channell, James K., Calculated Radiation Doses From Deposition of Material Released in Hypothetical Transportation Accidents Involving WIPP-Related Radioactive Wastes, November 1980.
- EEG-6 Geotechnical Considerations for Radiological Hazard Assessment of WIPP. A Report of a Meeting Held on January 17-18, 1980, April 1980.
- EEG-7 Chaturvedi, Lokesh, WIPP Site and Vicinity Geological Field Trip. A Report of a Field Trip to the Proposed Waste Isolation Pilot Plant Project in Southeastern New Mexico, June 16 to 18, 1980, November 1980.
- EEG-8 Wofsy, Carla, The Significance of Certain Rustler Aquifer Parameters for Predicting Long-Term Radiation Doses from WIPP, September 1980.
- EEG-9 Spiegler, Peter, An Approach to Calculating Upper Bounds on Maximum Individual Doses From the Use of Contaminated Well Water Following a WIPP Repository Breach, September 1981.
- EEG-10 Radiological Health Review of the Final Environmental Impact Statement (DOE/EIS-0026) Waste Isolation Pilot Plant, U. S. Department of Energy, January 1981.
- EEG-11 Channell, James K., Calculated Radiation Doses From Radionuclides Brought to the Surface if Future Drilling Intercepts the WIPP Repository and Pressurized Brine, January 1982.
- EEG-12 Little, Marshall S., Potential Release Scenario and Radiological Consequence Evaluation of Mineral Resources at WIPP, May 1982.
- EEG-13 Spiegler, Peter, Analysis of the Potential Formation of a Breccia Chimney Beneath the WIPP Repository, May, 1982.
- EEG-14 Not published.
- EEG-15 Bard, Stephen T., Estimated Radiation Doses Resulting if an Exploratory Borehole Penetrates a Pressurized Brine Reservoir Assumed to Exist Below the WIPP Repository Horizon, March 1982.
- EEG-16 Radionuclide Release, Transport and Consequence Modeling for WIPP. A Report of a Workshop Held on September 16-17, 1981, February 1982.

- EEG-17 Spiegler, Peter, Hydrologic Analyses of Two Brine Encounters in the Vicinity of the Waste Isolation Pilot Plant (WIPP) Site, December 1982.
- EEG-18 Spiegler, Peter, Origin of the Brines Near WIPP from the Drill Holes ERDA-6 and WIPP-12 Based on Stable Isotope Concentration of Hydrogen and Oxygen, March 1983.
- EEG-19 Channell, James K., Review Comments on Environmental Analysis Cost Reduction Proposals WIPP/DOE-136 July 1982, November 1982.
- EEG-20 Baca, Thomas E., An Evaluation of the Non-radiological Environmental Problems Relating to the WIPP, February 1983.
- EEG-21 Faith, Stuart, Peter Spiegler and Kenneth Rehfeldt, The Geochemistry of Two Pressurized Brines From the Castile Formation in the Vicinity of the Waste Isolation Pilot Plant (WIPP) Site, April 1983.
- EEG-22 EEG Review Comments on the Geotechnical Reports Provided by DOE to EEG Under the Stipulated Agreement Through March 1, 1983, April 1983.
- EEG-23 Neill, Robert H., James K. Channell, Lokesh Chaturvedi, Marshall S. Little, Kenneth Rehfeldt and Peter Spiegler, Evaluation of the Suitability of the WIPP Site, May 1983.
- EEG-24 Neill, Robert H. and James K. Channell, Potential Problems From Shipment of High-Curie Content Contact-Handled Transuranic (CH-TRU) Waste to WIPP, August 1983.
- EEG-25 Chaturvedi, Lokesh, Occurrence of Gases in the Salado Formation, March 1984.
- EEG-26 Spiegler, Peter, Environmental Evaluation Group's Environmental Monitoring Program for WIPP, October 1984.
- EEG-27 Rehfeldt, Kenneth, Sensitivity Analysis of Solute Transport in Fractures and Determination of Anisotropy Within the Culebra Dolomite, September 1984.
- EEG-28 Knowles, H. B., Radiation Shielding in the Hot Cell Facility at the Waste Isolation Pilot Plant: A Review, November 1984.
- EEG-29 Little, Marshall S., Evaluation of the Safety Analysis Report for the Waste Isolation Pilot Plant Project, May 1985.
- EEG-30 Dougherty, Frank, Tenera Corporation, Evaluation of the Waste Isolation Pilot Plant Classification of Systems, Structures and Components, July 1985.
- EEG-31 Ramey, Dan, Chemistry of the Rustler Fluids, July 1985.
- EEG-32 Chaturvedi, Lokesh and James K. Channell, The Rustler Formation as a Transport Medium for Contaminated Groundwater, December 1985.
- EEG-33 Channell, James K., John C. Rodgers and Robert H. Neill, Adequacy of TRUPACT-I Design for Transporting Contact-Handled Transuranic Wastes to WIPP, June 1986.
- EEG-34 Chaturvedi, Lokesh, (ed.), The Rustler Formation at the WIPP Site, January 1987.
- EEG-35 Chapman, Jenny B., Stable Isotopes in Southeastern New Mexico Groundwater: Implications for Dating Recharge in the WIPP Area, October 1986.

- EEG-36 Lowenstein, Tim K., Post Burial Alteration of the Permian Rustler Formation Evaporites, WIPP Site, New Mexico, April 1987.
- EEG-37 Rodgers, John C., Exhaust Stack Monitoring Issues at the Waste Isolation Pilot Plant, November 1987.
- EEG-38 Rodgers, John C., Jim W. Kenney, A Critical Assessment of Continuous Air Monitoring Systems At he Waste Isolation Pilot Plant, March 1988.
- EEG-39 Chapman, Jenny B., Chemical and Radiochemical Characteristics of Groundwater in the Culebra Dolomite, Southeastern New Mexico, March 1988.
- EEG-40 Review of the Final Safety Analysis Report (Draft), DOE Waste Isolation Pilot Plant, May 1989.
- EEG-41 Review of the Draft Supplement Environmental Impact Statement, DOE Waste Isolation Pilot Plant, July 1989.
- EEG-42 Chaturvedi, Lokesh, Evaluation of the DOE Plans for Radioactive Experiments and Operational Demonstration at WIPP, September, 1989.
- EEG-43 Kenney, Jim W., John C. Rodgers, Jenny B. Chapman and Kevin J. Shenk, Preoperational Radiation Surveillance of the WIPP Project by EEG, 1985-1988, January 1990.
- EEG-44 Greenfield, Moses A., Probabilities of a Catastrophic Waste Hoist Accident at the Waste Isolation Pilot Plant, January 1990.
- EEG-45 Silva, Matthew K., Preliminary Investigation into the Explosion Potential of Volatile Organic Compounds in WIPP CH-TRU Waste, June 1990.
- EEG-46 Gallegos, Anthony, and James K. Channell, Risk Analysis of the Transport of Contact Handled Transuranic (CH-TRU) Wastes to WIPP Along Selected Highway Routes in New Mexico Using RADTRAN IV, August 1990.
- EEG-47 Kenney, Jim W. and Sally C. Ballard, Preoperational Radiation Surveillance of the WIPP Project by EEG During 1989, December 1990.
- EEG-48 Silva, Matthew K., An Assessment of the Flammability and Explosion Potential of Transuranic Waste, June 1991.
- EEG-49 Kenney, Jim W., Preoperational Radiation Surveillance of the WIPP Project by EEG During 1990, November 1991.
- EEG-50 Silva, Matthew K. and James K. Channell, Implications of Oil and Gas Leases at the WIPP on Compliance with EPA TRU Waste Disposal Standards, June 1992.
- EEG-51 Kenney, Jim W., Preoperational Radiation Surveillance of the WIPP Project by EEG During 1991, October 1992.
- EEG-52 Bartlett, William T., An Evaluation of Air Effluent and Workplace Radioactivity Monitoring at the Waste Isolation Pilot Plant, February 1993.
- EEG-53 Greenfield, Moses A., and Thomas J. Sargent, A Probabilistic Analysis of a Catastrophic Transuranic Waste Hoist Accident at the WIPP, June 1993.

- EEG-54 Kenney, Jim W., Preoperational Radiation Surveillance of the WIPP Project by EEG During 1992, February 1994.
- EEG-55 Silva, Matthew K., Implications of the Presence of Petroleum Resources on the Integrity of the WIPP, June 1994.
- EEG-56 Silva, Matthew K. and Robert H. Neill, Unresolved Issues for the Disposal of Remote-Handled Transuranic Waste in the Waste Isolation Pilot Plant, September 1994.
- EEG-57 Lee, William W.-L., Lokesh Chaturvedi, Matthew K. Silva, Ruth Weiner and Robert H. Neill, An Appraisal of the 1992 Preliminary Performance Assessment for the Waste Isolation Pilot Plant, September 1994.
- EEG-58 Kenney, Jim W., Paula S. Downes, Donald H. Gray and Sally C. Ballard, Radionuclide Baseline in Soil Near Project Gnome and the Waste Isolation Pilot Plant, July 1995.
- EEG-59 Greenfield, Moses A. and Thomas J. Sargent, An Analysis of the Annual Probability of Failure of the Waste Hoist Brake System at the Waste Isolation Pilot Plant (WIPP), November 1995.
- EEG-60 Bartlett, William T. and Ben A. Walker, The Influence of Salt Aerosol on Alpha Radiation Detection by WIPP Continuous Air Monitors, January 1996.
- EEG-61 Neill, Robert H., Lokesh Chaturvedi, William W.-L. Lee, Thomas M. Clemo, Matthew K. Silva, Jim W. Kenney, William T. Bartlett and Ben A. Walker, Review of the WIPP Draft Application to Show Compliance with EPA Transuranic Waste Disposal Standards, March 1996.
- EEG-62 Silva, Matthew K., Fluid Injection for Salt Water Disposal and Enhanced Oil Recovery as a Potential Problem for the WIPP: Proceedings of a June 1995 Workshop and Analysis, August 1996.
- EEG-63 Maleki, Hamid and Lokesh Chaturvedi, Stability Evaluation of the E140 Drift and Panel 1 Rooms at WIPP, August 1996.
- EEG-64 Neill, Robert H., James K. Channell and Peter Spiegler, Review of the Draft Supplement to the Environmental Impact Statement DOE/EIS-0026-S-2, April 1997.
- EEG-65 Greenfield, Moses A. and Thomas J. Sargent, Probability of Failure of the Waste Hoist Brake System at the Waste Isolation Pilot Plant (WIPP), January 1998.
- EEG-66 Channell, James K. and Robert H. Neill, Individual Radiation Doses from Transuranic Waste Brought to the Surface by Human Intrusion at the WIPP, February 1998.
- EEG-67 Kenney, Jim W., Donald H. Gray and Sally C. Ballard, Preoperational Radiation Surveillance of the WIPP Project by EEG During 1993 through 1995, March 1998.
- EEG-68 Neill, Robert H., Lokesh Chaturvedi, Dale Rucker, Matthew Silva, Ben A. Walker, James K. Channell, and Thomas M. Clemo, Evaluation of the WIPP Project's Compliance with the EPA Radiation Protection Standards for Disposal of Transuranic Waste, March 1998.
- EEG-69 Rucker, Dale F., Sensitivity Analysis of Performance Parameters Used in Modeling the WIPP, May 1998.